Battelle
The Business of Innovation

August 5, 2013

U.S. Department of Transportation
Pipeline and Hazardous Materials
Safety Administration
1200 New Jersey Ave., SE
Washington DC 20590
RE: Contract DTPH56-11-T-000003
Comprehensive Study to Understand Longitudinal ERW Seam Failures

Dear: Steve

Battelle Memorial Institute, through its Corporate Operations (Battelle), is pleased to submit our interim task report for Task 2.6 dealing with ***Characterizing Aspects of Failure in ERW Line Pipe*** for your consideration. We look forward to its being posted for public access.

Sincerely,

Bruce A. Young

Project Manager

Battelle
The Business of Innovation

Final Interim Report – Task 2.6

Characterizing Failure in ERW Line Pipe

By

B. N. Leis
B. N. Leis, Consultant, Inc.,
Worthington, OH, 43085
and
J. B. Nestleroth,
Kiefner and Associates, Inc.,
Worthington OH, 43085

(with an annex by John Kiefner presenting KAI experience in characterizing failures in ERW seams)

Prepared for

U.S. Department of Transportation
Pipeline and Hazardous Materials
Safety Administration
1200 New Jersey Ave., SE
Washington DC 20590

Contract No. DTPH56-11-T-000003
Battelle Project No. G006084

August 5, 2013

Disclaimer

Battelle does not engage in research for advertising, sales promotion, or endorsement of our clients' interests including raising investment capital or recommending investments decisions, or other publicity purposes, or for any use in litigation.

Battelle endeavors at all times to produce work of the highest quality, consistent with our contract commitments. However, because of the research and/or experimental nature of this work the client undertakes the sole responsibility for the consequence of any use or misuse of, or inability to use, any information, apparatus, process or result obtained from Battelle, and Battelle, its employees, officers, or Directors have no legal liability for the accuracy, adequacy, or efficacy thereof.

Acknowledgments

Useful discussion and the assistance of current Battelle staff members in preparing this report – most notably Dr Daniel Kremser and Messrs E. B. (Ted) Clark and E. R. Beach – is gratefully acknowledged.

Executive Summary

The objectives of this report were to assess the possibility and merits of standardizing fractographic and metallographic practices for use in examining ERW seam failures. It was quickly clear that differences in the features causing failure, and the local microstructures, meant that case-by-case decisions were required regarding the fractographic and metallographic practices to be used. Recognizing that standardization was not possible, Annexes A and B were included to illustrate such practices and outline the expectations of good failure analysis and reporting practices. Thereafter, the work focused on 1) illustrating unique aspects associated with failure analysis of ERW seams, and 2) potentially new approaches for the same purpose.

It was found that the long used fractographic and metallographic practices for more homogeneous metals can be adapted for use with ERW seams, with care taken to account for aspects unique to such seams in regard to microstructural features, and the complexity they can lead to in the fracture processes. Two new technologies that rely on automated 3-D imaging and X-ray tomography were introduced as potential avenues to better understand and quantify ERW seam failures, which were supplemented by an adaptation of optical emission spectroscopy to identify the chemistry local to a fracture surface.

Significant shifting of the crack plane between differing microstructures as the fracture seeks a path of least resistance in an ERW seam were anticipated and observed using the 3-D approach, which revealed large jumps in the shift between planes. It also made clear that for CVN testing this shifting could complicate the practical interpretation of such measurements, and cause significant scatter in the measured energy and extent of ductility (measured by % shear area). Because differences in the initiation, propagation, and deformation components of fracture energy might be resolved through use of an instrumented striker in CVN testing, a minor change in the usual test practice could prove useful in interpreting seam toughness and related scatter. The utility of computed tomography was also clear in complement to the usual metallographic practices, particularly in choosing optimal planes for detailed metallographic analysis.

Conclusions drawn over the course of the task are presented throughout this report, with only the major conclusions noted here, as follows:

- differences in the features causing failure within an ERW seam, and in the related local microstructures, dictate case-by-case choices regarding fractographic and metallographic practices – while this effectively precludes standardizing such aspects, guidance is presented in two Annexes regarding good practice in characterizing such failures;
- thorough failure analysis and reporting is an essential aspect of integrity management as it helps to avoid the recurrence of similar failures;
- new approaches utilizing automated 3-D imaging and X-ray tomography were shown to be effective in complement to current fractographic and metallographic practices – and hold the potential to better understand the factors controlling failure, and to characterize the size, shape, and failure mechanisms involved;

- an adaptation of optical emission spectroscopy indicated that the averaged chemistry in the vicinity of the bondline of a well made ERW seam did not differ greatly from that remote to the bondline;
- differing microstructures in the seam were indicated to cause large shifts of the planes for crack initiation and propagation, as they seek the path of least resistance along and into an ERW seam; and
- complexity due to shifting crack planes and blunting of the notch in CVN testing were indicated to complicate direct use of measured energy and percent shear-area, which might be resolved if an instrumented impact striker were used to generate that data – which could improve failure pressure and other predictions for cases involving ERW seams.

Table of Contents

List of Figures

List of Tables

Page

List of Acronyms and Symbols

CT-CAT	computed tomography - computed axial tomography
CVN	Charpy-vee notch
DC	direct current
DNV	Det Norske Veritas
ECA	engineering critical assessment
EDS	energy dispersive spectrometer
ERW	electric resistance weld
FSE	full-size equivalent
FW	flash weld
HAZ	heat affected zone
HF (ERW)	high frequency (electric resistance weld)
ID	inside diameter, also used as (specimen) identification
ILI	inline inspection
ITD	in-the-ditch
KAI	Kiefner and Associates
LF (ERW)	low frequency (electric resistance weld)
NDE	nondestructive evaluation
OD	outside diameter
OES	optical emission spectrometry
SSC	selective seam corrosion
XRF	X-ray fluorescence
XRT	X-ray tomography
YS&T	Youngstown Sheet and Tube
% SA	percent shear-area
2-D	two dimensional
3-D	three dimensional
t	(wall) thickness
D	diameter

Characterizing Aspects of Failure in ERW Line Pipe

Introduction

This report presents the results of Subtask 2.6, whose purpose was to outline and illustrate practices useful in characterizing failures in line pipe produced using an electric resistance weld (ERW) as the basis to assess if such aspects could be standardized. Because ERW-seamed line pipes are unique compared to other seamed pipe only in the area of the upset and bondline, the planned focus was on fractographic, metallographic, and other related practices that are used or that might be adapted for this purpose.

As the term implies, fractography involves the study of fracture surfaces. Fractography is often done in a forensic setting to determine the cause of failure, but also is done to quantify phenomenology as the basis to develop models of crack nucleation and growth or evaluate such models. Less can be inferred from the term metallography, which involves the study of the physical structure of metals, whose understanding provides insight into various properties, processing history, and related aspects.

The basic concepts and related practices of these topics are detailed and illustrated in textbooks and handbooks[e.g.,1-4]. Text and handbooks dealing with fractography typically include topics such as history, modes of fracture, specimen preparation and preservation, documenting fracture surfaces, visual / (stereo) optical examination and light microscopy, scanning electron microscopy, transmission electron microscopy, quantitative fractography, fractal analysis, and so on. Handbooks and texts on metallography typically cover specimen preparation including sectioning and specimen extraction, interpretation concepts, types of structure, light and electron microscopy, digital imaging and quantitative analysis, macro vs micro structures, field practices, and so on. Finally, guidance is available that considers the generic principles in a pipeline-specific setting[e.g.,5]. Those interested in these well-established aspects should refer to the references cited, and in the many other such resources available for example online. In addition to such basic topics, technology that has been developed or adapted to ERW applications is presented, which is presented and discussed in more detail. Of particular note in this context are the sections on X-Ray Tomography (XRT), Three-Dimensional (3-D) Imaging, and Local Chemistry Screening.

As has been discussed in prior reporting for other subtasks[e.g.,6,7], the low frequency (LF) seam process and the contact as well as the non-contact high-frequency (HF) ERW seam processes all create a forged seam that reflects the effects of plastic-flow and localized melting that leads to an upset heat-affected zone (HAZ), which is inherently similar for all processes. Likewise, as has been detailed elsewhere[e.g.,8] and discussed in prior reporting of other subtasks[e.g.,6,7] the generic types of defects that can cause longitudinal (long) seam failures are similar. Because of the just-noted similarities, the outline and illustration of the long-practiced methods does not distinguish between these seam processes, aside from indicating differences in aspects that are unique or do show some specificity, such as metallographic etches.

This report first outlines and illustrates the long-practiced methods that have been used to characterize failures in applications specific to ERW seams in reference to metallography and fractography. Fractography is illustrated in reference to features typical of the many defect types and some etches that have been found effective over the years are illustrated through reference to typical cross-sections, with the details referenced to handbooks. Aspects of sample selection and preparation are briefly outlined, with cleaning and related issues also discussed. Characteristic cross-sections are presented in regard to both the bondline and the heat-affected zone (HAZ). Because the tools and techniques involved are documented in handbooks and other widely available resources, the focus here is on outcomes from their use rather than the equipment and practices involved.

Following an overview of the long-practiced aspects, technologies that offer some promise for adaptation to enhance interpretation of the failure processes are presented. As evident above, these include an XRT process and a 3-D imaging process, which are discussed relative to potential benefits versus issues, and some typical results presented to illustrate their utility. In conjunction with these new processes, an adaptation of a standard chemistry analysis practice will be presented in regard to understanding possible local differences that might act to promote failure. Finally, Annex A presents an introduction to good practices in developing and reporting failure analyses, and illustrates these. Annex B summarizes experience gained at KAI in regard to developing metallographic sections and fractography, which adds somewhat to similar information and discussion presented in prior reporting by Battelle[6] and KAI[7] in conjunction with DNV.

As needed, background and terminology specific to all topics considered is introduced. Finally, while standardized practices could evolve for all such approaches, this aspect was beyond the scope of this subtask.

Long-Practiced Characterization Technologies

Background

Characterizing the micro or macro structural and fracture features are but two of the many aspects that contribute to the direct-cause failure analysis process[e.g.,5]. In turn, a direct cause analysis in its most general form contributes to a root-cause analysis, which addresses systemic issues that carry well beyond aspects such as how and why it failed. As such, highlighting either of these topics here does not reflect their prominence relative to many other aspects, but rather simply reflects their role in understanding the failure behavior of an ERW seam, and the scope of the subtask being reported.

Metallography

Metallography is the key to understand the role of micro and macro structures that comprise an ERW seam weld. Metallography involves the selection and preparation of sections that in turn

can be examined to reveal the thermal-mechanical history/processing and the basic chemical makeup of the steel involved.

Sample selection and the planes to be sectioned are dictated by the purpose of the metallographic study. For example, when such work was involved during the transition from the LF to HF process in the US during the late 1950s and on into the early to mid 1960s, the specimens subject to study came from trial pipe production. In such work, the many process parameters were systematically varied and pipe seams were produced with the specific purpose of providing samples for sectioning – to correlate structure to processing. Multiple sections were cut from sites along the welds, with an early focus at the ends of the joints – although that concern diminished with the transition to continuous production[9]. Serial sections also were made with a view to understand short-term process variations.

In contrast to the study of processing effects on seam quality quantified by metallographic sections, where metallography is done to support a failure analysis the sections of primary interest are typically those reconstructed in the vicinity of the origin of the failure, as well as reference sections cut remote to the origin. While the same metallographic practices might be used, the focus of such studies differs case by case. In such cases the sections are evaluated to identify defects or other indicators of process upsets, as well as to identify indicators of possible in-service degradation. The literature indicates that metallography has played a critical role in the evolution of a quality ERW seam since the mid-1920s. This is evident for example in the view shown herein as Figure 1, reproduced from a handbook published in 1934[10], which discusses the quality and strength of tubes produced for high-pressure service according to concept and process patents granted in the early 1920s[11,12]. The arrangement of the roller electrodes, and the shape and confinement provided by the lateral pressure rollers noted therein were comparable to that in use until the LF ERW process was abandoned. Moreover, those and other related patents recognized the significance of process speed, upset force, current frequency, and temperature, all of which contribute to the quality evident in the microstructure shown in Figure 1. The only big difference then versus now lies in the equipment used, and the convenience and quality that are afforded by technology. This is evident, for example, for metallography in the realization that the low-magnification view in Figure 1 is a montage. Inspection of this figure suggests that the field of view then, even at low power, was limited to a small fraction of an inch which is in stark contrast to today's capabilities.

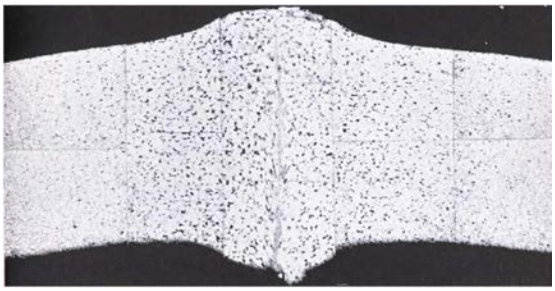

Figure 1. Cross-section montage through an ERW seam produced prior to 1934[10]

As-polished metallographic cross-sections can be effective in locating defects, such as small, tight cracks, which when small become very difficult to locate once the section is etched. Metallographic sections also can be instructive regarding the alignment of the seam, and can be help identify issues with edge preparation or over scarfing.

After etching to reveal the microstructure, the presence of the hard brittle phase known as martensite becomes evident, if present, and depending on the year produced when known can indicate a process upset. A skilled metallographer can infer much regarding the chemistry and processing of the skelp, and from study of the upset/HAZ can infer aspects of the thermal-mechanical process involved in making the seam. The presence of dirty constituents in the steel, such as sulfide stringers, becomes apparent, as do oxides in the bondline. Such information is instructive in regard to steel supply, as well as processing. A macro-etch can help to visualize the extent of the upset, which when inadequate is evident as an absence of out-bent fibers, which could contribute to the occurrence of a cold weld. Illustrative metallographic sections follow, although with limited discussion as these views often are largely self explanatory.

Figure 2 shows a cross-section through an early 1940s ERW seam produced by Youngstown Sheet and Tube (YS&T) from nominally 0.312-inch-thick skelp. As discussed in related project reporting[6], YS&T made use of a direct-current (DC) process. The cross-section shown in this image clearly illustrates a misaligned seam with inadequate trim on the inside diameter (ID) of the pipe, which likely traces to the misalignment. There is also a nick on the outside diameter (OD) that appears due to a slightly over-scarfd seam, and misaligned trim tool.

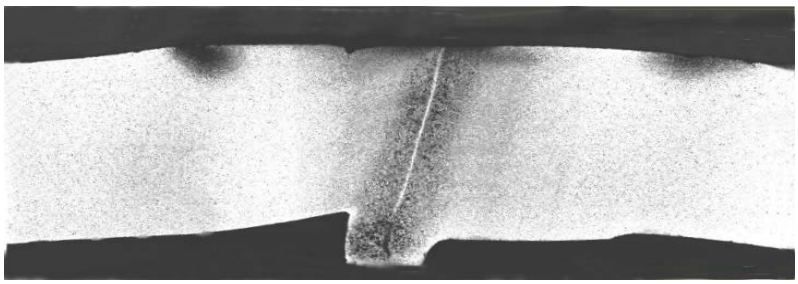

Figure 2. Section through a misaligned 1940s YS&T seam: t = 0.312”

It is evident from this view that misalignment coupled with a close scarf on the OD can lead to cases where the wall thickness is much reduced when compared to nominal, even considering typical production tolerances. While not apparent in this case, misalignment such as this opens to the formation of a lip that can roll from one side of the seam over the flash onto the other side of the seam, which creates an ID stress raiser that could serve as a site that nucleates axial cracking. It follows that serious misalignment opens to a number of potential integrity threats. While the microstructure is poorly characterized in the copy of report that this image was captured from, the skelp was not indicated to be a concern. The white band that tracks along the bondline is ferrite, and is commonly observed in such seams (in varying thicknesses) as it reflects steel that has been heated and decarbuized prior to upsetting, but not ejected from the bondline. The darker fields that appear on the OD about a wall-thickness to either side of the

seam are contact marks, where the wheel electrode rode along the pipe wall. While not an issue for this weld, these areas can contain untempered martensite, and develop cracks if the process control is upset.

Figure 3 shows a cross-section through the other early DC seam process known as a flash weld, which was uniquely used by the A O Smith Corporation from the late 1920s through 1970. While the OD seam was slightly over-scarf'd for such pipe, this ID view is characteristic of the flash-weld (FW) seam shape. As is evident from this figure, the skelp used to produce this 0.281-inch thick pipe was very dirty, and showed numerous sizeable silicate films in the vicinity of the fracture-origin.

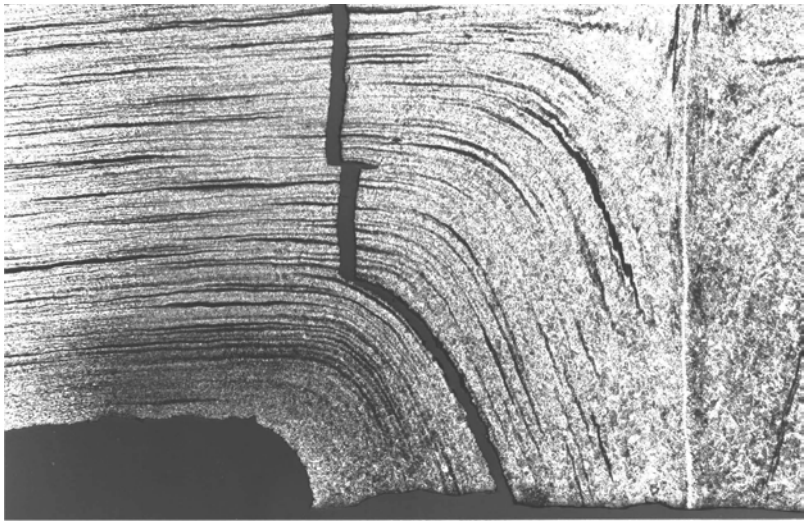

Figure 3. Section through 1950's FW seam showing about one-half of the wall thickness

The crack shown in the cross-section in Figure 3 is characteristic of hook cracks that form along 'out-bent fibers', whose shape reflects the macro-flow that occurs during the upset developed in the ERW seam process. This type of cracking is not driven by a process upset nor does it require misalignment. Rather, it occurs simply because the dirty steel contains concentrations of impurities that are strung-out and flattened during rolling of the skelp. The dirtier the steel, the more widespread are such features – which in very dirty steels lead to rather thick films and/or bands of pancaked inclusion stringers. Because the interfaces between the bands of impurities are weakly bonded to the adjacent pancaked steel grains, this layered structure is anisotropic and provides little strength or ductility in response to loading across such interfaces.

Figure 4 shows a cross-section through a 1941 ERW seam also produced by YS&T, which in this case involved nominally 0.250-inch-thick skelp. While this cross- section includes some of the traits evident in Figure 2, it has been included to illustrate brittle failure through untempered martensite scattered about the vicinity of the bondline. While the pipe produced in this era by YS&T did not include a post-weld heat treatment, the related patent literature[13] indicates that the pre-cut lengths of skelp were heated prior to forming the cans. This, coupled with the limited

number of failures involving untempered martensite, suggests that residual pre-heat served to limit the occurrence of this hard, brittle phase.

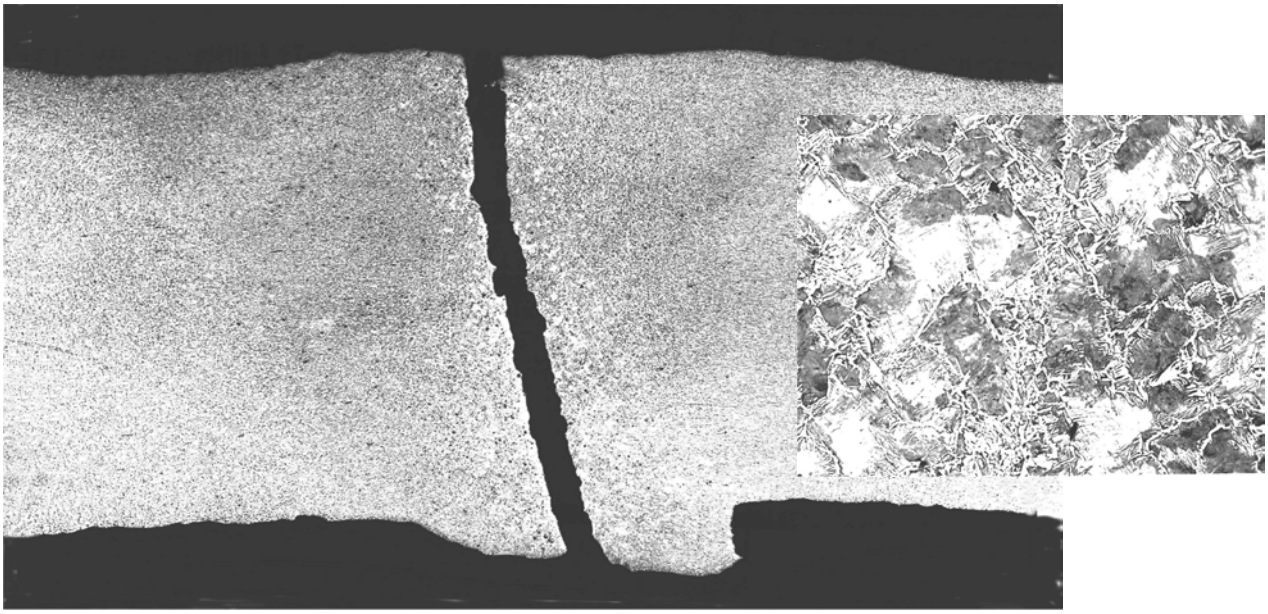

Figure 4. Cracking along a path with scattered areas of untempered martensite: t =0.250”

The primary image in Figure 4 characterizes an overview of the seam and the crack path, which shows patches of coarse ferrite along the bondline. The inset image was initially captured at 500 times magnification in the usual 4x5-inch film format, which can be used to infer the scale of the microstructural features evident in the inset. The light grey fields are untempered martensite, the white fields are ferritic, while the dark grey fields are bainitic. As might be expected, cracking through patches of untempered martensite shows little evidence of ductility, and experiences limited resistance to its continued advance.

Many other metallographic sections through ERW seams are illustrated and discussed in detail in Reference 4, with such discussion also presented in Reference 5. While these references also illustrate metallographic sections that involve general as well as selective-seam corrosion (SSC), Reference 14 deals specifically with this topic. Readers interested in the further details should consult those or other comparable resources. Aside from some edge-preparation issues, the cross-sections shown here and in the above references reflect the range of what can typically be encountered: thus it suffices now to summarize the range of the cracking paths that can be encountered. This is done relative to origins in the bondline or in the upset/HAZ in regard to the schematics shown in Figure 5. These schematics characterize a geometrically symmetric ERW seam modeled after the appearance of a FW joint, for circumstances absent corrosion. Figure 5a shows idealized views of cracking paths from origins in the bondline, whereas Figure 5b shows such paths from upset/HAZ origins.

In regard to Figure 5a, note that three origins are commonly observed. That labeled ‘a’ initiates in the bondline from the OD or ID of the pipe, and can range in depth from very shallow up to

the full depth of the seam – with a leak initially prevented by oxides that are compacted in the breach. The crack designated 'b' is similar to that just discussed, except that its origin is other than from the surface – often within a mixed structure that embeds oxides and other trapped impurities that the upset process failed to expel. Finally, the path designated as 'c' has been included to indicate that origins in the bondline do not always track along that path if/when they grow. In seams that involve dirty steel, a bondline origin can shift onto a hook path, and grow along that interface, as shown by the path designated 'c'. Likewise, in cases where a brittle phase lies parallel to and in proximity to the bondline, a bondline origin can shift into that brittle phase, and continue to grow in the phase or jump back into the bondline. As such, the crack seeks the path of least resistance – which can reflect both strength and ductility considerations.

a) bondline origins **b) upset/HAZ origins**

Figure 5. Schematics of bondline and upset/HAZ cracking paths

Figure 5b parallels the intent of Figure 5a for cracking that initiates in the upset/HAZ, which as indicated above develops in a layered microstructure that forms due to dirty steel. Origins can develop from the OD or the ID, or on both surfaces, at any site across or along the upset/HAZ. The case designated 'a' in Figure 5b reflects a single hook origin from either surface, or both as shown for 'b1' and 'b2'. Because the interface between the layers of pancacked steel grains and the plane of impurities is weak, the cracking tends to track this interface. Depending on the pressure and other forces that drive the maximum principal stress, and the relative strength and ductility of the structures involved, this hook cracking eventually turns from the interface onto a path that is perpendicular to that stress. As the schematic crack designated 'a1' shows, this shift onto a perpendicular plane can occur after differing amounts of growth in the interface, which is determined by the level of maximum principal stress, and the relative strength and ductility of the structures involved. Particularly where high pressure (local tensile stress) is involved, this shift onto a perpendicular plane tends to occur after little growth along the interface, and in the process can jump back onto the bondline, as indicated by path designated 'a2'.

Because this layered microstructure is present through the pipe wall, once the crack turns to grow through-wall it can intersect other such interfaces. This can give rise to a complex stepped crack path as it grows through-wall, which fractographers sometimes called 'woody', but more generally it is a hook crack. Figure 6 illustrates such fracture behavior, for which the origin lies along the upper margin of the photograph. Because of the initiation and growth in, along, and across multiple bands in the layered upset structure exposed at the pipe's surface, this image shows clear macroscopic evidence of such layering and failure in the above-noted interfaces.

Figure 5b also shows a pair of hook origins that initiated at both surfaces, designated as 'b1' and 'b2', which depending on the pressure and resistance encountered by the growing cracks can

lead to well developed hook cracking from one or both surfaces. Such cracking initiates independently, and also grows largely absent any influence of the second crack, as has just been discussed for the case of a single origin. However, as these cracks deepen, and coalesce through-wall leading to failure, they can interact, which tends to accelerate their growth.

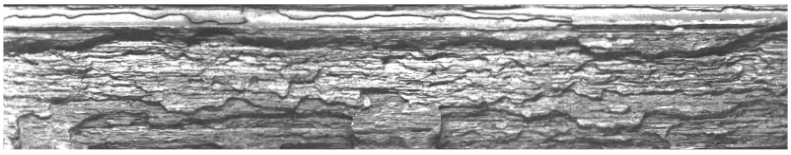

Figure 6. So-called woody fracture features in a mid-1960s HF ERW seam: t = 0.325”

Useful Etches for ERW Seams

An etch in a metallographic context serves to optically highlight structural features, which can be macroscopic in scale such as flow lines, or microscopic in scale such as grain or phase boundaries or other features. Figure 3 illustrates the effects of a macro-etchant, whereas the inset in Figure 4 shows the phases highlighted by a micro-etchant.

Etching selectively alters various structural features based on factors such their crystal structure, composition, or the stress they have been subjected to. While a variety of techniques have been used for this purpose, only the most common practice that uses selective chemical attack is considered herein. With this technique, the etchant reacts with aspects of the feature to decorate it or selectively expose it. Such etchants typically involve a mixture of acids or bases with oxidizing or reducing agents.

Over the years, work at Battelle has relied on various concentrations of a group of etchants to emphasize certain aspects of an ERW seam. A few of the more commonly used etchants include: Nital (100 ml ethanol + 1-10 ml nitric acid); Picral (100 ml ethanol + 2-4 g picric acid); Stead’s Reagent (10g cupric chloride, 40g magnesium chloride, 20ml hydrochloric acid (concentrated), alcohol to make 1L); Sodium Bisulfite; 1 g Sodium Tridecylbenzene Sulfonate in 100 ml saturated aqueous solution of Picric Acid; and hot Hydrochloric Acid. Figures 7 and 8 are instructive in regard to etches and the structures they help to characterize.

Figure 7 shows a macro-etched view of a cross-section through a failure in a FW seam in pipe made using 0.281-inch semi-killed steel. While the history of the skelp is unclear, views as shown in Figure 7 tend to reflect differences between the edges and the centerline characteristics of skelp that has been split from a much wider coil, to provide the width required. Although nominally the same skelp with the same base chemistry and processing is involved either side of the FW bondline, and the same etch was swabbed over this area for the same time period prior to washing and drying the mount, it is clear from this image that use of a given macro-etchant can give rise to significantly different results. As such, choosing an etchant and the exposure time can be a trial and error process whose results can depend on the samples being evaluated, and on the purpose of each metallographic cross-section. Thus, it is difficult to offer standardized guidance in such applications.

In contrast, Figure 8 illustrates results developed by way of a micro-etchant, which for these views is Picral applied to early 1960s samples of skelp. Detailed study indicates that both views present ferritic-pearlitic microstructures that otherwise differ in terms of grain size and uniformity. Such differences are not unusual between skelp producers, as is the case here, with the differences in uniformity and grain size tracing to aspects such as rolling practices, finishing temperature, and temperature in the coil. Also in contrast to Figure 7, largely because microscopic images capture a relatively small area over which the chemistry and processing are more uniform than across a bondline, such results tend to produce more uniform pictures of the structure.

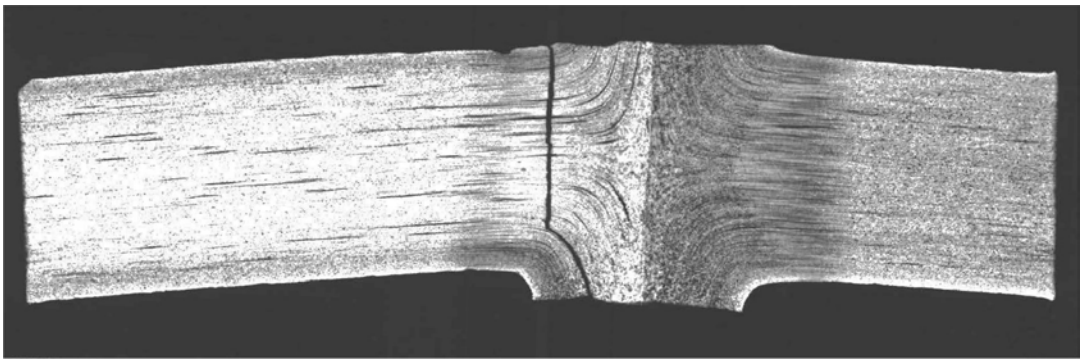

Figure 7. Differing effects of the same etchant in otherwise identical skelp: t = 0-281”

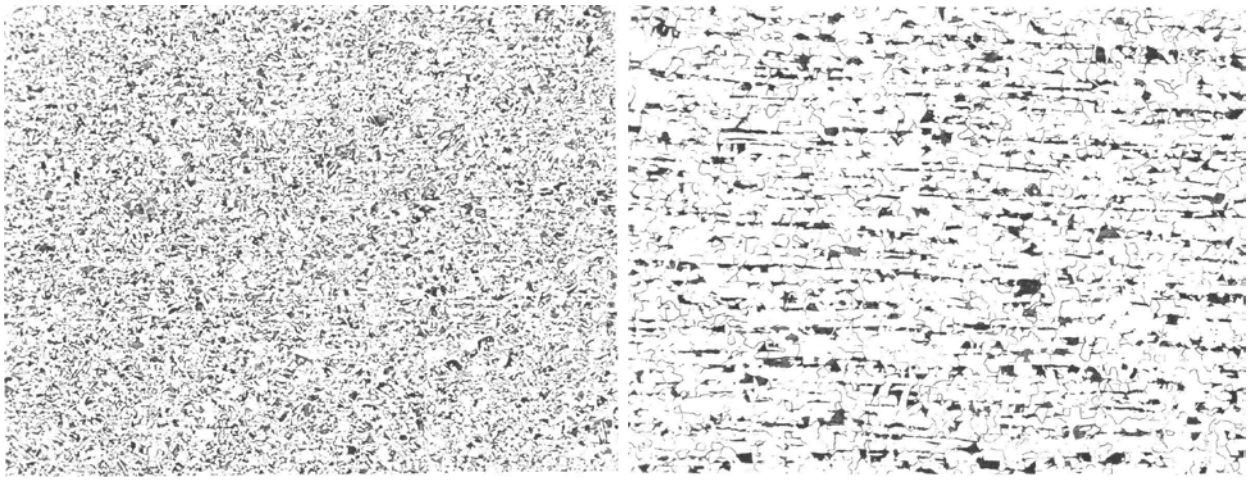

a) skelp supply A **b) skelp supply B**

Figure 8. Comparable effects of the micro-etchant Picral, both shown at ~100X

Fractography

Fractography involves the study of fracture surfaces to determine the cause of failure in engineering structures for forensic purposes, and to develop a phenomenological basis to build and/or evaluate models of crack initiation and growth response. The forensic process typically involves benchmark features that are characteristics of specific crack growth mechanism, such as fatigue, stress corrosion cracking, SSC, hydrogen embrittlement, and so on, as their traits tend to be unique depending on the material, its stressing, and other factors. Accordingly, the study of

fracture features requires consideration of all such aspects, with overall pattern of cracking at a macroscale as important as the features identified at the microscale. It also requires insight about the material, as microstructural features can exert a strong influence on the features evident. Study at a macroscale involves optical or stereo-optical microscopy, whereas a range of electron microscopy is available to support study at the microscale. As for metallography, the equipment and techniques are well established and presented in handbooks[(e.g.,1)].

Sample selection is critical in the evaluation of fracture features, particularly because at higher magnification the field of view shrinks to 'small speck on a large wall'. Thus, it is critical to understand the purpose of the study, and on that basis to then select fields of interest for study at higher magnification – with very high magnification often not needed, or considered last in the process. As the focus here is pipeline related failures, which in the mainline often involves an axial split, the assumption of similar resistance to cracking and loading indicates that the mid-length of the split can be a good place to start. The presence of local reversed curvature along the fracture, as shown for example in Figure 9 is likewise a good starting point. Notice in comparing the images shown in Figure 9 that the presence and extent of such reversed curvature depends on the pipe's geometric stiffness quantified relative ratio of its diameter to its thickness, denoted D/t, pressure stiffening quantified by the pressure at failure, and other factors. On that basis, care must be taken in each case considered to capture the benefits of past experience in light of differences in the circumstances that can control the failure process and how it presents itself in one scenario versus another.

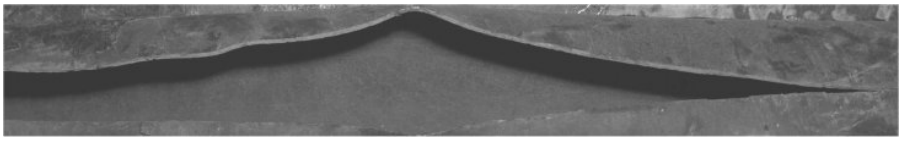

a) D/t = 51 at high pressure

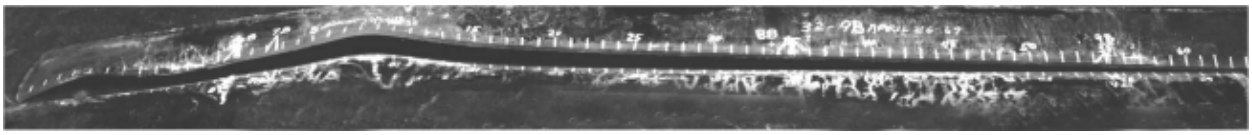

b) D/t = 74 at moderate pressure

Figure 9. Bulging and kinks along axial splits in ERW longitudinal seams

It is always necessary to first document the site, and to use clues in that process as to propagation direction to confirm indications as evident in Figure 9 as the origin. The surface of the pipe as well as that of the fracture should be considered in this context, with a macroscopic map of the fracture sequence developed in this context. Brittle-like fracture paths in such cases often show 'chevrons' that point back toward the origin, as evident for example in Figure 10a. In contrast, ductile fractures can show evidence of 'arrowheads' that point in the direction of crack advance, as illustrated in Figure 10b. While pressure is often the primary driving force for cracking, in selecting origins it is also important to consider secondary loadings, which tend to be more important in diagnosing failures in station piping or equipment.

Other situations are not as simple as indicated in the above figure, which is particularly the case when multiple crack paths are active, and possibly several joints of pipe are involved. While it is always necessary to first document the site, in such cases it is clearly beneficial to reassemble the marked pieces – physically as well as graphically – and to use clues noted above to infer the propagation direction as the basis to locate potential origins. Site details, such as the shape of the crater, as well as the surface of the pipe can be used to supplement the information gleaned from fracture surface, with a macroscopic map of the fracture sequence developed in this context, such as that shown in Figure 11.

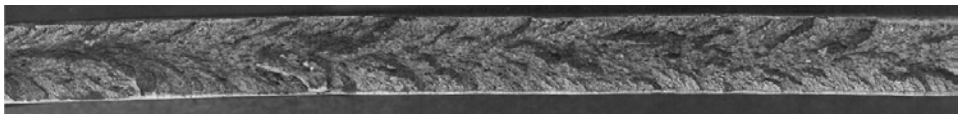

a) chevrons, with origin to the left: t = 0.375”

b) arrowheads, with origin to the right: t = 0.560”

Figure 10. Views of visual clues concerning cracking direction

Figure 11 shows the fracture map for an ERW seam failure, for which the extent of the axial cracking was contained by the girth welds at either end of the joint that failed. It is usual to present the pipe with the longitudinal seam (if present) or some clock position noted central to the surface of the pipe as if the pipe were unrolled. Thus, the line placed at mid-height in this figure shows the location of the ERW seam, with the path of the cracks located on the unrolled pipe, with one-half the circumference shown either side of the seam. The arrows placed along the crack paths indicate the direction of the cracking determined in this case by the presence of chevrons on the fracture surfaces. Once the segment containing the origin as indicated in the mapping was identified, the investigation shifted into the laboratory wherein the details along the seam led to identification of the origin as a cold weld.

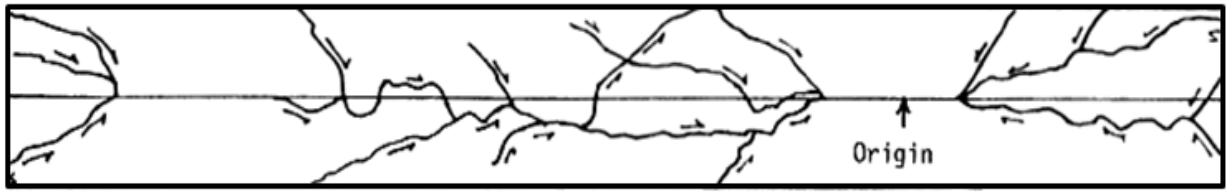

Figure 11. Fracture mapping for an early vintage ERW seam

Once candidate origins are identified, it is usual to create a more detailed fracture surface map in the vicinity of the apparent local direction(s) of the crack paths, and consider the implications of other evidence, such as the known loadings. High-level guidance for pipeline-related work can be found in Reference 5. Care must be taken in this context to incorporate consideration of the pipe’s geometry, as smaller diameter or heavier wall pipe does not deform to the same extent that

occurs for less stiff cross-sections such as the thin-wall case evident in Figure 9. Likewise, care must be taken to seek out the subtle or initially latent clues relative to the circumstances at hand.

Because the images discussed above in regard to Figure 10 reflect failures in the pipe body, such behavior does not always translate directly when an ERW seam is involved. For example, because of through-thickness differences in properties, features like the chevrons in Figure 10a can be incompletely or poorly developed, or develop on only a part of the fracture surface. Such a situation is shown in Figure 12, which shows the fracture surface near the origin of a split in a 1951 vintage FW seam. It is evident from that image that the seam was partially filled with 'black oxide', which gave rise to chevrons only over portions of the pipe wall.

Figure 12. Chevrons over portions of the thickness of the pipe wall: t = 0.281"

Likewise, because process upsets are periodic, and the quality of the seam can be strongly influenced by process upsets, the appearance of fracture along a seam can vary significantly over short distances along a fracture surface. This is illustrated for example in Figure 13, which captures images along a seam split that lay sequentially within a few feet of each other. Figure 13a has an appearance that is similar to some well characterized hook crack failures: a shallow origin lies on the upper (OD) edge of the photograph, with the darker area along the lower edge being shear. In contrast, the view in part b) of this figure is more typical of coarse stitching, although the lower edge (ID) is decorated with what appear to be cold welds that contain a shallow layer of black oxide. Adjacent to this area, the features are again similar to those of hook cracking, as shown in Figure 13c. This image shows a well developed hook crack, which runs much deeper than that in part a) of this figure, and was sufficiently open to take-up contrast paint applied to the OD prior to field inspection.

a) area 3

b) area 4

c) area 5

Figure 13. Features in close axial proximity along a fracture surface: t = 0.281"

It follows that care must be taken when assessing the nature of ERW seam failures, with cross-sections through the seam often necessary to conclusively determine the cause of the failure. Such differences within feet of each other complicate standardizing practices for the failure analysis of ERW seams.

Confusion also can arise in regard to the portion of the fracture surface that triggered the failure, with the presence of oxides and debris originating in pipe making, in-service, or due to the failure, for example due to fire or environmental exposure also being complicating factors.

Cleaning Fracture Surfaces

Once all aspects of the surface deposits, films, debris have been quantified to the extent needed, and samples obtained, the fracture surfaces should be cleaned to facilitate evaluation. In so doing it should be recognized that the deposits, films, and/or debris can be stratified, with differing compositions present depending on when over time or during the failure process they formed. It follows that the layering and each of the layers of deposits, oxides, etc can provide information about the chronology and the aggressive species that gave rise to the reaction products. Thus, it is wise to map differences in coloration, topography, etc, and to use replica tape or other techniques to capture this surface record. Likewise, cleaning should be progressive, and at times and certain places selective, which must be assessed case by case. In addition, care must be taken not to damage or otherwise alter the features of interest, such that it is good practice to expose a reference near-polished surface to the cleaning process.

Usual cleaning practices can be found in handbooks. Once past the brushes and scrubbing aspects, cleaning relies on the use of cleaning agents, such as an Endox or Citronox solution, assisted by the use of an ultrasonic tub. More aggressive practices also can be found documented in the literature, such as an Alconox solution, with commercially available inhibited acids being still more aggressive. Given such methods are more aggressive, they must be used with care as the chance exists to damage / obliterate fine fracture features. Because there practices are routine and well documented elsewhere, those interested in these methods should refer to the handbooks, or online documentation.

The purpose here is to briefly focus on one lesser known practice that involves a variation of cathodic cleaning[(e.g.,15)]. With this practice, the specimen is made the cathode in an electrolytic cell, wherein the liberated hydrogen gas bubbles act to mechanically pop-off the reaction product(s) and/or debris. An inert anode, such as platinum or carbon, should be used to avoid contaminating the fracture surface, with thiscleaning done in conjunction with an ultrasonic tub. A variety of electrolytes have been used to clean the fracture features on line pipe that are mildly aggressive, but because this cleaning occurs largely by the mechanical effects of hydrogen liberation and involves short-exposure, the technique generally leave the fracture surface untouched. Battelle primarily makes use of an electrolyte based on Endox-214, with that and the current levels and exposure times chosen case-by-case. To ensure that no damage is done to any of the fine fracture features, it is usual to include a near-polished surface on the sample, such as

that created by a diamond cutoff wheel. That surface is monitored, with tarnishing used as a measure of the potential to obliterate fracture features. Cycles of cathodic cleaning are coupled with an Alconox wash or scrub and de-ionized water rinse until the desired outcome is achieved.

Adapting Characterization Technologies

Background

Methods and practices developed in other areas of science and technology open the door to parallel developments in other applications. This section outlines two parallel developments that have been adapted through other work underway at Battelle, which show promise in applications to better understand the complex interplay between the unique micro- and macro-structures that can coexist in an ERW long seam. As noted earlier in the introduction, these adaptations capitalize on X-Ray tomography and 3-D imaging processes. In addition, a 'poor-mans' scheme to characterize local chemistry is presented. Suffice it here to note that the basic capability in each adaptation is not new – as 3-D imaging and XRT have been available for decades. What is new is the efficiency and convenience in their use, and in the clarity of the characterization and convenience the use of their results. Both will be presented relative to their potential benefits versus issues, with some typical results presented to illustrate their utility and the implications. In addition, an adaptation of usual chemistry analysis will be presented in regard to understanding possible local differences that can act to promote failure.

3-D Imaging

Introduction: As indicated above, 3-D imaging is not new. Scanning electron microscopy provided depth of field that was not available with optical microscopy, with the ability to capture a pair of images at appropriate positions, such that a 3-D perspective could be created. This pair of images was then shifted manually below a viewer until the correct positions were found, at which point a 3-D perspective popped into view. While this practice has been available now for many decades, it found limited use for several reasons. First, the process was manual, with the outcome evident to only the person at the viewer. Second, depending on the scale of the features being viewed, obtaining a panoramic view of the feature and its surroundings could require that many pairs of images must be captured, but still only on pair could be viewed at any point in time. Third, each pair of printed-film-images took several minutes to create, with the outcome of each pair limited to an area dictated by the magnification used, such that pairs of images sufficient to create a montage had to be captured, but again only one pair could be observed at any point in time. On this basis, while the capability has existed to create 3-D images for decades, it was expensive, inconvenient, and lacked any panoramic capability even at the level of two adjacent pairs of stereo photos.

Offsetting the just-listed issues requires software that can automatically drive appropriate sensors to capture and manage what has in past been visually captured and manually managed. It also requires massive storage capacity, to handle the file size that develops as multiple robust image files are automatically matched and 'stitched' together to create a detailed 3-D image. Finally, it

requires hardware capable of information transfer at reasonable rates, and other software to manage manipulating the stitched montage for viewing from various positions, and support any related image analysis. It is only since ~2008 that hardware and software in terms of sensors, digital storage, processing speed, and other aspects have existed to adequately capture images and manage such data[(e.g.,16)].

Results: Images typical of the 3-D panoramic views that can be created today in seconds to minutes and then manipulated in real-time are presented shortly in the context of Figures 14 to 19. These images provide perspective for the 3-D technology relative to the corresponding two-dimensional (2-D) images shown for comparison. These 3-D images present macroscopic features that have developed in and along the plane of an LF ERW seam that has failed in testing Charpy V-notch (CVN) specimens. Specimen blanks for these tests have been located and cut such that failure would initiate in and along the plane of the bondline. Thereafter, care was taken to machine and notch the blanks to ensure the target plane for cracking was actually evaluated in each test. A second group of specimens were similarly prepared except that the notch was located slightly offset from to the bondline, with the outcome being initiation in the upset/HAZ of the seam. Typical results for tests targeting failure in the bondline are shown in Figures 14 to 16, whereas results for samples that targeted the upset/HAZ are shown in Figures 17 to 19. These results have been chosen to cover a wide range of test temperatures that were selected to develop fractures from lower-shelf energy values up toward higher energies, to reflect the anticipated transition from brittle to ductile response over the fracture surface. After imaging, each of the specimens was sectioned for metallographic characterization and chemistry analysis. One half of the specimen was sectioned on a plane perpendicular to the bondline, while the second was sectioned immediately below the fracture surface.

Each of the Figures 14 to 19 includes a 2-D image that presents the fracture features as typically viewed to estimate the percent-shear-area (%SA), which by standard practice must be reported along with the energy to fail the specimen. This image shows the two halves of the broken specimen setting side by side in part a) of each figure. This macro-view is supported for each figure by a pair of images that show either side of the broken specimen in the vicinity of the fracture plane, which is shown as part b) of each figure. Side views are useful because they clarify 1) whether the crack nucleated at the base of the notch, or was offset to the flanks of the notch, 2) if the cracking continued on the plane it initiated, which assists in associating the measured %SA and energy with the correct plane of propagation, 3) whether significant blunting occurred prior to the onset of crack initiation and propagation, and the extent of laminar cracking associated with out-bent fibers. These views thus can be instructive in understanding whether planes adjacent to the primary crack plane also develop cracks, or otherwise are involved with the failure process. This assists in partitioning the energy dissipated in reference to the bondline or the upset/HAZ, and whether the resulting failure developed from the root of the CVN notch, or was somewhat offset to that notch root, indicating that initiation occurred at a site of lesser resistance and whether cracking continued on that weaker plane.

Energy and values of %SA associated with Figures 14 to 19 are as detailed in Table 1, along with the test conditions. The key to map the test conditions in this table to the figures is the specimen identification (ID) listed in the table. The notation FSE in the table and elsewhere denotes the full-size equivalent energy determined for these half-size specimens by an assumed linear correlation of energy with thickness, which while a common practice might be questioned based on some literature data[(e.g.,17)].

ID	Temp, °F	FSE ft-lb	%SA
7-1	70	4.5	3
7-5	170	11.1	47
7-13	195	18	72
7-7	220	17.8	75
7-8	245	18	98
7-10	220	20	90

Table 1. Conditions and results for Figures 14 through 19

Inspection of Figures 14, 15, and 16, which targeted and ran in or largely in the bondline, show that failure in the bondline can range from planar brittle response at lower energies (and values of %SA as in Figure 14), through somewhat rougher fracture surfaces as in Figures 15 and 16. As evident in these figures, the rougher fracture surfaces lead to correspondingly higher shear areas and energies for testing done at higher temperatures – as expected – with this ductile response containing a still brittle field that lies in the bondline. Notice from the 3-D images that very little stretch develops at the origin for the lower-energy result, whereas there is significant stretching prior to crack initiation at the notch for the two slightly higher energy cases. Thus, the deformation component of the energy is becoming larger for the higher temperature more ductile cases in Table 1. This suggests that developing such data for ERW seam resistance using an instrumented CVN machine could provide increased understanding of why the resistance of the seam to fracture is increasing as temperature increases. These results suggest that the seam has remained rather brittle in spite of the temperature increasing up to 195°F, and that the apparent increase in toughness is due to the blunting and local deformation prior to initiation. The increased resistance also could reflect the fact that the crack runs in the seam only over the initial portion of the cracking, with the transition off-plane possibly due to the increased specimen rotation that develops in testing at slightly higher temperatures.

Because the extent of blunting evident in Figures 15 and 16 leads to an increased stretching at the notch, and correspondingly deformation within the zone that cracks, sufficient force develops for these specimens to open laminar cracking on out-bent planes in the upset of the weld. In the figures that show the sides of the CVN specimens, this response is denoted ‘laminar separations’. Such planes reflect the pancaked layers of grains and the presence of flattened strung-out zones of Manganese Sulfide inclusions. While still somewhat brittle, the increased toughness in the bondline with increasing test temperature means that the crack plane seeks a path through less resistant material. The same planes of laminar weakness evident on the surface of the specimen

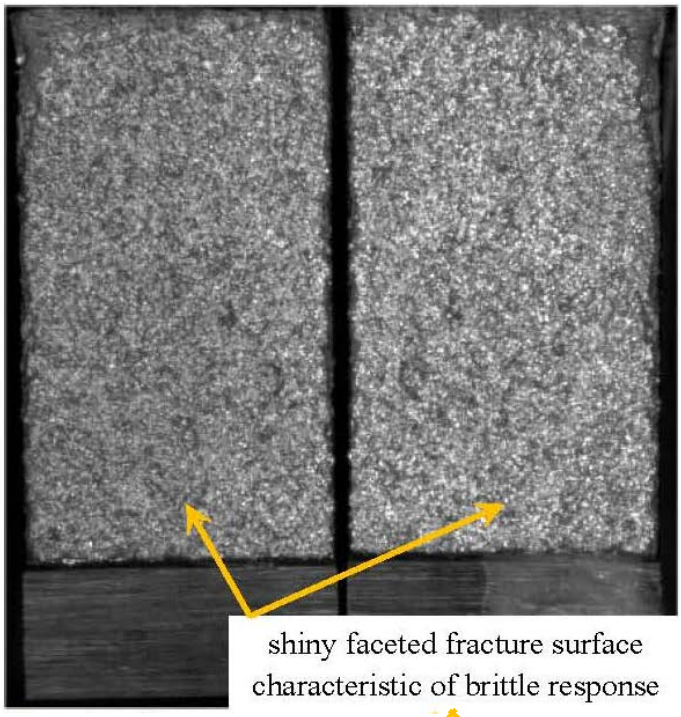

a) 2-D fracture images

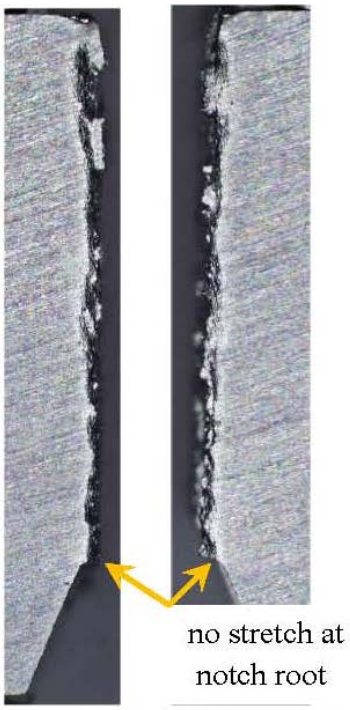

b) 2-D view of the specimen sides

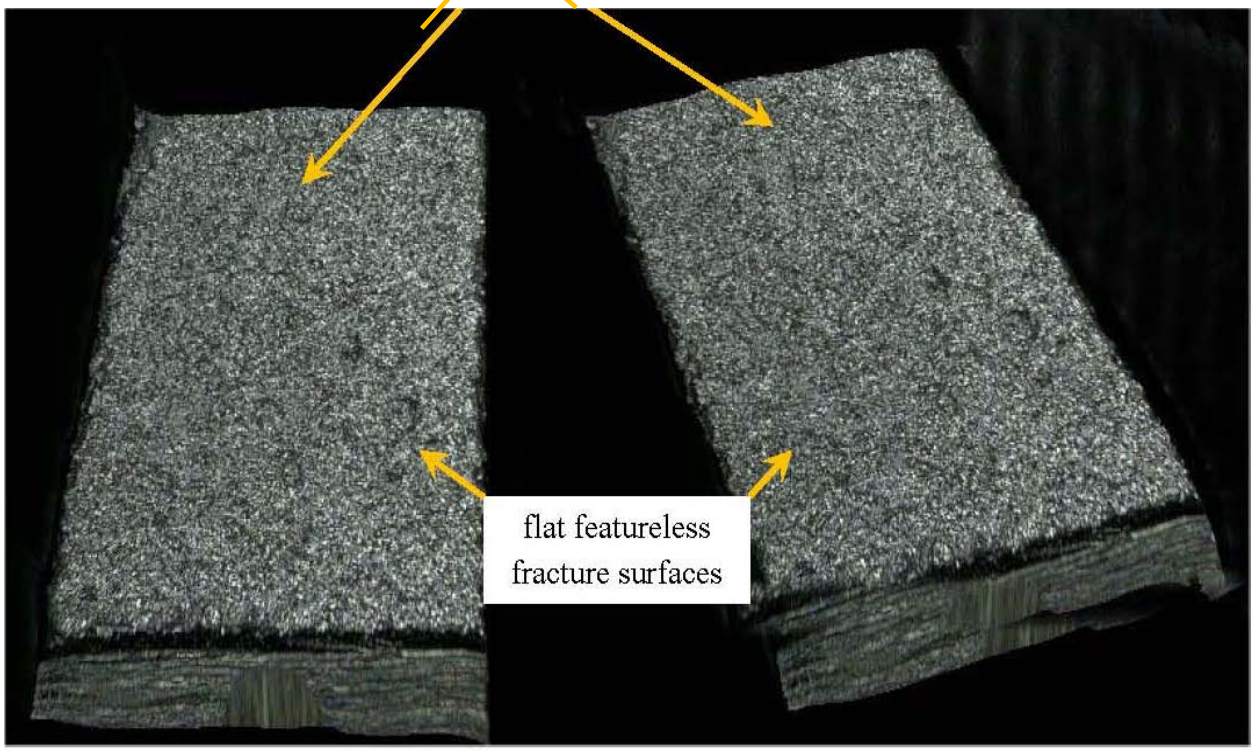

c) 3-D views of the fracture features – notch forward

Figure 14. Half-size CVN specimen # 7-1 in the bondline: 4.5 ft-lb (FSE) & 3% SA

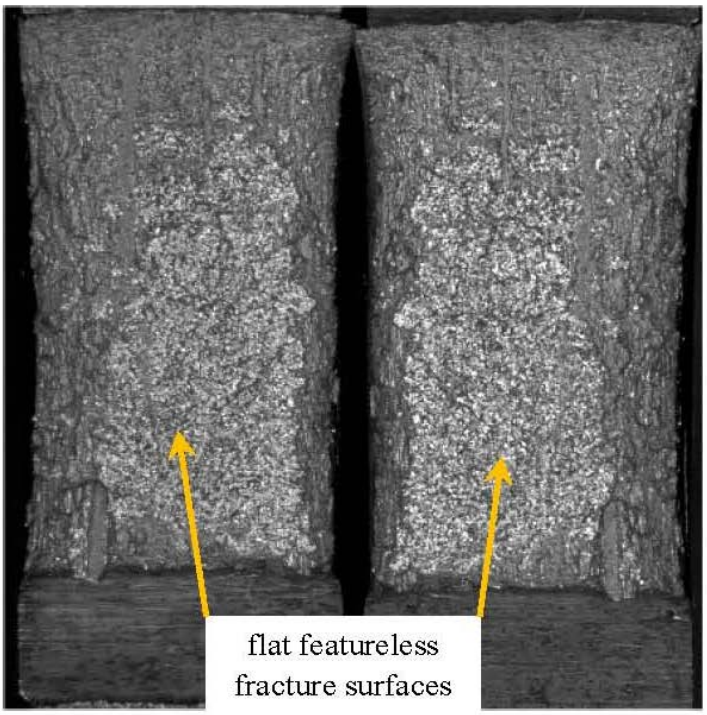

a) 2-D fracture images

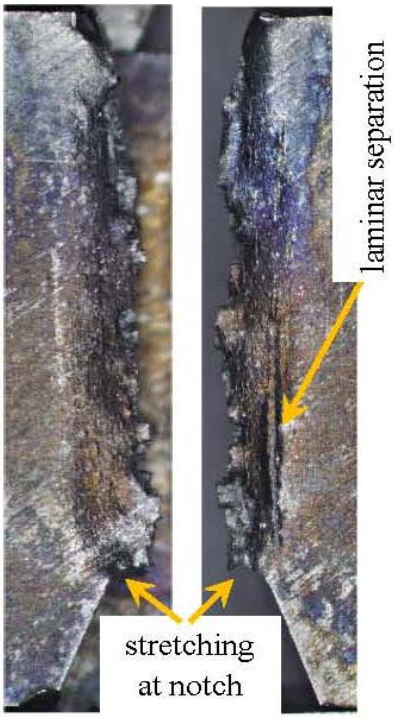

b) 2-D view of the specimen sides

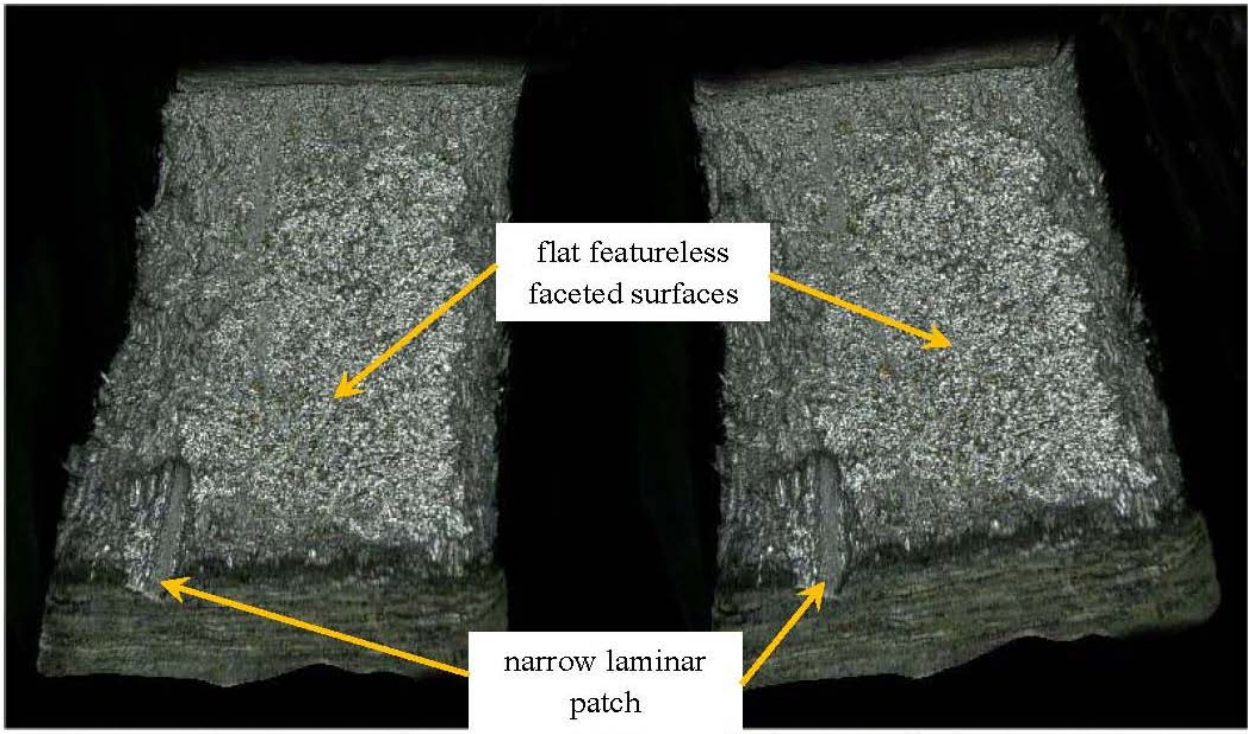

c) 3-D views of the fracture features – notch forward: about half in the still brittle bondline

Figure 15. Half-size CVN specimen # 7-5 through the seam: 11.1 ft-lb (FSE) & 47% SA

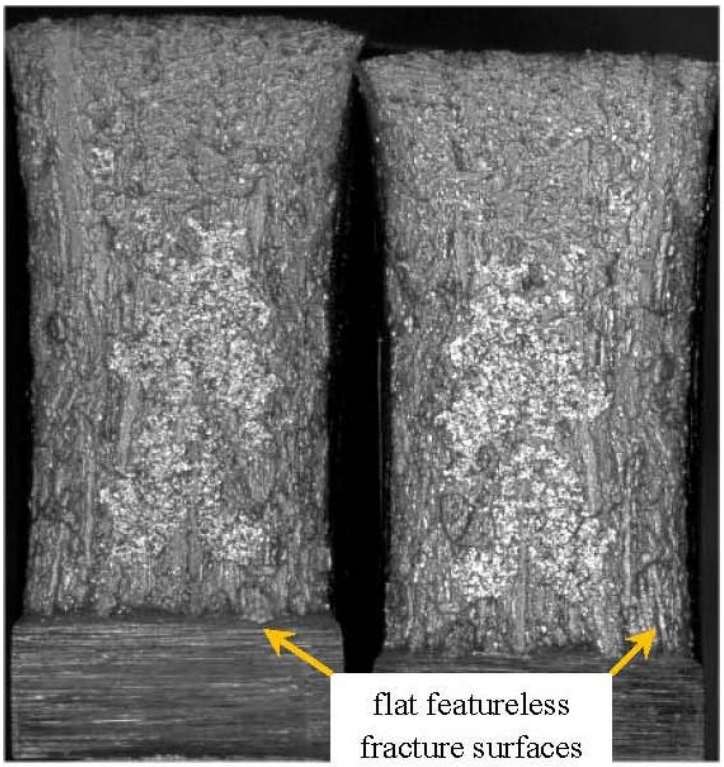

a) 2-D fracture images

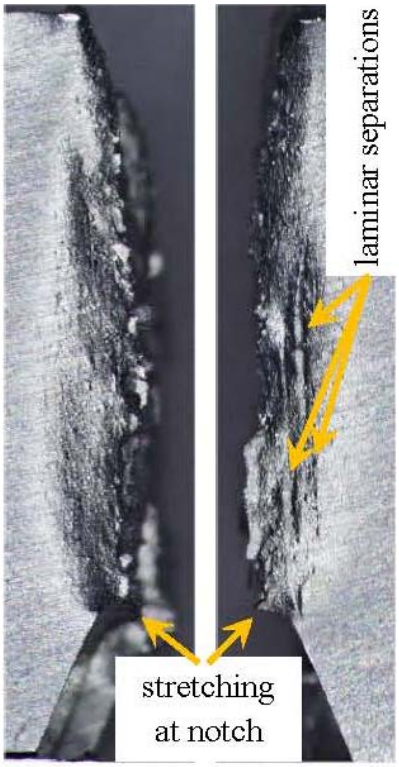

b) 2-D view of the specimen sides

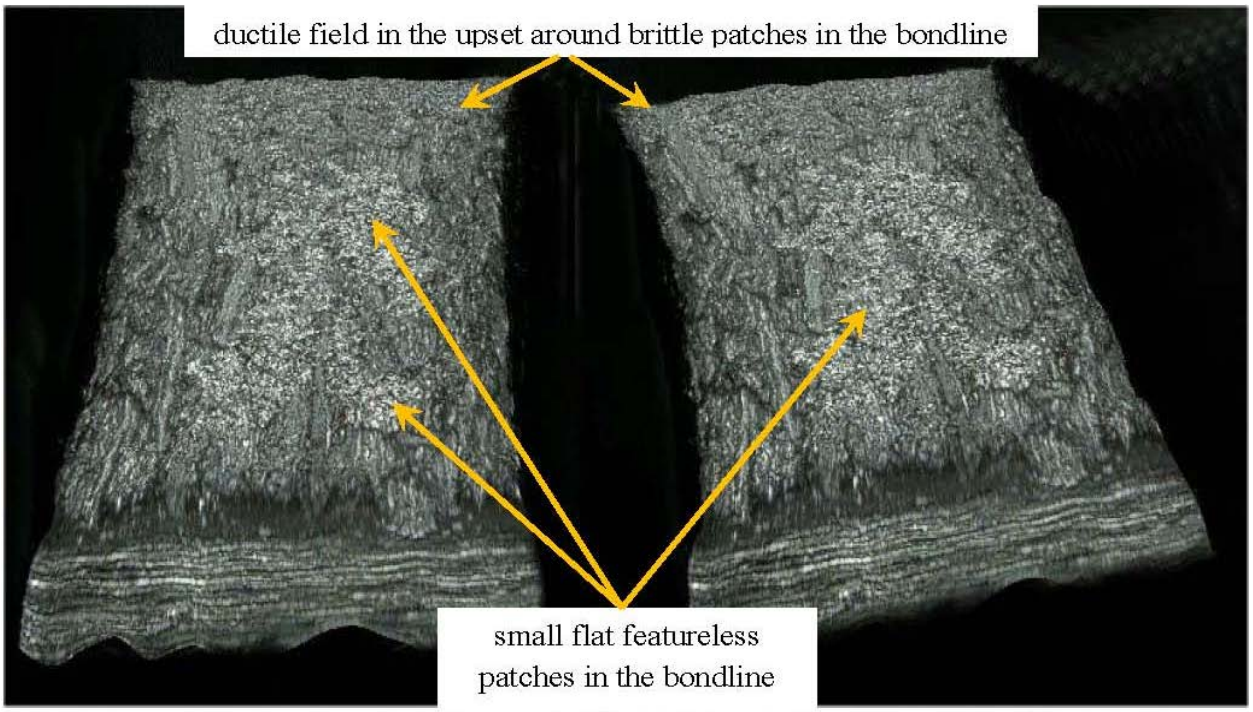

c) 3-D views of the fracture features – notch forward: mostly off the still brittle bondline

Figure 16. Half-size CVN specimen # 7-13 in the seam: 18 ft-lb (FSE) & 72% SA

a) 2-D fracture images

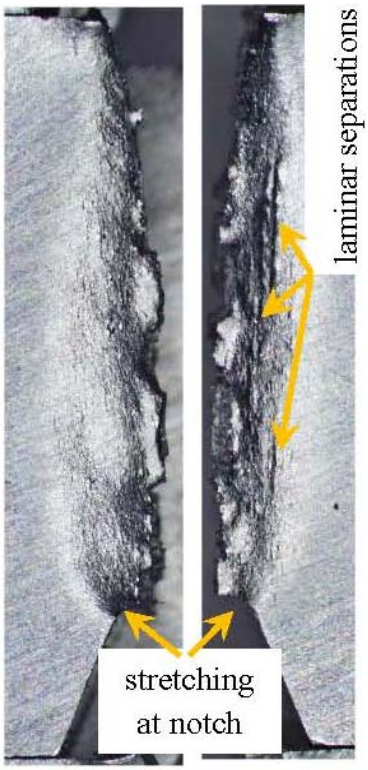

b) 2-D view of the specimen sides

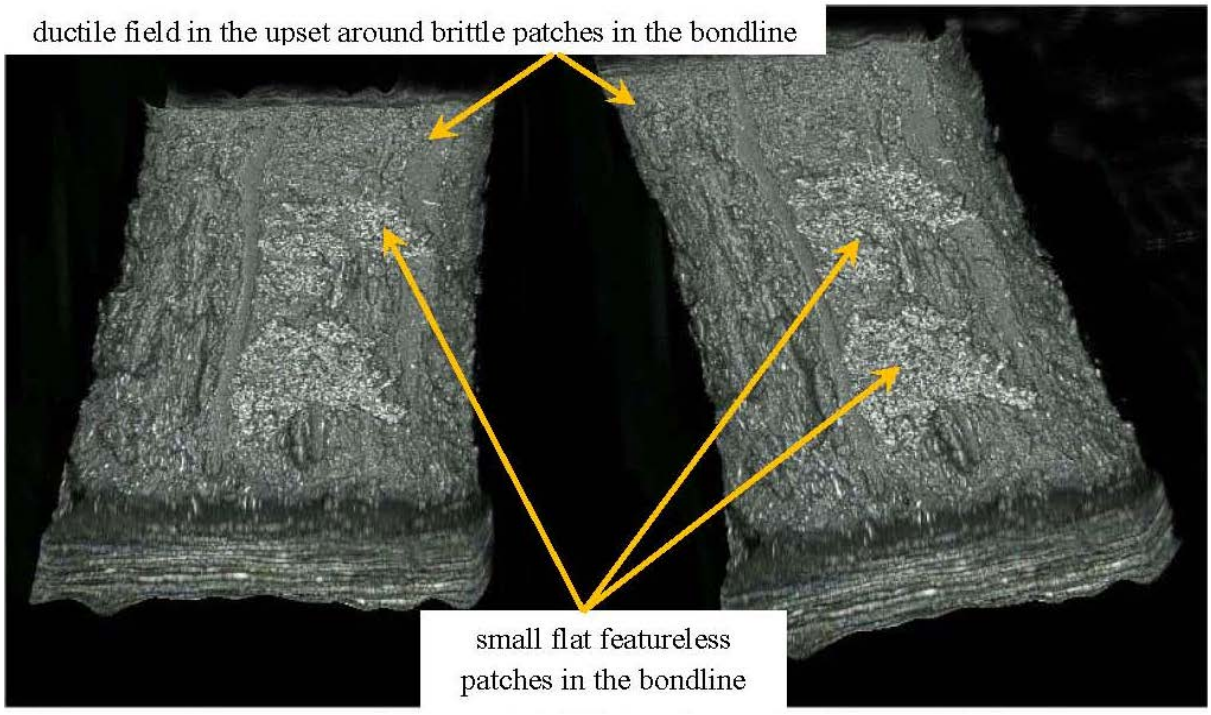

c) 3-D views of the fracture features – notch forward: mostly off the brittle bondline

Figure 17. Half-size CVN specimen # 7-7 in the seam: 17.8 ft-lb (FSE) & 75% SA

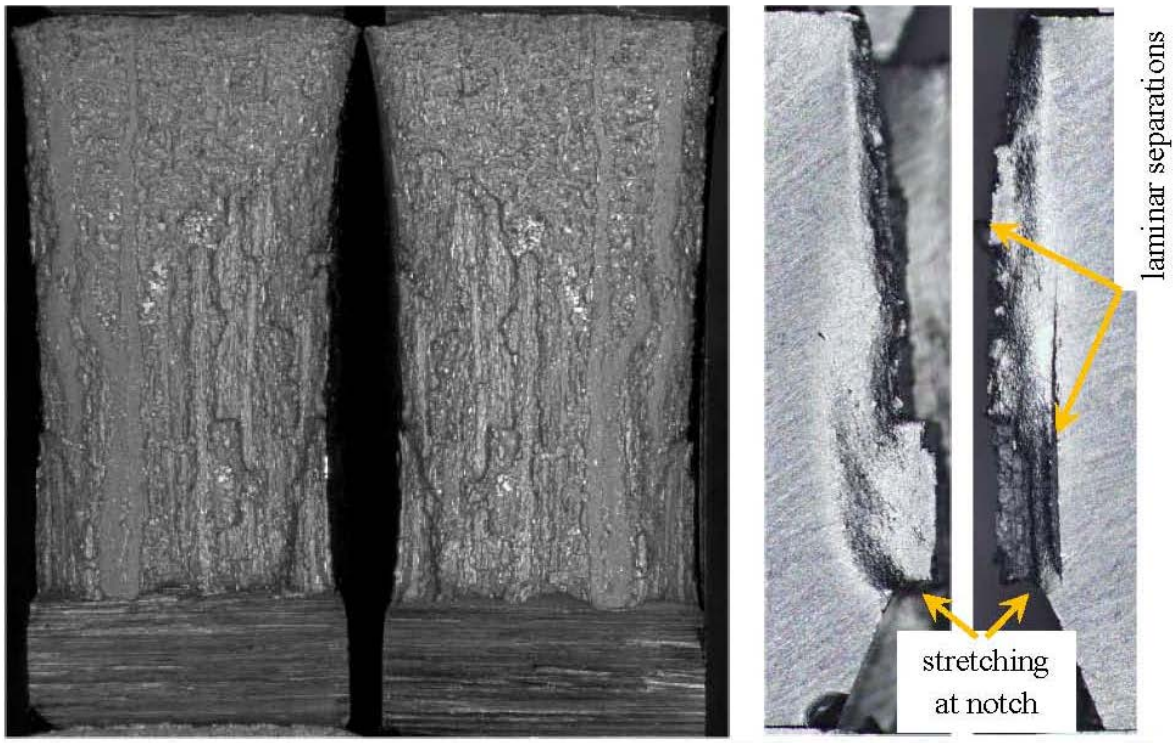

a) 2-D fracture images **b) 2-D view of the specimen sides**

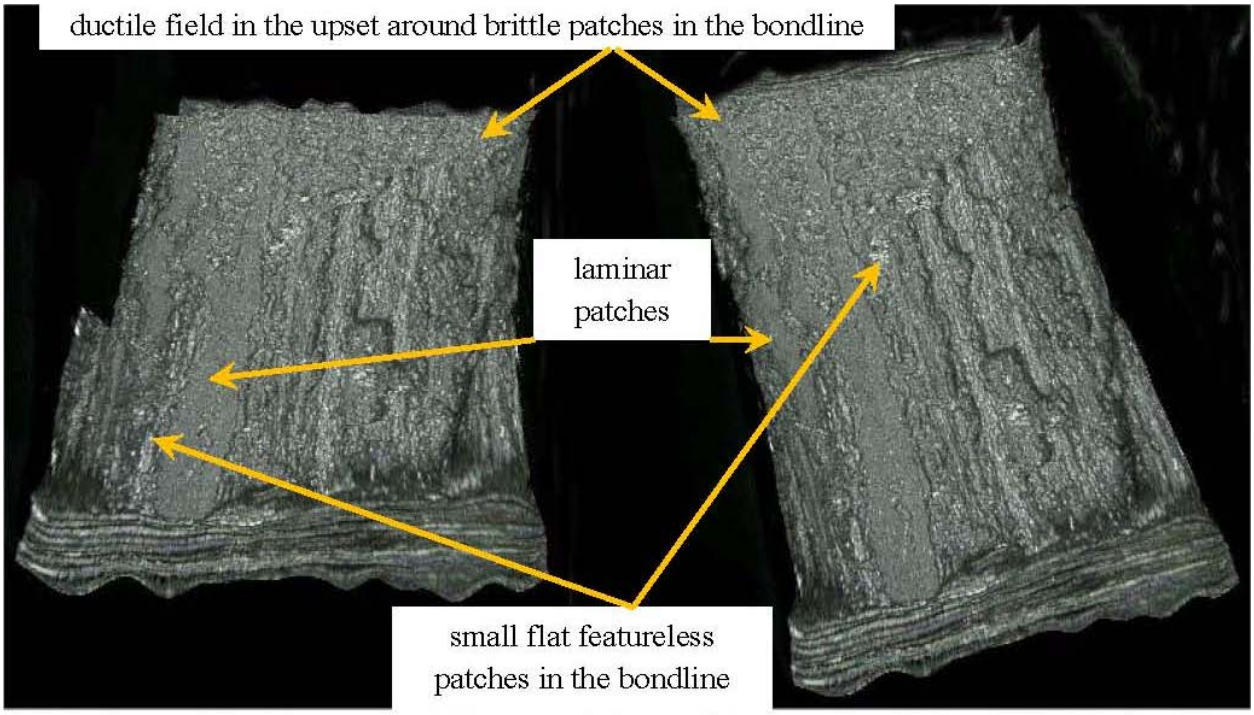

c) 3-D views of the fracture features – notch forward; primarily off the still brittle bondline

Figure 18. Half-size CVN specimen # 7-8 in the seam: 18 ft-lb (FSE) & 98% SA

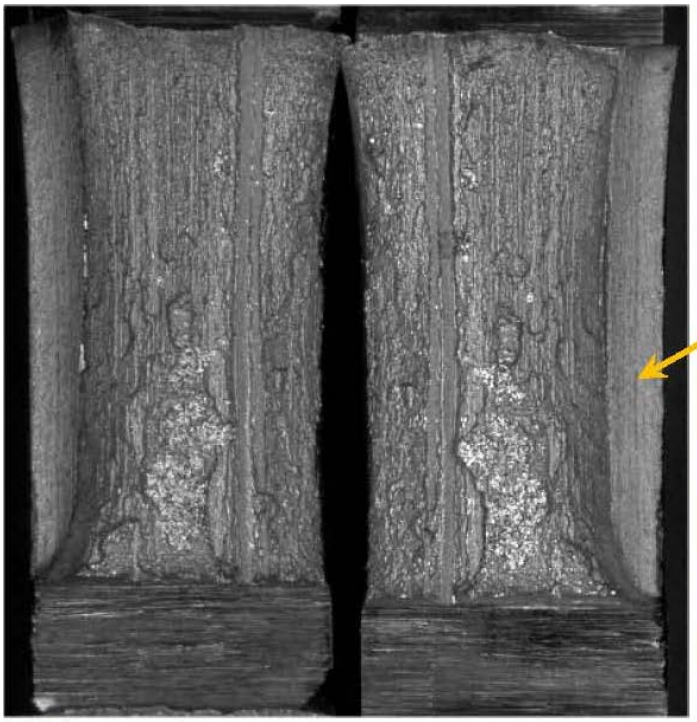

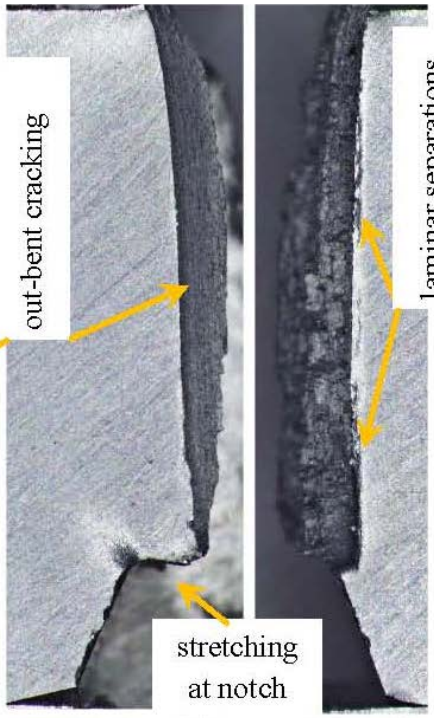

a) 2-D fracture images **b) 2-D view of the specimen sides**

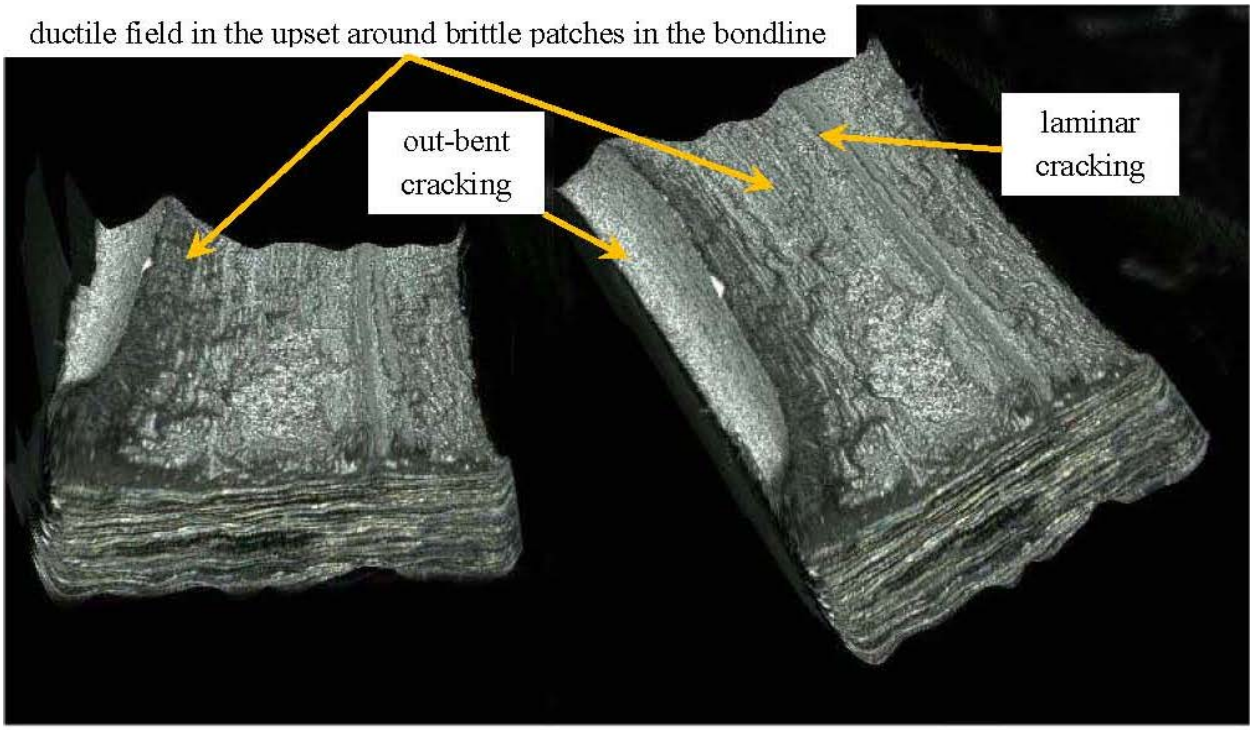

c) 3-D views of the fracture features – notch forward; largely off the still brittle bondline

Figure 19. Half-size CVN specimen # 7-10 in the seam: 20 ft-lb (FSE) & 90%SA

are likewise present in the interior, and become evident on the fracture surfaces as the bondline becomes increasingly tough. One small laminar patch is identified in Figure 15, near the root of the V-notch. While not called out in Figure 16, they are more widespread in this view that represents still higher toughness.

As the energy to deform the notch, and then initiate cracking and grow the crack across the CVN specimen (i.e., toughness) increases, the crack more actively shifts between microstructurally different planes as it seeks the path of least resistance – first for initiation, and then also for propagation. For this reason it was difficult to initiate cracking off the bondline (i.e., in the upset/HAZ), and continue cracking on that plane. Rather, where initiation was targeted off the bondline the crack path it quickly stepped from that origin in the upset/HAZ back onto the less tough / weaker plane containing the bondline and continued therein. Once that transition onto the plane of the bondline occurred, the fracture features reflect those evident for origins on the bondline, like that discussed above – and as such are not included herein.

This transition from resistant to less resistant cracking planes was most evident at higher test temperatures for origins that targeted the upset/HAZ, because the differential energy to initiate and propagate failure increases as the response becomes more ductile. This is most apparent for Figures 17, 18, and 19 in the side views of the specimens, wherein the extent of the plastic flow at the notch root shows strong blunting, with lateral contraction also evident in these images. Blunting has a major effect on the apparent toughness of the seam[18], and becomes increasingly dominant as the toughness increases. Even so, as the temperature increases it is clear from Figures 17, 18, and 19 that the area occupied by the still brittle response that occurs in the boldline is decreasing. It is also clear, particularly in reference to the 3-D images that are included in part c) of those figures, that the cracking has shifted off the bondline to involve other microstructures that are either less resistant, or become active due to the increased rotation of the net ligament in the specimen as the crack grows.

It is apparent from these 3-D images that the fracture morphology has the potential to be very complex. Figures 18 and 19 are good examples of the role of laminar separations / cracking. In Figure 18 the pancaked microstructure that underlies this mechanism leads to large elongated planar zones that form due to separations between bands of this structure. The image in Figure 19 likewise shows such planar zones, and as well shows the area where such zones have rotated normal to the rolling direction as out-bent fibers, which is the genesis of the hook cracks seen in field failures[e.g.,6,7]. As becomes evident shortly, such 3-D images facilitate improved understanding of the dissipative processes that comprise the ‘toughness’ quantified by a CVN specimen cut in an ERW seam, and provide a basis to determine if the cracking developed in the bondline versus sound material in the upset/HAZ. In turn, this has implications regarding energy partitioning between the bondline versus the upset/HAZ, and in establishing the corresponding %SA, which are used in predictive models of failure pressure for seam defects[e.g.,19,20].

It is evident from detailed study of these 3-D images that the increase in energy for failure as the CVN test temperature is not physically due only to a transition in fracture response within the

bondline from brittle to ductile behavior. Rather, the increased blunting as temperature increases leads to a complex fracture that includes portions of the bondline as well as the upset. Figure 20 includes various views that serve to illustrate this complexity.

Evidence of blunting is clear in Figures 20a and 20b. The origin for the image in Figure 20a is slightly up the flank from the more highly stressed notch-root, with the cracking in this case tracking the bondline over the full depth of the sample, but only over a portion of the specimen's thickness. The origin for the image in Figure 20b is somewhat closer to the more highly stressed notch-root than in the prior case. Whereas for Figure 20a the cracking continued along the same plane, it is clear from Figure 20b that the crack quickly shifts cracking planes. It is clear from Figures 20a and 20b that the blunting causes local lateral contraction along the root of the notch. In turn, this lateral contraction can appreciable change the energy dissipation in a sub-size specimen, and cause nonlinearity in the usual linear scaling of the sub-size energy to determine its FSE energy[18]. While for more homogeneous metals this tends to be less significant for the lower toughness steels, its influence in the context of an ERW seam has not yet been explored.

Transitions between planes reflects the tendency for the crack to select the path of least resistance along the crack tip – which can be influenced by the resistance offered by different microstructures over the thickness of the CVN specimen. Weak interfaces, as can occur between differing phases, separate easily, and show no evidence of deformation. Figure 20c is a good example of a strong shift in crack path. This view shows just a portion of the fracture plane, as it has been taken after the specimen half has been sectioned along its mid-thickness. The cracking in this image developed from the notch-root, which lies at the right-hand side of this image and propagates toward the left side of the view. The primary crack plane for this case lay in the bondline, which is the plane along the upper edge of this image. Some brittle patches are evident on this plane as is a patch of laminar cracking near the notch root. In addition to this primary plane there is a secondary plane of cracking, which grew in from the surface of the CVN specimen, and undercuts that plane. As this secondary plane deepened, its effects on the stress field in the specimen were recognized by the primary crack, such that it transitions from the primary plane down to this secondary plane – as indicated by the dashed crack path. Given the toughness of the brittle patches, cracking along the primary crack plane must be considered a path of minimal resistance. Its transition onto an out-bent-fiber interface suggests that such interfaces have even less resistance, and form as precursors to the primary crack – as implied by the undercutting of the primary plane by the out-bent plane.

Figure 20d provides another view of a complex crack path and the related features, which formed under similar test conditions to that for Figure 20c. As for Figure 20c, the origin of this cracking is to the RHS of the picture, although the orientation is slightly shifted, and the primary crack plane lies partially in the bondline, as evident in the presence of the brittle patches and a cross-section made on the other half of this CVN specimen. As above, there is clear evidence of a laminar crack that developed on an out-bent plane along the side of this CVN specimen, which runs from below the notch to the back face of the specimen. It is clear from this orientation that

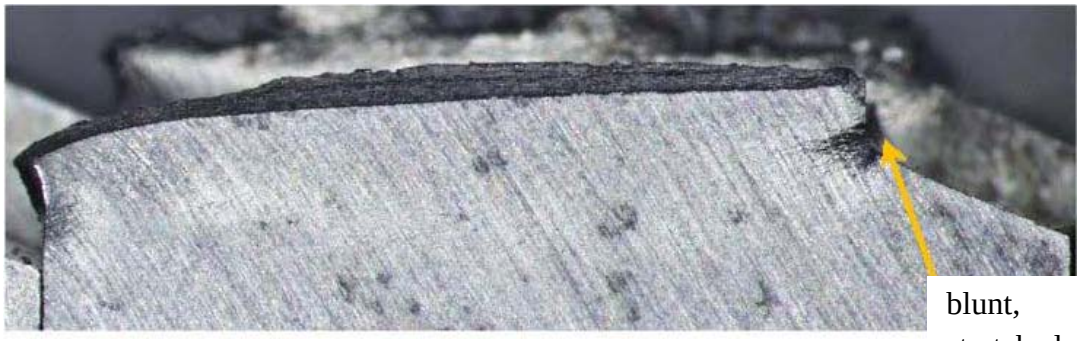

a) blunted notch with cracking continuing on the same plane

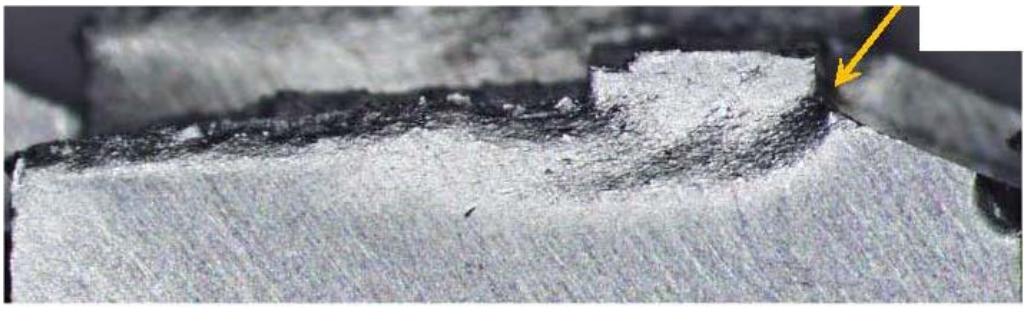

b) blunted notch with cracking shifting on the initiating plane

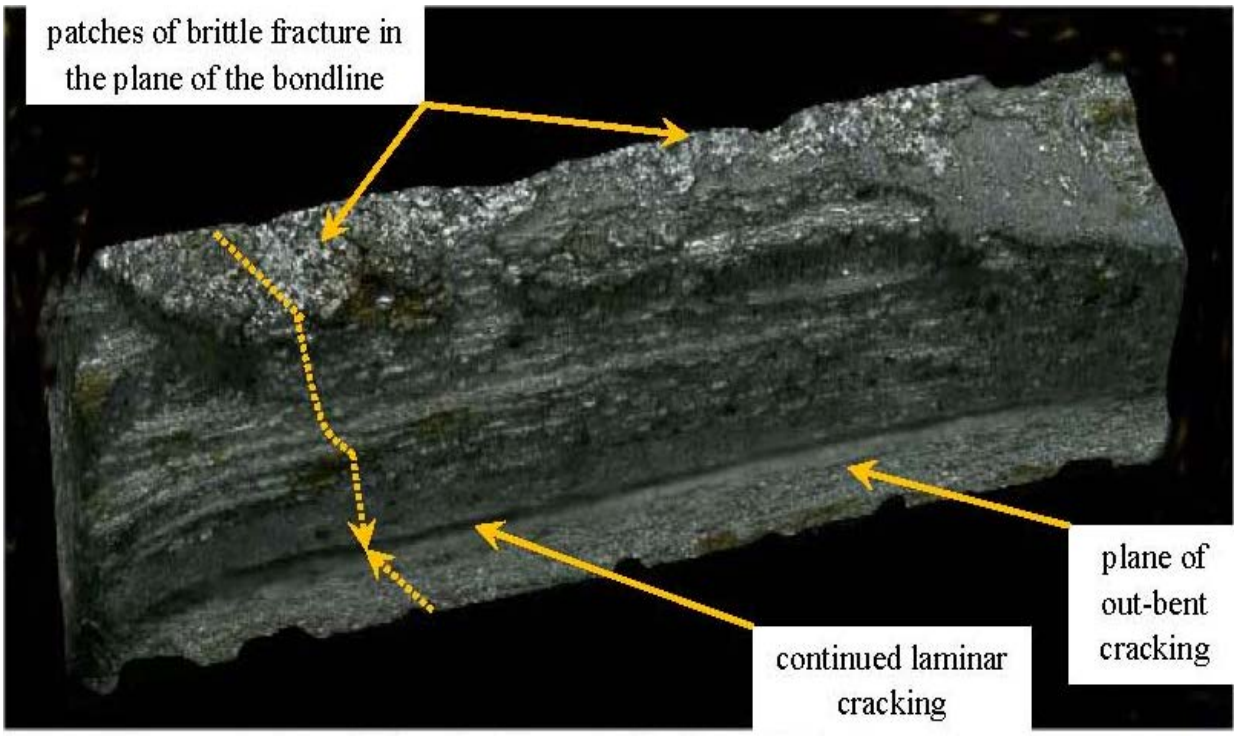

c) view of the crack plane shifting to intersect a hook-crack plane

Figure 20. Views illustrating the complex nature of ERW seam cracking

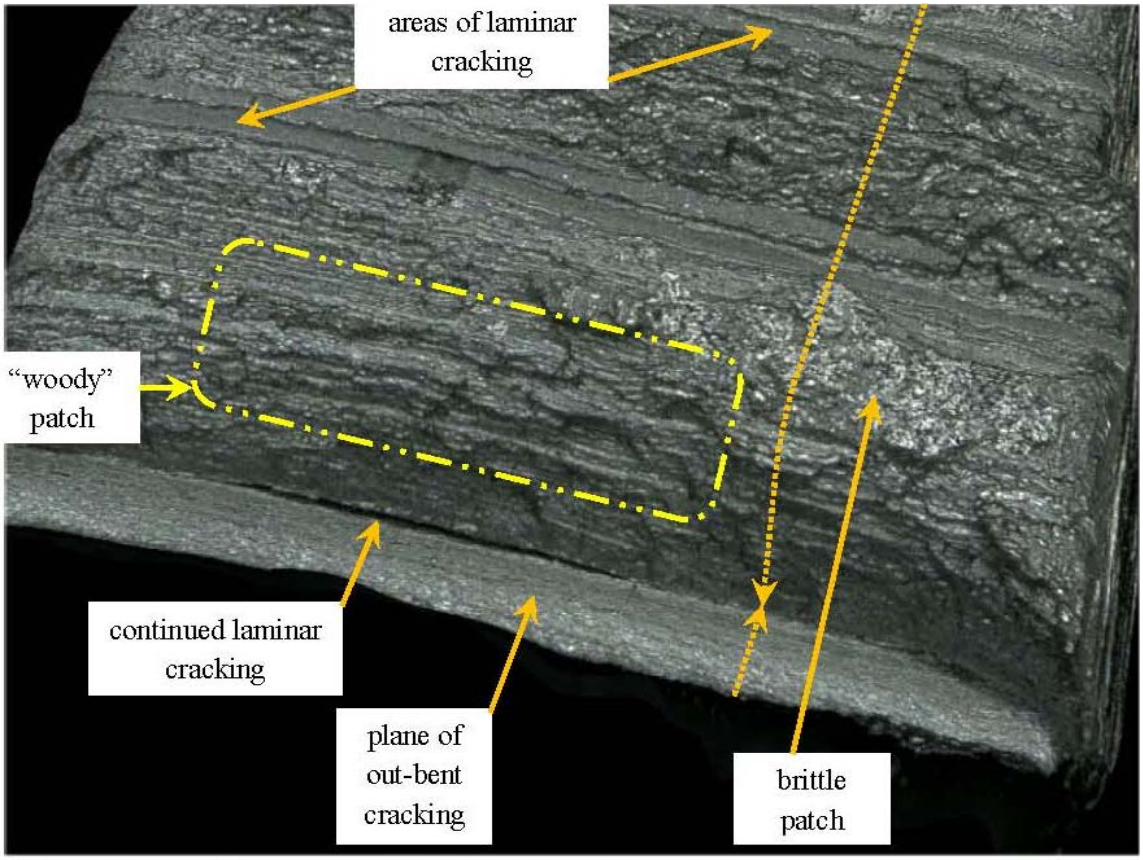

d) view of a transition comparable to that shown in part c)

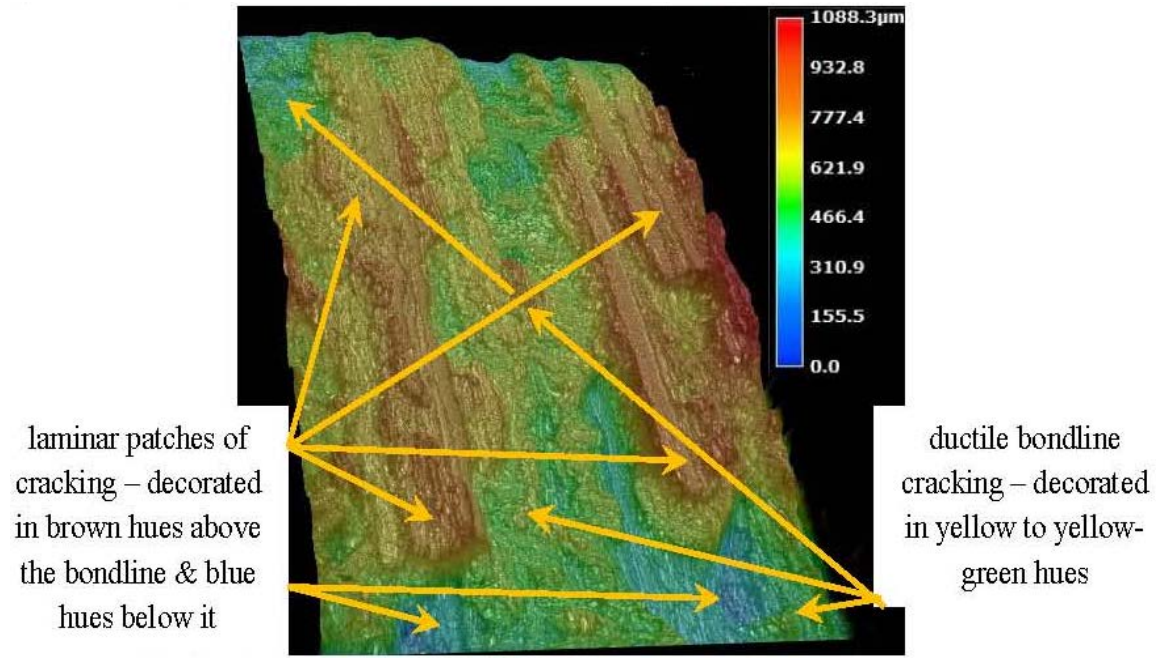

e) vertically colorized 3D view; ductile cracking mostly in the bondline (20 ft-lb FSE, 98 %SA @245°F) – scale in microns covers a ~0.044 inch vertical slice

Figure 20. concluded

this laminar cracking on the out-bent plane undercuts the primary crack plane, which indicates its formation prior to the intersection of this cracking by the primary crack plane. For this reason the cracking path leading to failure is as indicated by the dotted lines on this figure – with the vertical step evident in this image being large – the order of 0.040 inch. Because the cracking on the out-bent plane precedes that of the main crack plane one can conclude that such interfaces between out-bent fibers are paths of minimal resistance, and very weak. This weakness suggests the portion of the cross-section occupied by this out-bent fiber might be excluded from the area used to calculate the FSE value of fracture energy. Given that such response was repeatable, further assessment of FSE in regard to an effective area, while outside the scope of this subtask, could prove instructive. Other features evident in Figure 20d include patches of laminar cracking on a plane parallel and very close to that of the bondline, and a zone of so-called woody fracture, wherein the features are similar to that shown earlier in Figure 6. As noted there, this appearance reflects cracking that jumps between layers of pancaked grains that are separated by a weak interface, as for example that due to roll-flattened Manganese Sulfide stringers.

Further understanding of the fracture-surface area that contributes to the fracture response of a CVN specimen cut across an ERW seam is available through software based manipulation and enhancement of the 3D image file, once it has been captured. For example, the image file can be manipulated to reorient it such that the bondline defines a plane, after which the image can be colorized to indicate the distance from the fracture surface relative to that plane. Figure 20e illustrates results that develop through use of this technique. These data represent testing done at 245°F, which relative to Table 1 was the highest temperature represented by the images discussed earlier in regard to Figures 14 to 19. The resulting FSE energy was 20 ft-lb, at 98% SA. The length scale included in this image represents a ~0.044-inch-thick slice. As noted in the figure, the yellow to yellow-green hues correspond to the bondline, which at the scale shown and based on the related metallography for this seam represents a layer a few grains thick. It is apparent from related images that very few brittle patches remain in the bondline, which at 245°F is effectively ductile (98% SA). Figure 20e indicates that for cracking that targeted the bondline ~40% of the area of the fracture surface actually develops in that microstructure, with the rest occurring in the adjacent upset HAZ. Some of this cracking lies in zones of laminar cracking, with a significant fraction in fracture paths that jump between the weaker interfaces that exist in this rather dirty steel.

Using the colorization technique makes clear that the brittle patches evident in the prior images on the plane of the bondline are absent, consistent with the 98% SA. It follows that the increase in fracture resistance is due increased resistance in the bondline as well as to cracking on other planes. Although the fracture actually shifts off the bondline, and the fracture resistance is now five times that evident for Figure 14, the CVN energy developed for this mix of cracking can be used to quantify the bondline's resistance. This is because the energy measured reflects a lower bound to the energy required to continue propagation in the bondline. But, as noted above, the effective area that contributes to that resistance might be open to question if the energy based on

such results is used in models of seam failure pressure predictions. It is clear that weak interfaces underlie field failures[e.g.,6,7], and will be the first to fail in such applications as was evident for the CVN specimen testing. It is also evident that the mixed fracture response that develops in one CVN test at a given temperature will differ specimen to specimen, due to differences in the mix of microstructures that are sampled where a given specimen is cut from the seam. While this could contribute to data scatter beyond that typically evident for CVN testing in the pipe body, this tendency is not evident in the testing done in the seam[21] for the steel considered in this report. It also is not evident for testing focused in the seam versus the pipe body for the other steels that were evaluated in this project.[21,22]

Because a CVN specimen interrogates a rather small segment of a pipeline seam that can be thousands of miles long, the mix of microstructures evaluated even in extensive testing will reflect a negligible amount of that seam in relative terms. For this reason, it is best to focus such testing in pipe segments located immediately adjacent to seam splits, or in joints where reliable nondestructive evaluation (NDE) has indicated the presence of seam anomalies. But, because issues with seam quality develop due to ERW process upsets, even this practice does not ensure that the CVN testing represents the worst case mix of microstructures evident in the field. The strong temperature dependence of impact resistance tends to exasperate this situation, with no obvious alternatives currently available.

Screening Local Chemistry

Introduction: The improved imaging results indicate that significant differences in fracture energy can result depending on whether the fracture runs in the bondline versus the upset/HAZ. Such differences in fracture resistance and cracking plane indicate that corresponding differences must exist in the chemistry and microstructure. As for the basic skills presented earlier in regard to fractography and metallography, books have been written[e.g.,23] in reference to microchemistry analysis that are applicable to metals

Surface analysis of local chemistry can be done using a scanning electron microscope (SEM) equipped with an energy dispersive spectrometer (EDS), which can give spot analyses of minute particles. The electron probe likewise can be an effective tool for similar purposes, as can a variety of other micron-scale technologies. Such nondestructive analysis brings with it a high capital and use cost, with related practices being tedious, which make such methods very expensive for day-to-day use. Because of their cost, such technology is not readily available, although some “portable” units are available that help offset the concern for accessible. While access is a consideration, the capital and usage cost are much bigger constraints to their use.

Given the high cost, an adaptation of the much less expensive optical emission spectrometry (OES) technique was evaluated for potential use in such applications. OES utilizes a high-energy spark created across an argon-filled gap between an electrode and the sample to be analyzed, which causes emission of radiation from the excited sample surface whose wavelengths are characteristic of the elemental composition. The radiation is separated into the

lines specific to a given element, after which the intensity for each is measured and converted into concentration values for the elements identified.

OES continues to be the primary technique for the production analysis of solid metallic samples. While an established practice in that context, it makes use of a relatively large sampling area in a standard sized blank. This requirement precludes its use to quantify the chemistry differences in the pipe body, or in the upset/HAZ, versus that local to a fracture plane that is as small, as occurs for a half-size CVN specimen – unless this scale constraint can be offset. For present purposes, data was sought on local chemistry immediately below the fracture surface, which was removed for such analysis using a wafer saw with a 0.012-inch thick blade. In reference to Figure 21, the cut-plane to remove the fracture surface was perpendicular to the face of the specimen, and located as indicated by the line designated 'A' in this image. This plane was located to just remove the fracture features intact, but no deeper. Given that failure of the many CVN specimens tested fell on paths that ranged from in the bondline through well out into the upset region it was expected that this plane would intersect those microstructures. As such, it was anticipated that approach would quantify the nature of the near-seam chemistry, which could then be contrasted with the nominal chemistry, which was measured on the cut-plane designated as 'B' in Figure 21, which lay well remote to any of the heating or the upset used to create the seam.

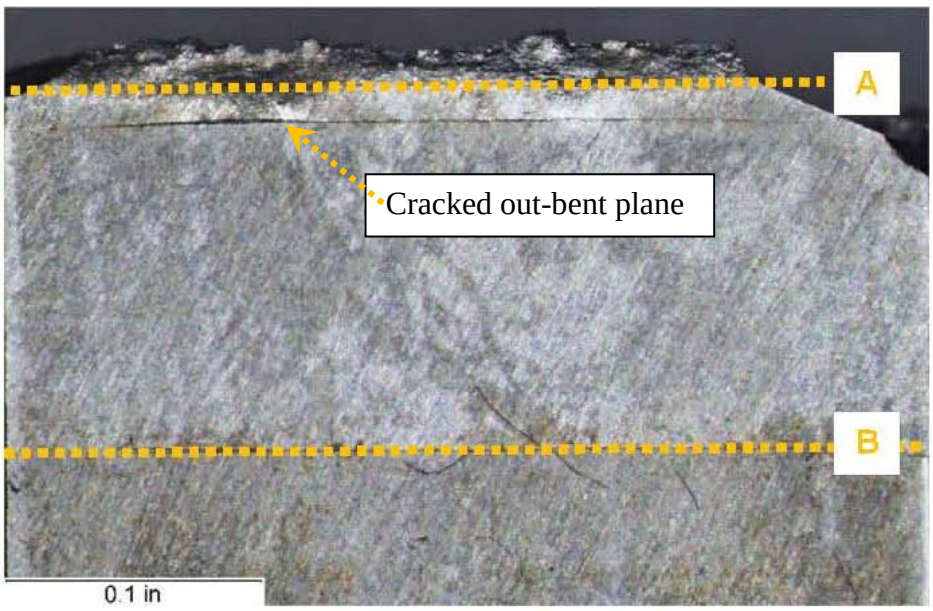

Figure 21. CVN sample sectioning planes for local chemistry comparative analysis

To limit contamination, a new blade was used or the blade was washed for these cuts, with an otherwise pristine setup utilized. To generate sufficient area for the OES sampling, the stubs remaining below cut-planes A and B were compressed mechanically, with the resulting plastic flattening significantly increasing the overall area of the sample, with care again taken to limit contamination. The purpose at this juncture was not to develop quantitatively accurate and precise data from specific sites below the fracture surface, but rather to qualitatively assess the

extent to which differences in chemistry could be identified via triplicate sampling using this adaptation.

Results: Table 2 presents chemistry results in weight-percent based on the limited use of the just noted adaptation of OES. It is apparent in comparing the chemistry local to the bondline – which using the above approach leads to an averaged outcome within a layer of about 1/16-inch centered about the bondline – that there is no clear indication of differences to the third decimal point. This outcome is not surprising, because a forged (autogenous) weld does not introduce deposited metal and so, aside from trapped oxides and some decarburization, there is no reason for the chemistry to differ.

	C	Mn	P	S	Si	Cu	Sn	Ni	Cr	Mo	Al	V	Nb	Zr	Ti	B	Ca	Co
Near Bondline	0.305	1.136	0.009	0.019	0.013	0.011	0.001	0.009	0.013	0.006	0.007	0.000	0.001	0.002	0.002	0.000	0.001	0.006
Nominal	0.302	1.130	0.009	0.018	0.012	0.011	0.001	0.008	0.013	0.006	0.004	0.000	0.001	0.002	0.001	0.0001	0.0005	0.005

Table 2. Comparative averaged chemistry data near versus remote to the fracture plane

While the above adaptation of OES leads to an outcome that is rational for an autogenous weld, the results are not conclusive. Should it be considered necessary to confirm this outcome, two micro-beam based techniques could be used to probe the local chemical composition, which because of the smaller spot-size could reveal differences not evident at the averaged scale of the OES technique as used above.

The first of these micro-beam approaches uses the SEM as the source for the energetic beam to generate characteristic x-rays, which are called characteristic because the energy of the X-rays detected via EDS is characteristic of each element present. The energy of the incident electron beam controls the volume of steel interrogated. A higher energy electron beam can generate x-rays at a depth of up to 5µm in the material; however, more typically used conditions localize the interaction volume to 2 - 3µm below the surface. The SEM can focus the electron beam on an area smaller than 1µm x 1µm on the surface of the sample (areas up to 0.5 mm x 0.5 mm can be surveyed also), but the real volume from which the x-rays are generated is controlled by the electron beam energy that in turn controls the depth of penetration. The SEM-EDS technique is good for qualitative analyses, and can be used for quantitative analysis of elements ranging from boron (B) up to uranium (U) in atomic number. The semi-quantitative software built into an EDS system is accurate to 0.1 weight percent, such that the results in Table 3 indicate greater resolution is required, which necessitates quantitative analysis that in turn is referenced to elemental standards.

Another technique that is similar to the SEM-EDS technique for local chemical analysis is micro x-ray fluorescence (micro-XRF). This uses an incident x-ray beam to fluoresce characteristic x-rays from the sample. The interaction volume is similar to the SEM; however, the smallest area that can be looked at is on the order of 10 µm x 10 µm with micro-XRF. Typically areas surveyed are more on the order of 100 µm x 100 µm. The micro-XRF uses an EDS detector to rapidly quantify the elements found in the specimen, very similar to the SEM-EDS. Micro-XRF

is good for analyzing elements ranging from sodium (Na) to U and is not good for quantitative analysis of light elements.

Either of the techniques noted could be used to probe the local chemistry, such as near the fracture surface, near the weld, or in other areas of interest in comparison to the bulk chemistry. While these techniques could identify localized differences due to contaminants that have been missed via the averaged OES technique, it is not clear yet that the value of such details justifies the effort.

X-Ray Tomography

Introduction: X-ray computed tomography, more commonly called a computed tomography (CT) scan or computed axial tomography (CAT) scan, is a commonly applied medical imaging procedure that utilizes X-rays to produce images of the body. This technology is gaining use in industrial applications for quality control including dimensional analysis, and defect assessment. After acquiring a large series of two-dimensional X-ray images taken around a single axis of rotation, tomographic processing algorithms are used to generate a 3-D representation of density inside the body or an object. Post processing programs slice the three dimensional volume into two dimensional images that find cancers in the body and anomalies in objects.

The potential of tomography was investigated to support the metallographic and fractographic characterization of ERW seam anomalies. As discussed above, a goal of the metallography is to characterize the microstructure in the vicinity of the anomalies, and to identify the extent to which microstructure contributes to a failure. Metallography also can be used in the context of serial sections, to quantify structure as a function of position relative to the anomaly, with the added benefit of quantifying the size of the anomaly on the sectioned planes. Fractography works in complement to metallography: it seeks to quantify the depth and length of the feature, and the mechanisms of crack initiation and growth. Both metallography and fractography occur at a point in time well after failure.

In contrast to destructive practices such as serial sectioning, in-the-ditch (ITD) and other assessments occur at a time when the anomaly is intact – when the need exists to understand the significance of the anomaly as part of an engineering critical assessment (ECA). As was the case for the post-failure techniques noted above, this requires information concerning the axial extent of a feature and its depth, and where possible inference of the nature of the growth process. Because the seam remains intact, ITD methods must provide a nondestructive evaluation. CT has the potential to quantify these parameters via NDE. But, while CT can determine the geometry of an anomaly and other traits, details such as the grain structure and chemistry, which might be needed in some applications, would require the use of complementary technologies.

Background: While the reconstruction algorithms and display software of industrial and medical tomography are similar, the implementation is very different. In medical CT, the X-ray source and detector rotate about the body, whereas the reverse applies in the currently deployed

industrial CT setup. This is clear in Figure 22, which shows a typical industrial CT setup, where it is apparent that the object to be imaged rotates while the source and detector remain stationary.

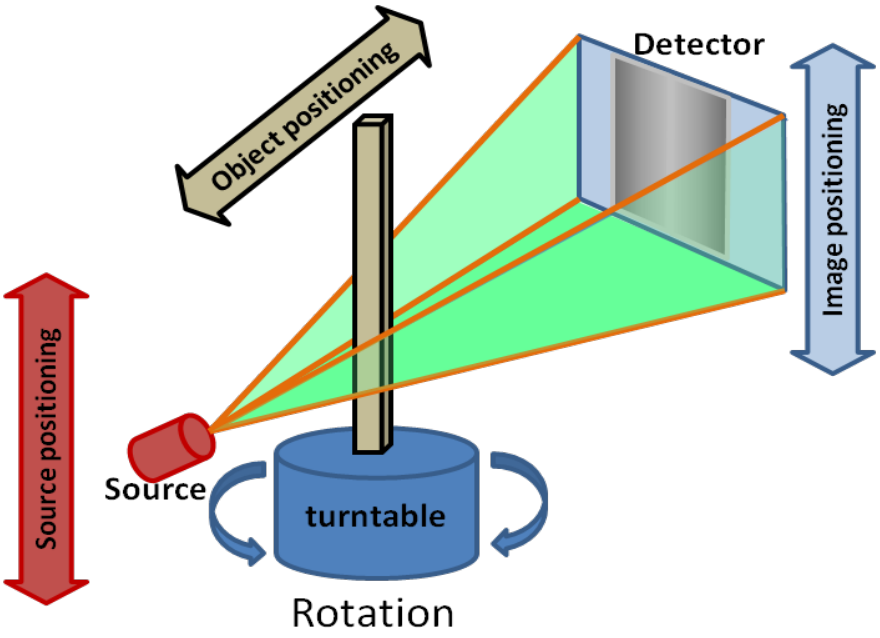

Figure 22. Industrial CT image acquisition configuration

In view of the schematic of the setup shown in Figure 22, the current industrial CT practice can work in complement to post-failure analyses via metallography and fractography using samples that contain anomalies of interest that have been excised from the seam. However, because the field analog of what is done for medical tomography does not exist, and is unlikely to provide adequate resolution in such a setup, CT is unlikely to support an ECA.

Accordingly, this section considers CT of a sample that was excised from an ERW seam as the basis to assess the potential utility of this technology to quantify the presence and extent of anomalies. If such work showed great utility and sufficient resolution, what is destructive for present purposes could transition to an NDE practice – provided the investment was justified.

As Figure 22 shows, the object to be evaluated is rotated in increments, typically between 0.1 and 0.5 degrees per step. Finer increments provide higher resolution images, while coarser increments reduce scanning time. The source is an X-ray tube that can generate very small focal spot sizes, typically below 50 µm in diameter, referred to as a micro-focus source. To produce a full volumetric reconstruction, the width of the object must be less than the width of the detector. When the object is significantly smaller, higher resolution images can be acquired by a magnification process. For example, if the object is 4 times smaller than the detector, the object is moved closer to the source and the resulting image spans the entire detector. With magnification, all the pixels in the detector are used, effectively enhancing the resolution. If the object is longer than the height of the detector, the source and detector can be positioned to

image to object in segments. The computer controlled position system enables the volume to be combined for a full assessment.

Test Configuration: This assessment of the potential of CT to detect and size seam weld anomalies made use of a 200 x 200-mm (nominally 4 x 4 inch) detector with a 1024 x 1024 pixel resolution. For optimum resolution, the seam weld region of the pipe is trimmed so that only the HAZ remains or the wall thickness, whichever is larger. The process could be optimized trading resolution for time, although this has not been considered. For screening larger areas, a lower resolution can be used; with specific areas of the anomaly reexamined at a higher resolution.

The output of the process is a digital file that represents the relative ability of X-ray energy to pass through a particular point in the material. The values in the three dimensional file are referred to as the radiodensity, x-ray density, or just density. Materials that inhibit the passage of X-ray are called dense, while those that allow radiation to pass more freely are referred to as lucent. When displayed in a grey scale image, a white appearance indicates the densest materials, compared with the relatively darker appearance of less dense materials.

The digital CT file can be sliced in many planes, as apparent in Figures 23 to 25.

Figure 23c shows the circumferential-radial cross section plane. This is the usual plane evaluated in metallographic sectioning to assess the microstructural features at some point along the length of a seam weld defect. Other views evident in Figure 23 include the axial – circumferential plane, as evident in Figure 23a, the axial – radial view shown in Figure 23b, and the perspective shown in Figure 23d.

The seam weld also can be easily seen in Figures 23a and 23b, but is more difficult to see in the perspective view. The hook crack evident in the cross-section in Figure 23c is clearly and faithfully characterized by CT based on a direct comparison of the image developed in the corresponding metallographic section. The section Figure 23c also shows a punch mark that serves as a benchmark to correlate inspection results. The length of the crack can be assessed by examining the axial – circumferential plane, results for which are shown in Figure 24a, and is comparable in that view is to what is observed in a magnetic particle inspection. The axial – radial plane, Figure 25b, provides a general view along the seam weld and is most useful to display anomalies in the bond line. This is because wandering cracks and hook cracks can appear in this view as varying in radial depth, whereas in reality they are actually varying slightly in circumferential position.

Example Results for Seam Welds: Two ERW seam weld were examined using computed tomography, which are characterized in Table 3. The specimens were extracted from pipes that had seam weld anomalies as detected by magnetic particle testing and sized using phased array ultrasonic technique. Both pipe samples were hydrostatically tested to burst, with failure occurring in other anomalies.

The slicing planes that were illustrated in Figures 23 to 25 were images from sample 1, pipe ID 22-11. The hook crack seen in these figures was relatively consistent in depth and shape along

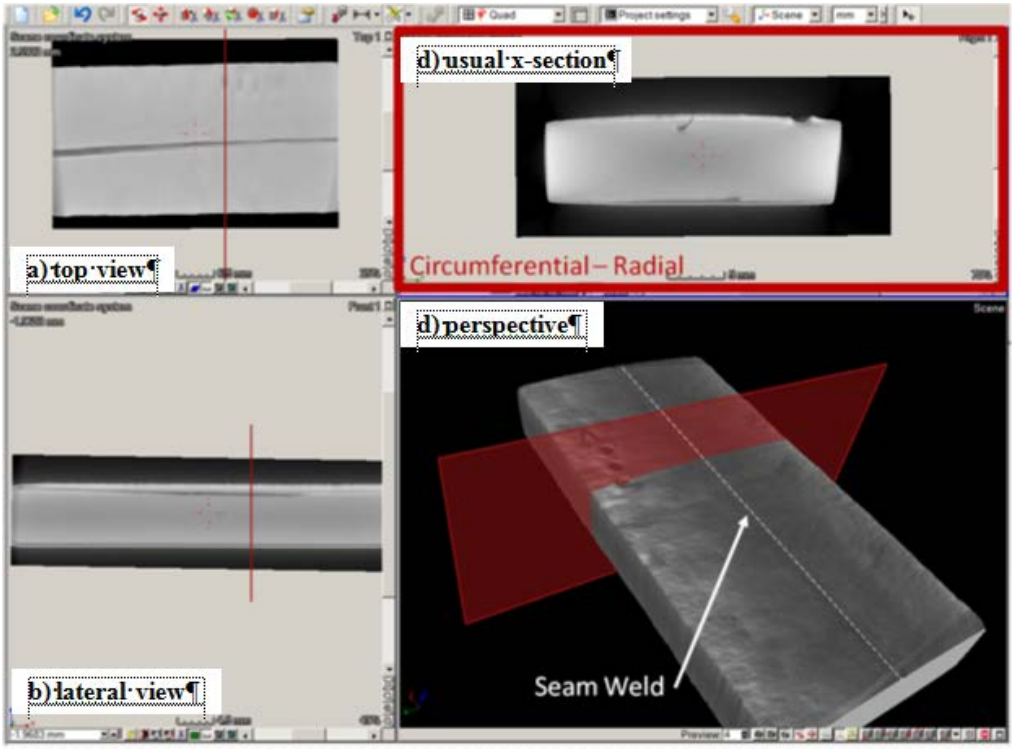

Figure 23. Tomography data sliced on the traditional circumferential-radial cross section plane used in metallography to assess seam weld defects

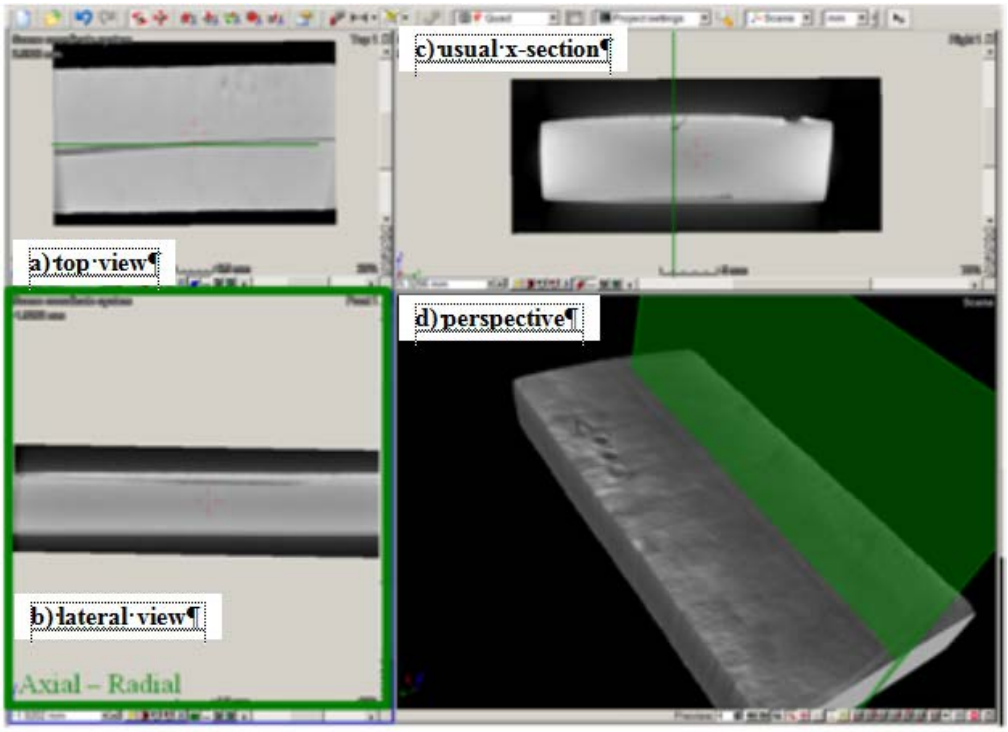

Figure 24. Tomography data sliced in the axial-circumferential cross section plane just below the surface can be compared to magnetic particle imaging results

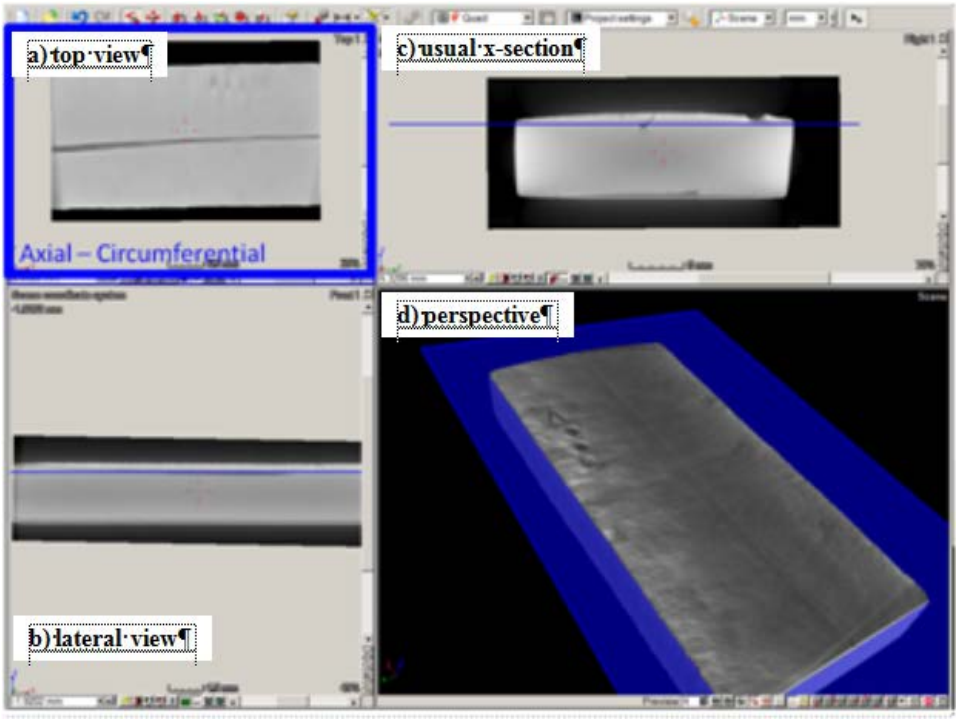

Figure 25. Tomography data sliced in the axial – radial plane, which provides a general view along the seam weld

Table 3. Traits of the pipes and their weld-samples evaluated using CT

	Sample 1	Sample 2	Units
Pipe ID (Diameter - #)	22 - 11	16 - 16	-
Diameter	22	16	inch
Nominal wall thickness	0.280	0.260	inch
Anomaly ID	Seam A 03	#1	-
Anomaly length Magnetic Particle	83	4	inch
Anomaly depth (Phased array)	0.045	0.038	inch
Anomaly depth (Phased array)	16%	15%	Percent
Test pressure (no failure)	130%	94%	%SYMS
HAZ width	0.5	0.25	inches
Scanned length	2		inches
Magnification	16x		-
2-D Pixel size	0.00025		inches

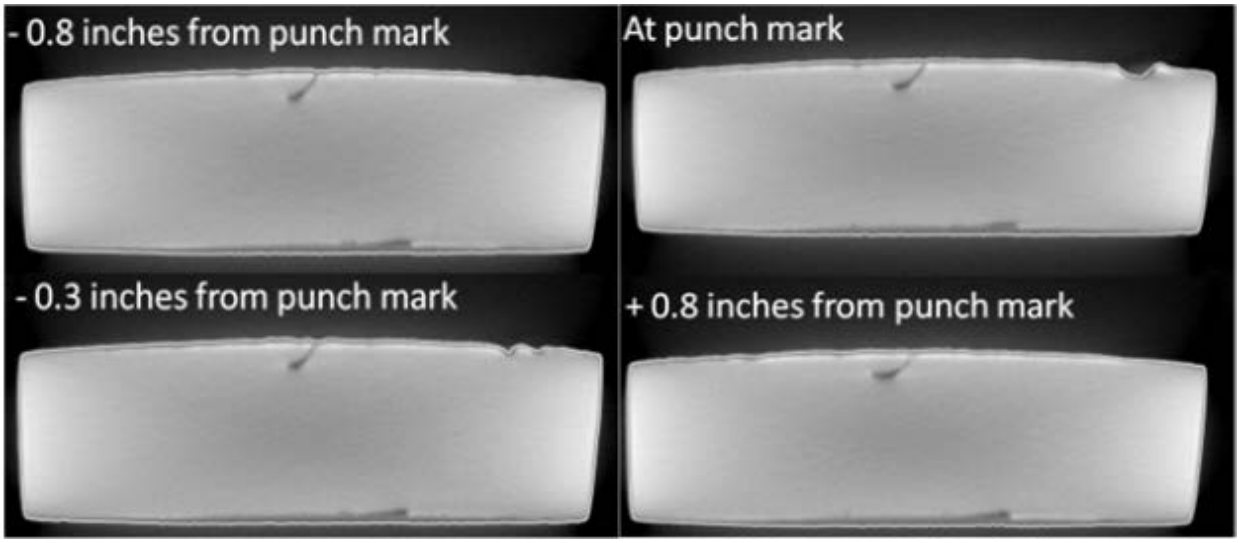

Figure 26. Views of the hook crack from serial CT sections in specimen 22-11

the seam weld, as shown in Figure 26. The depth can be accurately measured and is 18.4% of wall thickness. This compares well to the in-the- ditch inspection result noted in Table 3 as 16%.

Figure 27 shows a few typical tomographic views and that for the metallographic section thru the deepest point for this area of the weld seam based on the CT results for the second sample, pipe 16-16. Note that the sharper images is a results of the smaller sample; the magnification of this sample, and hence the resolution, differs by a factor of 2x. The tomograph in the traditional cross-section plane, Figure 27d, and the metallograph, Figure 27e, show the main crack is connected to the OD and is nominally 40% thru the wall of the pipe. While apparent in the metallograph, but not easily seen in the tomograph, a fine crack is evident growing from the ID surface. This provides some insight into the resolution of the tomographic setup; higher magnification would be required to detect the fine crack with tomography. The other two cross sectional views, Figure 27b and 27c, show that the anomaly is not continuous, but rather is three distinct shorter cracks. All three anomalies appear to have about the same depth.

It is evident from Figures 23 to 26 that computed tomography is an effective complement to the usual metallographic practices when dealing with seam-weld anomalies. While just a few images were presented to illustrate the technique, the entire anomaly can be visualized via CT in a matter of minutes using a personal computer once the data is acquired and processed. In this context computed tomography provides the means to choose slicing planes for detailed metallographic analysis. While CT can determine the geometry of an anomaly, the details of grain structure and other details needed for full seam assessment still requires metallographic sectioning in the areas of concern.

Imaging seam welds with anomalies requires high resolution systems and the capability to manage high magnifications. A raw pixel size in the 2-D raw data recording that translates less than 1/1000 of an inch or less is needed; with better results seen for a pixel size of 1/4000 of an

inch than as compared to 1/2000. Relative to metallography, the cost to scan a sample is the order of that to create a few sections, indicating that this technology provides an economical means for the preliminary assessment of seam-weld anomalies that have been detected with ITD or ILI inspection methods. While not likely practical for in the ditch applications in the near term, computed tomography can be a useful tool in complement to metallography and fractographic practices.

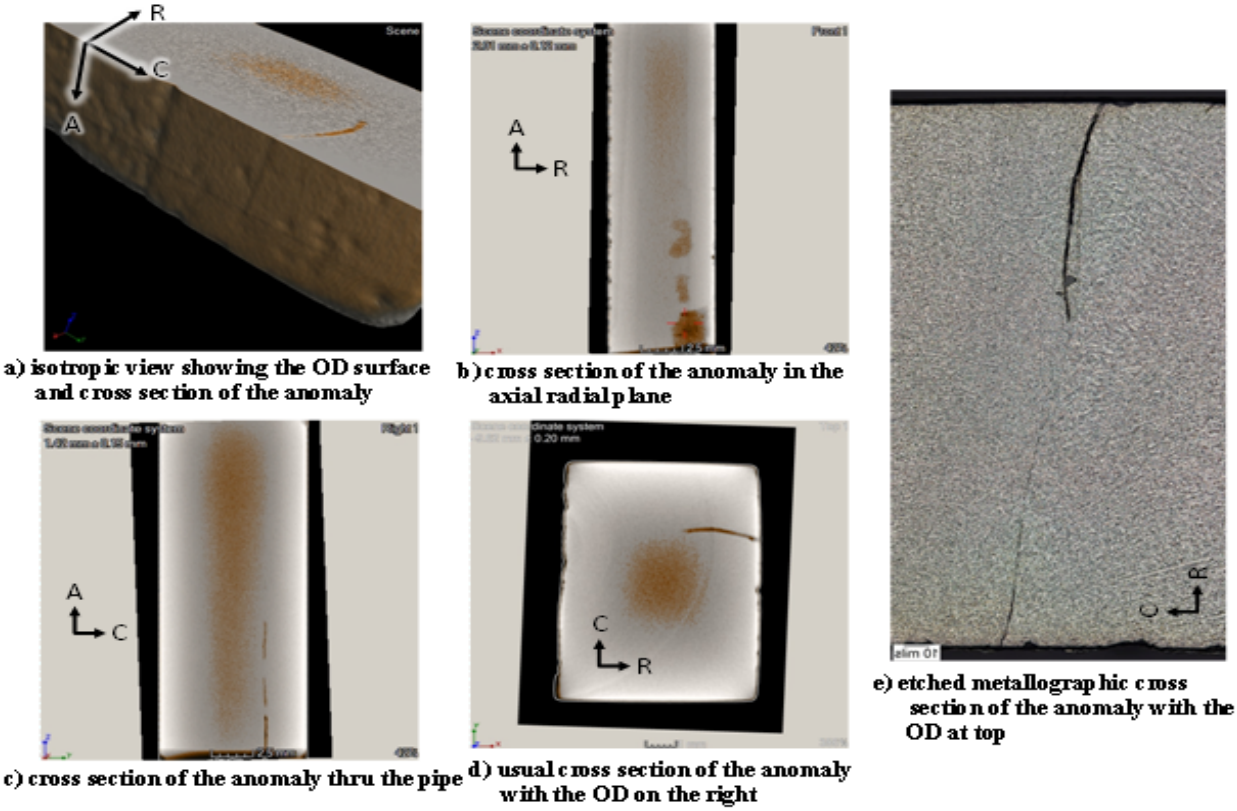

Figure 27. Tomography and metallography of a seam anomaly in pipe 16-16

Standardizing Practices in Support of ERW Seam Failure Analysis

As planned, this task was to consider the possibility and merits of standardizing fractographic and metallographic practices in regard to examining ERW seam failures. It quickly became clear that because of differences in the features causing failure, and in the related local microstructures, that their analysis required case-by-case decisions on the fractographic and metallographic practices to be used.

Figure 7, which as discussed earlier, shows a view of the macrostructure of a FW seam, serves to illustrate such differences in regard to microstructure. This image shows the clear differences that existed for this pipe across the bondline of this FW seam. The macro-etchant that was effective in delineating the flow on one side of this bondline was far less effective in regard to the flow and chemistry present under otherwise nominally identical thermal and mechanical upset conditions. While such differences could trace to the use of split skelp or plate, the fact

remains that nominally the same steel in regard to chemistry and processing behaved in a manner that effectively precludes one "recipe" for use as the etchant. Once aspects as basic as the choice of the etchant are open to question, the remaining decisions beyond the high-level guidance in handbooks becomes unclear. Similar observations can be made in the context of fractography in regard to Figure 13. Because it was not found possible to standardize such practices, Annexes A and B were developed to illustrate good practice and indicate what is expected in the context of failure analysis and related reporting in regard to ERW seams.

As the complexity of the ERW seam made clear the limitations regarding standardizing practices or protocols beyond the guidance in handbooks, the focus of the effort shifted to illustrating the unique aspects associated with ERW seam failure relative to the usual aspects of failure analysis. This was done to provide some insight into the use of such techniques beyond the generic direction provided by handbooks. In addition, potentially new approaches were elaborated that had the potential to complement the usual techniques. As such, while this task did not result in standardized procedures and protocols, it has demonstrated the usual practices in applications to ERW seam failure in Annexes A and B, and introduced new technologies that can augment the traditional practices, whose use will broaden understanding of the ERW seam failures.

Summary and Conclusions

As planned, this task was to consider the possibility and merits of standardizing fractographic and metallographic practices for use in examining ERW seam failures. It quickly became clear that differences in the features causing failure, and the related local microstructures, required case-by-case decisions regarding which fractographic and metallographic practices should be used. Recognizing that standardization was not possible, Annexes A and B were included to illustrate such practices and outline the expectations of good failure analysis and reporting practices. Thereafter, the work focused on 1) illustrating unique aspects associated with failure analysis of ERW seams, and 2) potentially new approaches for the same purpose.

It was found that the fractographic and metallographic practices used for more homogeneous metals can be adapted in applications to ERW seams, with care taken to account for aspects unique to such seams in regard to microstructural features, and the complexity they can lead to in the fracture processes. Two new technologies that rely on automated 3-D imaging and X-ray tomography were introduced as potential avenues to better understand and quantify ERW seam failures, which were supplemented by an adaptation of optical emission spectroscopy to identify the chemistry local to a fracture surface.

It was apparent that significant shifting of the crack plane between differing microstructures was due to the cracking seeking the path of least resistance in the ERW seam. While this behavior was anticipated, the significant distance involved in the shifting between cracking planes revealed by the 3-D imaging was not. This imaging also made clear that for CVN testing shifting of the crack from the plane or structure targeted by the notch could complicate the practical interpretation of such measurements, and lead to significant scatter in the measured

energy and %SA. Finally, because deformation at the notch appeared to be significant, it was postulated that such CVN data should be generated with an instrumented striker, in order to better understand how to use the results of a CVN test in failure pressure and other predictions made for an ERW seam.

The potential utility of computed tomography in complement to the usual metallographic practices was evident in dealing with seam-weld anomalies. While just a few images were presented to illustrate the technique, the entire anomaly can be visualized via CT in a matter of minutes using a personal computer once the data is acquired and processed. In this context computed tomography provides the means to choose slicing planes for detailed metallographic analysis. While CT can determine the geometry of an anomaly, the details of grain structure and other details needed for full seam assessment still requires metallographic sectioning in the areas of concern.

It was clear that imaging seam welds with anomalies using computed tomography requires high resolution systems and the capability to manage high magnifications. It was equally clear that this technology provides an economical means for the preliminary assessment of seam-weld anomalies that have been detected with ITD or ILI inspection methods.

Important conclusions drawn over the course of the task follow:

- differences in the features causing failure within an ERW seam, and in the related local microstructures requires case-by-case decisions on the fractographic and metallographic practices to be used – because this effectively precludes standardizing such aspects, two Annexes were presented regarding good practice in characterizing such failures as guidance beyond that available in handbooks and textbooks;
- thorough failure analysis and reporting is an essential aspect of integrity management as it helps to avoid the recurrence of similar failures;
- new approaches for use in complement to fractographic and metallographic practices – specifically automated 3-D imaging and X-ray tomography – both offer promise to better understand the factors controlling failure, and to characterize the size, shape, and failure mechanisms involved;
- imaging seam welds with anomalies with high resolution 3-D imaging or computed tomography requires the capability to manage high magnifications and the large volumes of data they produce;
- an adaptation of optical emission spectroscopy indicated that the averaged chemistry in the vicinity of the bondline of a well made ERW seam did not differ greatly from that remote to the bondline;
- significant shifting of the crack plane between differing microstructures made clear that fracture initiation and propagation both seek a path of least resistance in an ERW seam – while this observation was anticipated the physical distances in such shifts was a surprise;

- complexity due to shifting crack planes and blunting of the notch in CVN testing in turn complicates the direct use of measured energy and percent shear-area, which might be resolved if such CVN data were generated using an instrumented striker, which could lead to improved failure pressure and other predictions for cases involving ERW seams; and
- shifting of the crack from the plane or structure targeted by the notch in CVN testing can lead to significant scatter in the measured energy and percent shear-area, which is often observed in such data for an ERW seam.

References

1. "Fractography and Atlas of Fractographs," Metals Handbook, Vol. 9, 8th Edition, American Society for Metals, Metals Park, OH, 1974; Mills, K., "Fractography," American Society of Metals (ASM) handbook, Volume 12, 1991.
2. "Metallography and Microstructures," Metals Handbook, Volume 09, Vander Voort, G. F., (editor) American Society of Metals, 2004
3. Habraken, L., de Brouwer, J-L., Schrader, A., Rose, A., Pokorny, A. and Pokorny, J., "De Ferri Metallographia", Volumes I, II, and III, Institut de Researches de la Siderurgie, Francaise, W B Saunders Co, 1967
4. "Failure Analysis," Chapter 11 of Fatigue Design Handbook, 2nd Edition, AE-10, Society of Automotive Engineers, Rice, R. C., Leis, B. N., and Nelson, D. V., (Editors), 1988.
5. Kadnar, J., "Metallurgical Laboratory Failure Examination Protocol," a PHMSA Guidance document on failure analysis, www.
6. Leis, B. N. and Nestleroth, J. B., "Battelle's Experience with ERW and Flash Weld Seam Failures: Causes and Implications," Battelle Interim Report, Subtask 1.4, US DoT Contract No. DTPH56-11-T-000003, September 20, 2013.
7. Kiefner, J. F. and Kolovitch, K. M., "ERW and Flash Weld Seam Failures," KAI Interim Report on Task 1.4, September, 2012
8. Nichols, R. K., "Common HF Welding Defects," Thermatool Corp., (www.thermatool.com/.../common-hf-welding-defects.pdf), undated
9. Leis, B. N. and Nestleroth, J. B., "Time-Trending and Like-Similar Analysis for ERW-Seam Failures," Battelle Interim Report, Subtask 4.2, US DoT Contract No. DTPH56-11-T-000003, April 15, 2013.
10. Anon., Handbook of Electric-Weld Tubing, Steel and Tubes Inc, 1934
11. Johnston, G. V., "Method and Apparatus for Butt Welding Thin Gage Tubing," US Patent 1,388,434, 23 August, 1921.
12. Johnston, G. V., (assigned to Elyria Iron & Steel Co) "Butt Welded Thin Walled Tubing," US Patent 1,435,306, 14 November, 1922.
13. Colby, I. A., (assigned to Youngstown Sheet and Tube) "Method of and Apparatus for Continuous Welding of Pipes and Tubes," US Patent 2,575,381, 20 November, 1951.
14. Brossia, C. S., "Selective Seam Weld Corrosion Literature Review," DNV Interim Report, Subtask 3.1, US DoT Contract No. DTPH56-11-T-000003, April 10, 2012.
15. Yuzawich, P. M. and Hughes, C. W., "An Improved Technique for Removal of Oxide Scale from Fractured Surfaces of Ferrous Materials," Practical Metallography, Vol 15, pp. 184-194, 1978.
16. Anon., Keyence Corporate Profile, Microscopy, http://www.keyence.com/dwn/corporate_profile_gn_ka.pdf, (last accessed January 2013)
17. Killmore, C. R., Barbaro, F. J., Williams, J. G., and Rothwell, A. B., "Limitations of the

Charpy Test for Specifying Fracture Propagation Resistance," WTIA \APIA \CRC-MW Specialists Seminar on Fracture Control in Gas Pipelines, Paper 4, University of Wollongong, Australia, June 1997.

18. Leis, B. N., "Charpy Impact Test and its Applications," J Pipeline Engineering – Special Volume on Fracture, Vol. pp. September 2013 (in press)
19. Kiefner, J. F. and Kolovitch, K. M., "Models for Predicting Failure Stress Levels for Defects Affecting ERW and Flash-Welded Seams," KAI Interim Report on Task 2.4, US DoT Contract No. DTPH56-11-T-000003, January, 2013.
20. Leis, B. N., "Battelle's Experience in Predictions of Failure Pressure for ERW and Flash Weld Seams," Interim Report on Task 2.4, Annex to Reference 19, KAI Interim Report on Task 2.4, US DoT Contract No. DTPH56-11-T-000003, January, 2013.
21. Leis, B. N. and Nestleroth, J. B., "Compare - Contrast Analysis of Inspection Data and Failure Predictions versus Burst-Test Outcomes for ERW-Seam Defects," Battelle Interim Report, Subtask 4.1, US DoT Contract No. DTPH56-11-T-000003, May 31, 2013.
22. G. T., Quickel "Characterization of the Toughness of Pipe Containing Seam Defects," DNV Interim Report on Task 2.3, US DoT Contract No. DTPH56-11-T-000003, February, 2013.
23. Behrens, H., "A Manual of Microchemical Analysis," MacMillan, 1994

Annex A: Guidance Regarding Failure Analysis for ERW Seams with a Focus on Fractographic and Metallographic Practices

This Annex discusses failure analysis of ERW seams and illustrates metallographic and fractographic practices in this application. Other interim project reports available on the PHMSA website also broadly illustrate the use of these practices – particularly those for Tasks 1 and 3 of Phase One of this project. Readers interested in further review of these aspects or in the characteristic features of ERW seam failures should consult the PHMSA website. (http://primis.phmsa.dot.gov/matrix/PrjHome.rdm?prj=390&btn=Go)

GUIDANCE REGARDING FAILURE ANALYSIS FOR ERW SEAMS

Background

Failure in a general context can be defined as the inability to perform as intended, leading to an incident. Failure can occur in simple components or structures, like a drive axel on a vehicle. Failure also can occur in more complex systems wherein failure is evident in terms of overall performance or more readily apparent as a structural breakdown at the scale of individual elements. In such complex settings, the consequences of a process upset or reactor malfunction can range from a faulty product through an explosion propagating through the entire chemical plant. Components can remain physically intact and yet still have failed, as for example where structural deformation upsets the fit-up of a seal or a bearing, which then malfunctions.

At the most basic level an incident can be characterized relative to the specific causal factors and susceptibilities that jeopardized functionality, in what is termed a direct-cause analysis. Incidents also can be characterized more generally at the level of organizational and/or systemic malfunction that contribute to or cause case-specific malfunction, in what is called root-cause analysis. Whether a direct-cause or a root-cause analysis is done depends on the complexity of the system or component, the scope of causal factors and susceptibilities, and the consequences of the incident. Major incidents with loss of life often dictate more comprehensive analysis than do those with relatively little consequence.

Much has been written on the subject of incident analysis as just outlined, from the conceptual generic level down into the details of the protocols, procedures, and techniques – with standards often available that establish acceptable practices. Properly performed, direct and root cause analyses provide critical insight into when, what, why, and how the circumstances uniquely combined with the design and as-built susceptibilities leading to a failure. In turn, this identifies corrective and preventive actions, and also helps develop diagnostic and predictive tools, all with the purpose of avoiding future failures, and achieving higher levels of quality and/or reliability – ultimately enhancing public and environmental safety without jeopardizing economic and other business metrics.

Whether such concepts are applied to an offshore failure of a platform or a pipeline the process is the same – but how it is applied and why differs because the causative factors and susceptibilities differ. The same can be said concerning such concepts in the context of the administrations that comprise the US Department of Transportation, like the Federal Aviation Administration (FAA). It is likewise the case at the level of the Pipeline and Hazardous Materials Safety Administration (PHMSA) in regard to hazardous materials or pipelines. While a webcrawl using keywords like FAA + "root cause analysis" will develop ~467,000 hits, the same in the context of the PHMSA leads to about 7000 hits. Similar disparity exists in the context of failure analysis. Notably, the PHMSA provides high-level guidance in regard to documenting failures in pipelines[(5)], which if coupled with literature guidance on processes and standard practices defines a viable starting point for any related failure report.

Scope of this Annex and Implications for Failure Analysis

The purpose here is not to address the above-noted gap, as whether it is the PHMSA or the FAA the concepts are the same. More critically, such concepts have been broadly documented both in the context of the Government, as well as by the private sector. Rather, the purpose here is to selectively illustrate aspects of the susceptibilities unique to ERW seams. The objective is to provide insight into how and why such aspects should be addressed if the outcome as a "failure analysis report" is to provide value to the industry by helping to offset future incidents.

The focus is direct-cause failure analysis of pipelines – specifically steel transmission pipelines. Incidents in steel pipelines, like most metallic structures, can occur by one of several modes of failure, with the mechanism of failure often dictating the mode. The primary failure modes are fracture, plastic collapse, and instability, while the plausible mechanisms for pipelines include brittle fracture, ductile fracture, tensile instability, fatigue, stress-corrosion cracking, and so on depending on the service loading and environment. Thus, a failure analysis should in general develop sufficient detail to establish both the mode and mechanism of failure.

Because as-built is not always as-designed, it is necessary to address the design basis for the pipeline to ensure that those aspects are in no way causative. Even when a "smoking gun" is found, it is necessary to review the overarching circumstances of the failure, to ensure other factors were not essential for that smoking gun to be causative. This requires an understanding of the routing, the soils, and all factors that potentially contribute to the loadings. It is equally essential to do a set of basic properties tests, to establish that the steel made grade, and that the pipe satisfied nominal requirements as specified. In cases where records are lacking, such testing might be more comprehensive than typical, to help better establish the design basis for the pipeline.

Recognizing that ERW pipe is typically used in onshore transmission pipelines wherein the loading is usually dominated by locally uniform pressure provides further guidance as to the minimal scope of a failure analysis. Because the loading is locally uniform, failure occurs where the local properties coupled with the local cross-section can no longer sustain that pressure. Thus, the failure analysis must address the local properties and the local cross-section to ensure that the origin and cause of failure as determined are mutually consistent with those circumstances.

It follows that this Annex should illustrate good practice supporting failure analysis of ERW seams. In general, this involves quantifying the local properties (e.g., typically strength, toughness, chemistry, and hardness), and characterizing the net cross-section in reference to the presence of defect(s) and their shape(s) and size(s). Finally, this involves presenting adequate metallography and fractography to identify the traits at the origin of failure and the mechanism(s) of growth leading to failure. Occasionally this is problematic, but as skill and experience develop what seemed complex becomes routine.

Perhaps the most critical step in any failure analysis is the certainty that the origin(s) has been correctly identified. Where the failure is brittle, which can be recognized by a fracture surface that lies perpendicular to the pipe's wall, this is relatively simple in cases where a single crack results in failure. As discussed in regard to Figure 10a in this report, features called "chevrons" form due to the nature of the brittle mechanism, which point back toward the origin. In such cases, the origin lies centrally between such chevrons. Where multiple brittle cracking paths form, as illustrated earlier in Figure 11, finding the origin is more complex. First, the shards must be reconstructed as shown in a fracture map, like that illustrated for example in Figure 11. Because a single origin gives rise to one crack at the onset of failure, the reconstructed shards eventually point back to a single crack path from which the multiple cracking propagated. Once that single path is located, finding the origin is as noted above.

In cases where the failure process is ductile, the origin gives rise to a single crack path – although in some cases more than one path can form. Where little axial growth is involved, the origin typically is centered within the length of the contained split. Such origins are easily identified in regard to metal loss or the presence of a defect that often is marked by a thumbnail, as evident in Figure A1. Because more energy is involved, some local bulging develops, with the energy released at rupture forming a pucker, such as those shown in Figure 9 in this report.

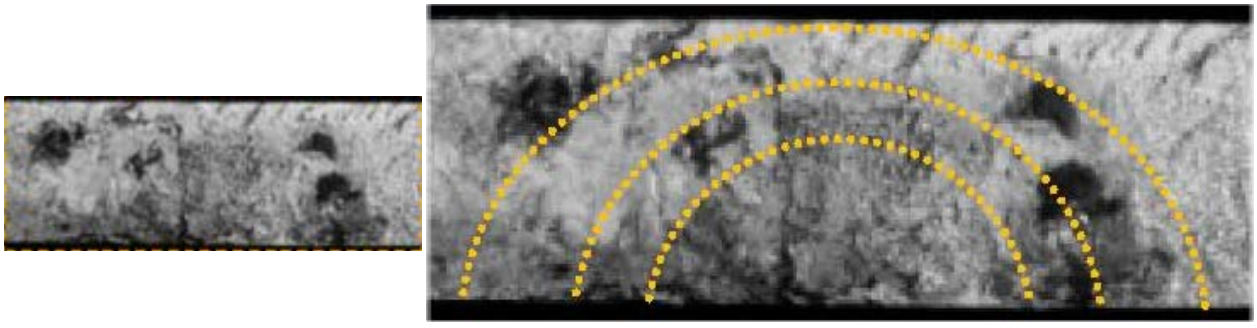

a) overview, t = 0.219" **b) nested thumbnails shown indicating subcritical advance**

Figure A1. Thumbnail feature formed in the bondline of a HF-ERW seam

While this report has covered some aspects of concern, many others have been dealt with in the reporting for other Subtasks completed as part of this project. For example, determining local properties has been discussed earlier herein, as well as in reporting for Task 1.4[6], Task 2.3[22], Task 4.1[21], and in the literature[e.g., A1]. Characterizing the net cross-section and its significance in reference to defect location in the bondline versus the upset, and shapes(s) and size(s) has been considered in reporting for Task 1.4[6,7], Task 2.4[19], and Task 4.1[21]. It remains here to focus on the metallographic and fractographic aspects.

Finally, failure in an early HF ERW seam can occur by the same mechanisms that cause failure in LF ERW seams – the exception being "stitching" that has been eliminated by the HF processes. Because the application of metallography and fractography tends to be similar if the failure occurs through bondline failure (at a cold weld or in selective seam corrosion (SSC)) or

through the upset (e.g., hook cracks), this Annex illustrate the use of these practices specifically in regard to hook cracks.

Metallography and Fractography Focused on ERW Hook Cracking

This section illustrates metallography and fractography in the context of a seam-related failure in a 12.75-inch-diameter pipeline with a 0.250-inch thick wall made of X46 with a LF ERW seam produced circa 1958 by Republic Steel. This crude oil line was operating at 1,210 psig (i.e., at 67 percent SMYS) local pressure at the time of failure. The section that leaked was subject to a pre-service hydrotest at 90% SMYS. It was retested in the mid-1970s and again in the late-1980s to 89% and 92% SMYS, respectively, prior to its failure toward the mid-1990s. The FSE CVN plateau energies of the base metal, HAZ, and weld bond line were 36, 27, and 19 ft-lbs respectively. Such values were considered excellent for this size and grade of pipe, with related analysis noted to indicate flow-controlled failure through all three regions of the pipe sampled.

Following site documentation as appropriate, consideration of the site and disposition of the pipe and visual review of the fracture features, the failed segment can be stabilized and fully protected as needed for removal and shipment to the laboratory. Recognizing that protection is needed local to the critical features, this site review must identify an origin with reasonable certainty otherwise all potential origins must be protected prior to shipping. Upon receipt, it is usual to document the “as-received” state, during which time all other preliminaries (like custody transfer, approvals, etc.) can be finalized. Thereafter, the in-shop phase of the failure analysis begins with a macro-fractographic review of the as-received section(s) (pups, joints, etc), which is directed at confirming the preliminary assessment of the location of the origin – or reassessing it as needed. Depending on the features presented, an acceptable plan for the study is developed and approved. With all approvals in place, key segments along the fracture paths are excised with practices that preserve the features. Initially larger pieces become more manageable as the initially larger segments are examined visually or under stereo optical microscopy (SOM), and decisions are made to slice them into more manageable portions to facilitate cleaning. All aspects are documented after which the smaller portions can be cleaned and evaluated in more detail.

As none of the cut-planes used to separate the smaller portions run through critical fracture features, a thin slice can be cut from sequential ends of these portions and then roughly polished to track the fracture path relative to the position of the bondline and upset. If the origin lies outside the upset, the failure is in the pipe body and usual practices apply. However, if the origin lies within the seam, then it can be instructive to mount adjacent sides of the fracture path on either side of the origin, to better understand the exact location and cause of the failure. In this regard metallography and fractography move forward together, with what is learned between them synergistically moving the analysis forward. In contrast to SOM to capture an overview of the fracture features, such metallographic sections are made using an optical microscope that provides a wide range of power, often from about 40 times upward of 1000 times, to facilitate detailed resolution of the structures.

The montage in Figure A2 shows a typical metallographic cross-section view through a LF ERW seam in pipe produced in 1956 by Lonestar. From a metallographic perspective the seam is narrow and relatively fine-grained, in skelp that shows some evidence of banding and upset MnS stringers. Both the ID and the OD of the seam are neatly scarf'd back even with the pipe body. The inset to the left shows the upper-third of the seam, which makes clear that failure occurred along the bondline as indicated in the full-thickness view. The inset to the right shows the lower-third of the seam, and from the swirl evident in the upset indicates that this side of the skelp was a little mismatched through the thickness, with the fold at the bottom evidence that the mismatch was accommodated by the upset. The small steps evident to either side of the seam suggest that while the failure occurred within the bondline there is microstructural weakness to either side of the bondline that contributed to this failure – as cold cracking tends to be feature free (planar).

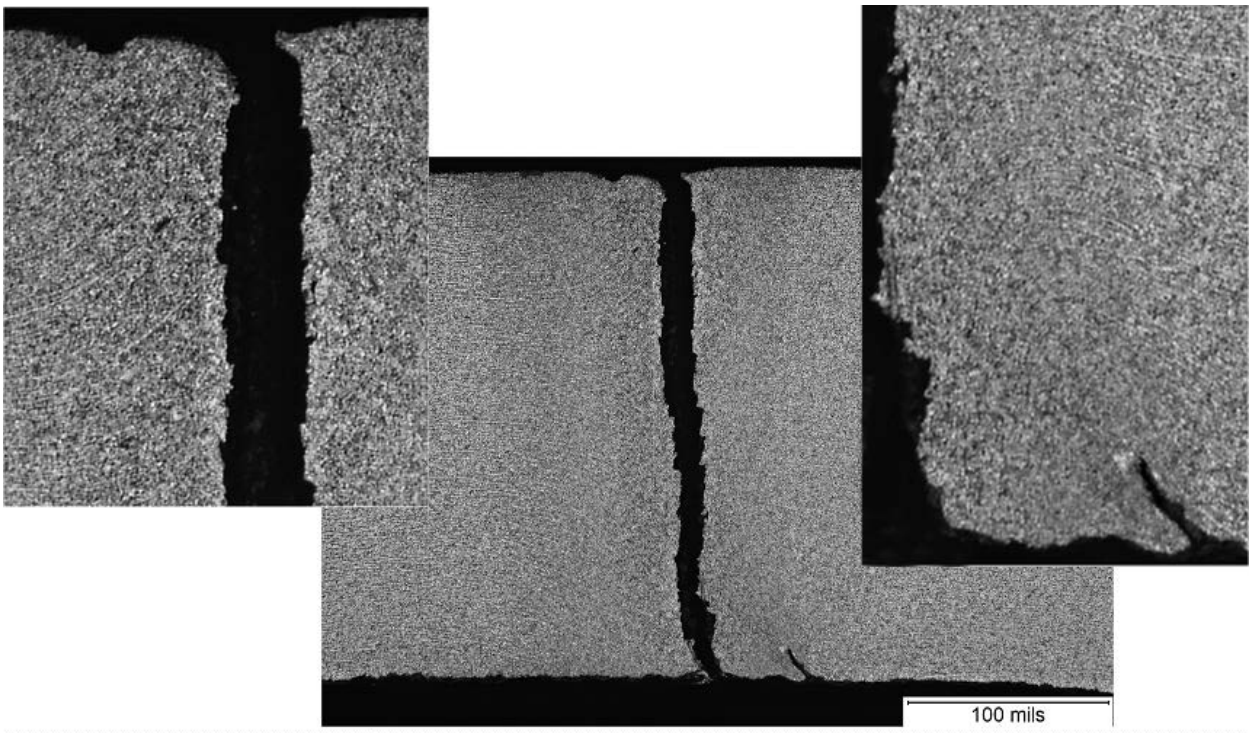

Figure A2 Metallographic section through a bondline failure, t = 0.250" (nominal)

Depending on the need, as-polished metallographic sections are effective to illustrate and track cracking paths through the thickness, while etched sections assist in understanding the role of the microstructure, and what it reveals of the fabrication process. As dictated by the situation and the need, metallographic sections are presented at a magnification from a few times, up to many hundred times as when resolving microstructural details such as the presence of martensite. That being said, it is useful to show typical structures at between 100 and 200 times magnification, such that a large enough area is captured to show a representative sample of the steel.

The remaining images considered in this Annex derive from scanning electron microscopy (SEM), light microscopy, and SOM in regard to hook cracks. The advantage of SEM over usual light microscopes lies in depth of field coupled with the ability to focus – which allows

evaluation of a large region on the fracture without loss of focus. Depending on the SEM, some allow lower-power down to several times magnification, up to levels well beyond anything of practical utility of typical pipeline failure analysis. This section deals with such results, beginning with the fractography, first as-received, and then after cathodic cleaning as outlined in the body of the report. Next, the results of the metallographic work are presented to illustrate how such work supports the fractography.

Visual Examination of the Pipe and Fracture Surfaces As-Received

The outside and inside pipe surfaces of the sample containing the fracture origin were visually evaluated, with no evidence of corrosion or other potentially contributory factors. However, there was evidence of usual manufacturing marks adjacent to the weld due to trimming the upset.

Examination of the fracture surfaces in the vicinity of the presumed origin showed the feature lay centrally across a local pucker as evident in Figure A3 – where the outside surface is oriented up. Such images should capture the overall appearance of the origin, and cover its full length. An indication of scale should be included, but this also can be accomplished by indicating the thickness for views captured perpendicular to the fracture surface. It is usual to provide some description of the key features. In regard to Figure A3 it is apparent that a dark band runs along the exterior of the pipe, which is typical of a hook crack. There is also evidence of crack advance below the original defect, which is evident in the form of long semielliptical thumbnail features.

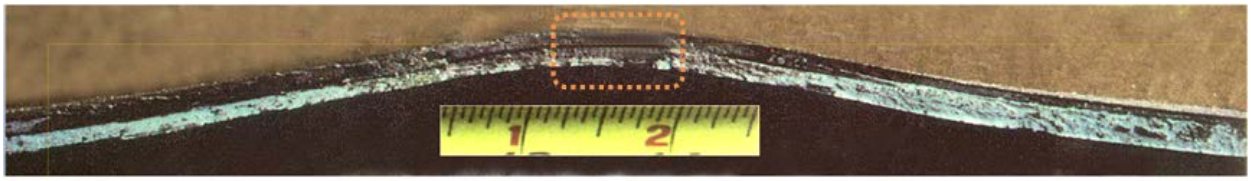

Figure A3. Overview of the origin

Adjacent to the origin an axially aligned linear feature was evident within the weld upset. Its length as evident on the surface was much less than that of the origin causing failure. This axial feature was broken open by cooling it in liquid nitrogen and then impacting it, with the resulting fracture surface shown in Figure a4 at a scale comparable to that in Figure A3. This feature also showed evidence of crack advance below the original defect that was evident in the form of a long semielliptical thumbnail feature. On the outer half of the wall thickness, the features in the secondary cracking appear to be similar to those at the origin.

Figure A4. Intact adjacent feature after exposing the fracture surface; t = 0.250” (nominal)

When the detail provided by an overview image does not adequately show the details, because these have to be captured at lower magnification to show their full length, it is usual to provide supplemental views at higher magnification. For example, in regard to Figure A4 an additional

view such as that in Figure A5 should be included, along with a description of the features and a comment as appropriate on their significance.

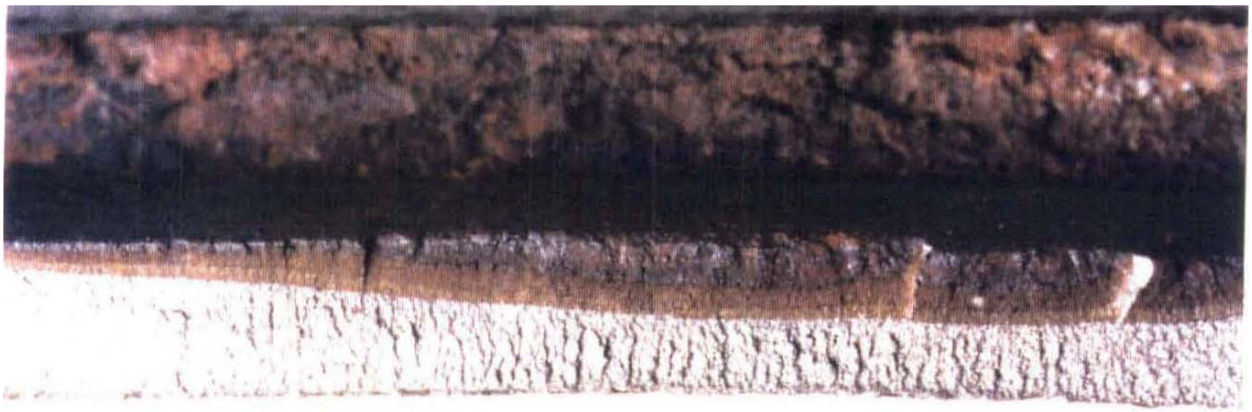

Figure A5. Detail in the boxed area of Figure A4

Figure A5 shows detail in the boxed region in Figure A4, and covers the full wall thickness. This view is centered at the origin for this long semielliptical thumbnail crack, which as evident from Figure A4 is one of such features that formed where the original defect grew from the mid-wall depth of the original defect toward the inside surface of the pipe. The features in this figure are comparable to those in the second similar feature. The gradation in the color of the corrosion products indicates that this growth occurred over different intervals. The steps within this growth that run from mid-wall to the ID surface of the pipe indicate that several cracks initiated on slightly different planes and linked as they grew.

Given this pipe segment experienced three hydrotests, it is plausible that the evidence of growth in steps marked by corrosion reaction products reflects those three steps. But given the subject pipeline also experienced a large daily pressure cycle it is also possible that this crack growth includes a fatigue component. Thus, the next step involved cleaning as outlined in the body of this report to facilitate both SOM and SEM examination. The features associated with this failure as just discussed motivate such detailed study, because further SOM and SEM could provide insight into systemic concerns. In contrast, where the circumstances do not indicate that benefit accrues from such details, and the observations available from metallographic analysis make the cause clear in a way that is consistent with all of the facts and site observations, further study is not needed or justified.

SEM and Metallographic Examination of the Origin

Visual study of the origin facilitated by low-power SOM was done to provide perspective for the failure process and the mechanisms that might be causal. That study confirmed that the origin lay in a long hook crack that developed along a segregation band. Because that band emanated from near the mid-thickness of the skelp, the originating defect ran into that depth before turning onto a plane oriented through-thickness. Such is typical of other hook crack origins, with the specific plane of weakness and its depth into the skelp leading to different appearing fracture features.

The SEM study sought to confirm that the failure occurred under flow-control and identify mechanism(s) leading to crack initiation and growth beyond the original mid-thickness depth of the hook crack. As outlined in the body of the report, the fracture surface was cleaned starting with solvents and a soft fiber brush to remove coating and loosely adhering soil and corrosion products. A quick look under SOM indicated this was inadequate, as is often the case, because the remnant corrosion products obscured the fine fracture details. Consequently, a second cleaning cycle was done using the cathodic cleaning process outlined in the report, working in conjunction with an alkaline bath[15]. The appearance of the fracture surface after cleaning is shown in Figure A6.

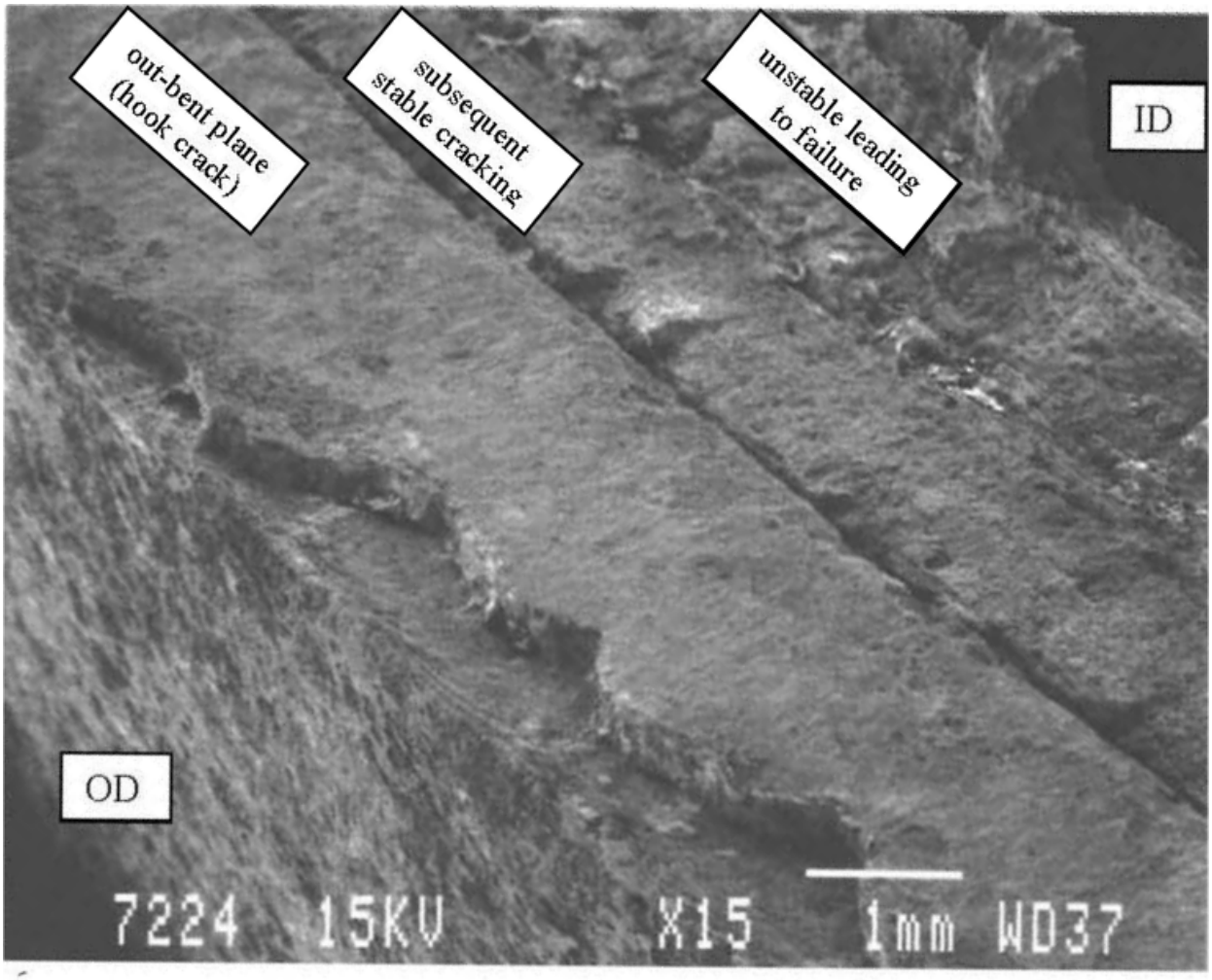

Figure A6. Detail in the boxed area of Figure A3

Five regions labeled in Figure A6, which from the left side are: 1) the OD surface of the pipe; 2) the hook crack; 3) the cracking below the initial defect (hook crack); 4) the unstable growth that breached the wall and led to rupture; and 5) the ID of the pipe. Given the twisted perspective used in Figure A6, these five regions are most easily visualized in reference to the cross-section shown in Figure A7. This section was cut immediately adjacent to the origin, where as apparent from this figure the final fracture plane below the defect had turned to shear.

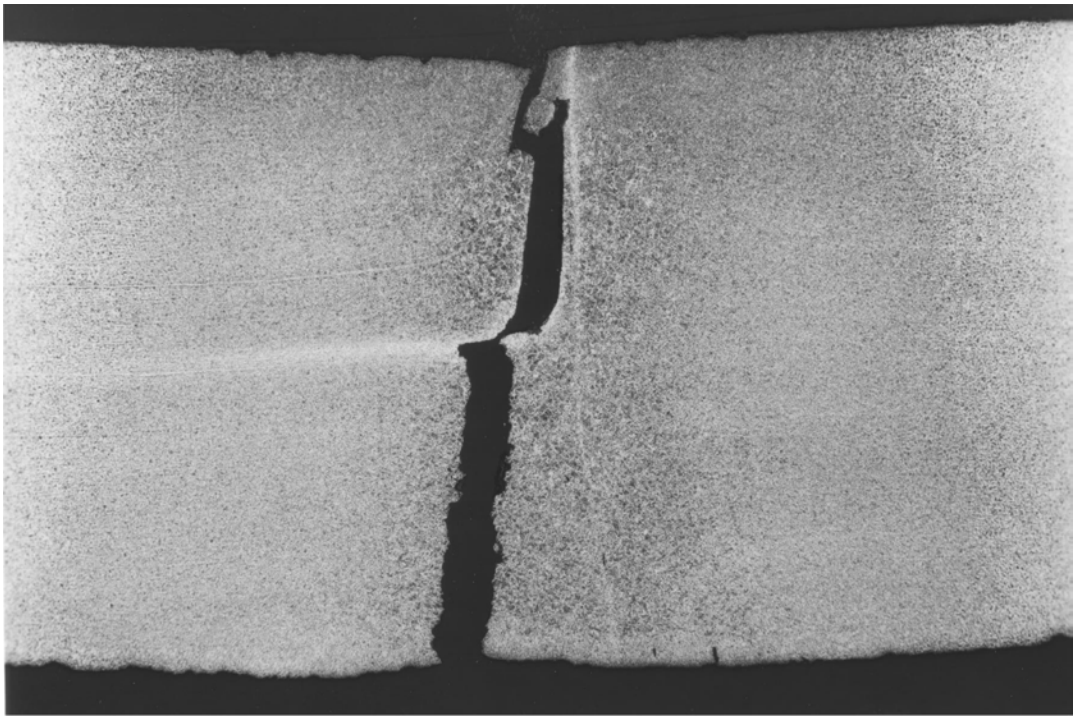

Figure A7 Metallographic section through the hook-crack origin, t = 0.250" (nominal)

Figure A7 captures the area of the neatly scarf'd upset out into the skelp beyond the effects of the ERW process covering a distance of about two wall-thicknesses. The OD surface is at the top of this image, such that the failure grew from the OD in toward the ID. The portion of the fracture surface from the OD surface of the pipe down to the mid-wall forms in association with two segregation bands (outbent fibers). One of these forms from centerline segregation and as such lies adjacent to but not in the bondline. The outbent plane evident in Figure A6 lies on the left side of the hook crack, while the ledge of material missing from that plane at the OD surface can be seen still attached to the opposite side of the fracture. Thus, the hook crack developed on two planes. The fact that the interface formed across a segregation band fails whereas the bondline remains intact indicates that this interface is weaker than the bondline. Such is also evident from the images shown in the body of the report as Figures 19 and 20. The curved portion of the crack formed as the crack tracked the outbent and extended a short distance essentially parallel to the pipe's surface along the segregation band at the mid-wall.

It is clearly evident from Figure A7 that the cracking into the pipe wall below the hook crack forms out toward the edge of the HAZ, but still lies within the area of the upset. This is the area pf the fracture surface that showed the gradation in color formed in the corrosion reaction products that remained within the crack. The detailed features in such areas merit further study, as insight gained can indicate the potential for stable tearing leading to pressure reversals, as well as susceptibility to fatigue crack propagation (FCP). Fatigue crack growth below a hook crack as well as stable tearing are both quite likely because hook cracks tend to be long and potentially form at initial depths up to a depth of half the wall thickness. That combination of length and depth gives rise to a crack driving force that easily exceeds the threshold for FCP, even for

modest pressure cycling. Likewise, it exceeds the threshold to initiate stable tearing except in cases where the steel's toughness is very high.

Etched cross sections as in Figure A7 provide entrée to the microstructural features associated with the failure, with adjacent slices made to support chemistry and microhardness analysis. Study of such aspects serves to eliminate them as contributory factors. While not shown here this work indicated that the segregation regions consist of bands of ferrite, which contained numerous nonmetallic inclusions. The bondline ran from near perpendicular to somewhat skewed, which indicates that some through-thickness misalignment occurred in the fin-pass. Away from the upset, the microstructure was banded and consisted of a mixture of ferrite and pearlite that was considered typical for a hot rolled X46 steel. The ferrite grain size was the order of ASTM 9, which suggests that fine-grained steel production practices were used. Overall, nothing untoward was evident from a microstructural perspective save for the presence of segregation bands indicative of somewhat dirty steel – the fundamental cause of hook cracks (and also SSC).

Figure A8 shows a low-power SEM view of the fracture surface spanning the lower half of the cross-section shown in Figure A7, on the right side of the fracture. The upper-half of this image is the cracking below the hook crack while the lower-half is the unstable tearing that breached the wall and led to the rupture.

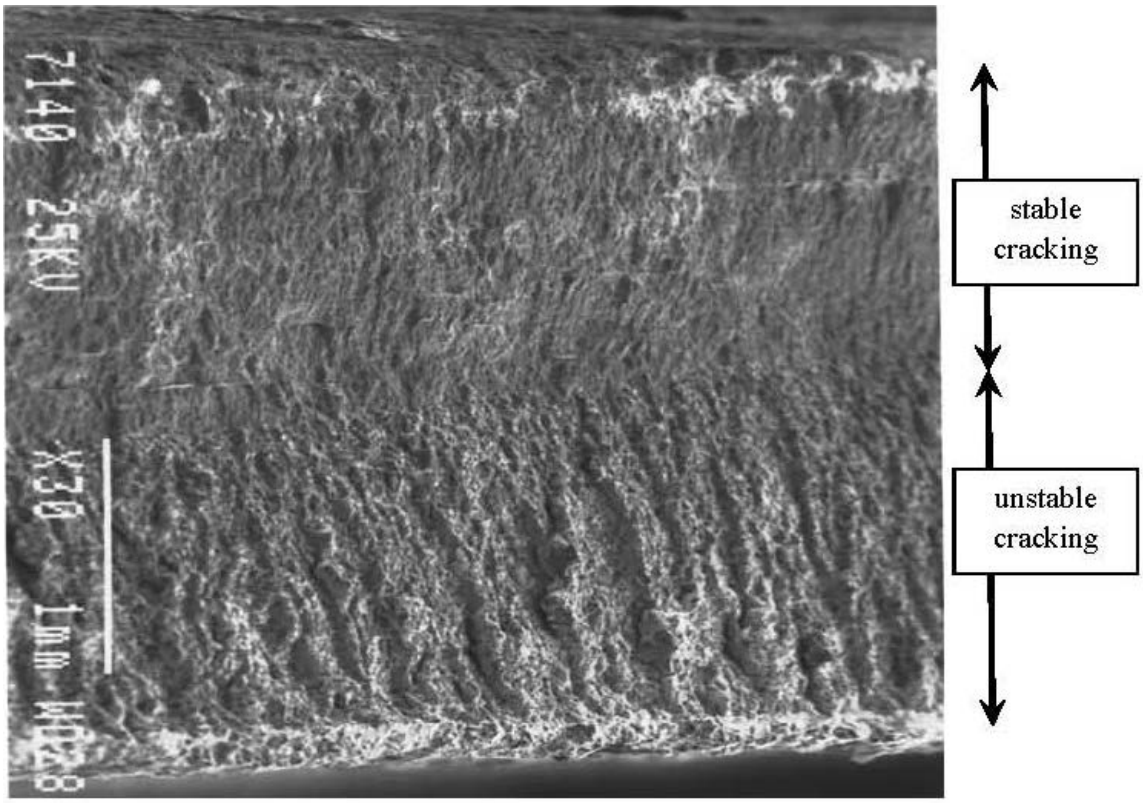

Figure A8. Fracture details below the hook crack

For the record, the image in Figure A8 was captured at an angle that shorten the vertical distance relative to the horizontal distance, such that the scale indicated in the image as 1 mm for the through-thickness direction corresponds to about 1.25 mm in the axial direction. While the portion of the fracture surface labeled stable cracking shows evidence of crack-arrest fronts, there are many more evident than the three that would correspond to the hydrotests history for this pipeline. It follows that these arrest fronts reflect a combination of the hydrotest events and a mechanism like stress-activated creep, or fatigue. While line pipe steels tend not to develop well-formed striations, the search for such evidence can be tedious – even when examining fracture surfaces on test specimens that failed under pipeline-like fatigue cycling.

The surface shown in Figure A8 was scanned for evidence of both stable tearing and fatigue. The zone immediately below the hook crack down through about one-third of wall thickness noted as stable cracking was relatively flat and exhibited coarse, blocky features typical of transgranular, stable tearing, the mechanism of ductile crack growth. This is the mechanism by which crack growth during a hydrotests causes pressure reversals. This zone appears to have been damaged by corrosion after that portion of the crack had formed. Below this zone is another axially oriented band that was characterized by somewhat axially oriented arrest fronts and woody appearance at lower magnification. Such macro-features often are observed on fracture surfaces of carbon steel where FCP has occurred, however well-defined striations were not observed at higher magnifications over this portion of the fracture surface. Below that zone lies an area bounded below by the onset of unstable fracture. This area contained axially aligned regions that showed features typical of stable tearing as can occur during a hydrotests, as well as evidence of crack extension due to cyclic loading in patches of ill-formed striations oriented consistent with through-wall growth. The view in Figure A9 illustrates such features, where the axial continuity persists across microstructural changes over a distance the order of three or four grain diameters.

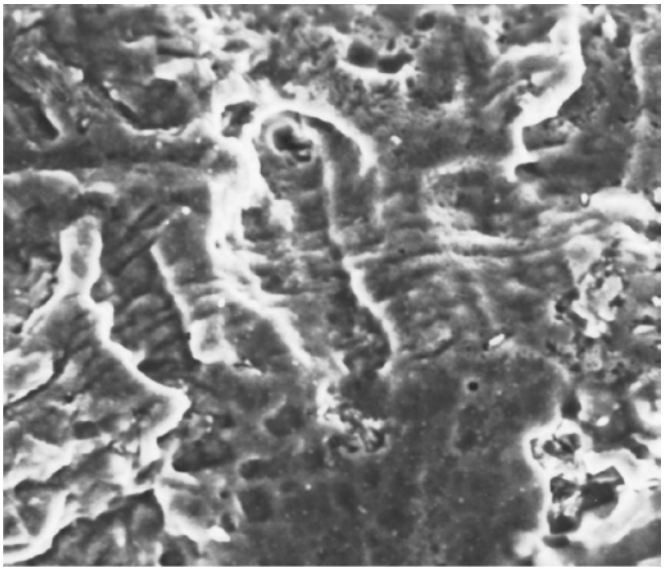

Figure A9. Small patch of ill-formed axially oriented striations

It follows that this pipeline was susceptible to FCP under typical service conditions. As hook cracking tends to be susceptible to fatigue by virtue of the shape of this type of defect, the operation of the line was revisited in light of its failure history to minimize the concern for this mechanism.

Summary and Conclusions

This annex has discussed practices associated with direct-cause and root cause analysis and identified good practices for failure analyses done in support of such work. Experience indicates that a good failure analysis can be an effective tool contributing to the integrity management plans for pipelines.

References New to Annex A

A1 Brian O. Hart, B, O., Bringers, P. H., Bubenik, T. B., and Vieth, P. H., "Early Generation Seam Welds," Final Report R3017-01R Under Joint Funding from DoT/OOS and PRCI, Project DTRS56-03-T-0002, CC Technologies, 2004

Annex B: Illustrations of Fractographic and Metallographic Practices Applied to ERW Seam Failures at Kiefner and Associates

This Annex presents results of failure analysis of ERW seams to illustrate metallographic and fractographic practices in this application. It is intended to provide further illustration of good practice in the context of ERW seam failures.

Other interim reports on the PHMSA website (http://primis.phmsa.dot.gov/matrix/PrjHome.rdm?prj=390&btn=Go) – particularly those for Tasks 1 and 3 of Phase One of this project – also broadly illustrate the use of these practices. Readers interested in further review of these aspects or in the characteristic features of ERW seam failures should consult the PHMSA website.

Final Report

Fractographic and Metallographic Practices Employed at Kiefner and Associates, Inc. for ERW Seams and Seam Failures

J. F. Kiefner

June 3, 2013

0533-1101

Intentionally blank

Final Report No. 13-106

Final Report

on

FRACTOGRAPHIC AND METALLOGRAPHIC PRACTICES EMPLOYED AT KIEFNER AND ASSOCIATES, INC. FOR ERW SEAMS AND SEAM FAILURES

to

BATTELLE

AS PART OF THE DELIVERABLE OF SUBTASK 2.6 ON
U.S. DEPARTMENT OF TRANSPORTATION
OTHER TRANSACTION AGREEMENT NO. DTPH56-11-T-000003

June 3, 2013

by

J.F. Kiefner

Kiefner and Associates, Inc.
585 Scherers Ct.
Columbus, OH 43085

0533-1101

B3

EXECUTIVE SUMMARY

This report describes the fractographic and metallographic practices employed by Kiefner and Associates, Inc.(Kiefner) in conjunction with investigations of ERW seams and seam failures. This work is Kiefner's contribution to Subtask 2.6 "Standardize Fractographic and Metallographic Practices for ERW Seam Failures" as part of "Understanding Low-Frequency ERW Pipeline Failures", **U.S. Department of Transportation Other Transaction Agreement No. DTPH56-11-T-000003.**

An attempt is made herein to show how one company has employed fractography and metallography over a period of more than 20 years to investigate and understand ERW and flash-welded pipe failures. The techniques described have been sufficient to identify causes of failures in most cases.

Examples of fractography and metallography are given herein in conjunction with failures caused by cold welds, hook cracks, selective seam weld corrosion, and pressure-cycle-induced fatigue. The intent is to show what was learned by means of these techniques. As will be seen, some failure origins are easy to characterize, while others are not. For example, the origins of failures arising from selective seam weld corrosion or pressure-cycle-induced fatigue have been relatively easy to identify and characterize. In contrast, failures that propagate along the bond line of an ERW seam often do not have easily recognizable origins. And, for failures involving multiple hook cracks and/or non-metallic layers, the dimensions of the effective originating defect may be next to impossible to ascertain.

The company has generally relied on standard optical fractography and metallography to analyze the causes of ERW and flash-welded seam failures. Fracture surfaces are scanned visually after appropriate cleaning to look for origins of failure. For identifiable origins the dimensions of the associated defect and the base metal properties are used to predict failure stresses to be compared with actual failure stresses. Photographs of fracture surfaces at magnifications ranging from 1X to 2.5X are taken. Metallographic sections are taken at appropriate locations to confirm types of defects, locations of crack paths relative to the bond line and other significant features. Microhardness measurements are used occasionally to confirm the presence of regions of excessive hardness.

The company has not been particularly successful using the aid of an electron microscope to identify fatigue crack growth on a scale where individual steps of crack advance are seen. Nevertheless, the use of the electron microscope can serve other purposes such as identifying areas of brittle or ductile fracture, confirming different stages of crack growth, and identifying chemical species that may be relevant to the cause of a failure.

The scope of this document is limited to showing how the techniques of fractography and metallography have been used by one company in the investigation of ERW and flash-welded seam failures. It is not meant to be the basis of a comprehensive guide. The hope is that the information offered will be of use in conjunction with similar information from other laboratories for anyone whose objective is to develop a comprehensive standard for the use of fractography and metallography for investigating ERW and flash-weld seam failures.

DISCLAIMER

This document presents findings and/ or recommendations based on engineering services performed by employees of Kiefner and Associates, Inc. The work addressed herein has been performed according to the authors' knowledge, information, and belief in accordance with commonly accepted procedures consistent with applicable standards of practice, and is not a guaranty or warranty, either expressed or implied.

The analysis and conclusions provided in this report are for the sole use and benefit of the Client. No information or representations contained herein are for the use or benefit of any party other than the party contracting with Kiefner. The scope of use of the information presented herein is limited to the facts as presented and examined, as outlined within the body of this document. No additional representations are made as to matters not specifically addressed within this report. Any additional facts or circumstances in existence but not described or considered within this report may change the analysis, outcomes and representations made in this report.

TABLE OF CONTENTS

LIST OF FIGURES

Fractographic and Metallographic Practices Employed at Kiefner and Associates, Inc. for ERW Seams and Seam Failures

J.F. Kiefner

INTRODUCTION

Described herein are the fractographic and metallographic practices employed by Kiefner and Associates, Inc. (Kiefner) in conjunction with investigations of ERW seams and seam failures. This work is Kiefner's contribution to Subtask 2.6 "Standardize Fractographic and Metallographic Practices for ERW Seam Failures" as part of "Understanding Low-Frequency ERW Pipeline Failures", **U.S. Department of Transportation Other Transaction Agreement No. DTPH56-11-T-000003.**

Described below are the features of ERW and flash-welded seams and ERW and flash-welded seam failures as seen via metallography and fractography. These are the typical techniques that have been used by Kiefner for more than 20 years for the investigation of ERW seam failures. Almost all metallographic work done by Kiefner over the years has involved macrophotography of fracture surfaces, and macro- and micro-examination of polished and etched cross sections of ERW seams and ERW seam failures. Many examinations have also involved micro-hardness measurements. On occasion, Kiefner has subcontracted to others (Edison Welding Institute, Worthington Steel) for scanning electron microscope examinations of fracture surfaces. Metallographic sections are typically cut, mounted, and polished to a 1 micron finish for viewing under a microscope. The commonly-used etchant for exposing the microstructure is a 5% nital solution. Defects in an ERW seam are sometimes broken open for examination by cooling the sample in liquid nitrogen and breaking the seam by impact to expose the surfaces of the defect.

It is noted that failure investigations of ERW pipe samples conducted at Kiefner always include the measurement of base metal tensile properties (yield strength, ultimate strength, and elongation), measurement of weld tensile strength, testing of Charpy V-notch specimens to establish the full-range fracture transition relationships for impact energy and shear area for the base metal, and determination of the alloy content of the base metal.

MORPHOLOGIES OF ERW AND FLASH-WELDED SEAMS

A metallographic section across a typical low-frequency-welded electric resistance welded (LF-ERW) seam is shown in Figure 1. LF-ERW seams were typically made with 120-cycle electric current. Excess material that was extruded toward the ID and OD surfaces during welding was trimmed flush.

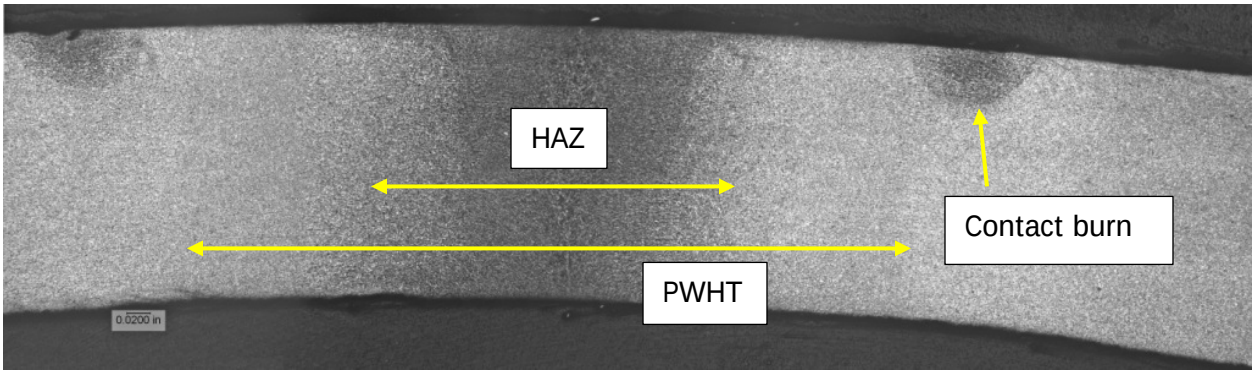

Figure 1. Morphology of a typical LF-ERW seam shown at 10X magnification

The bond line of this seam lies at the center of the photograph, but it is not readily visible in this material at this magnification. The visible features are the dark-colored rectangular weld heat affected zone (HAZ - about one wall thickness in extent) centered on the bond line, the moderately dark area extending about 1 wall-thickness-distance on either side of the heat affected zone represents material transformed by post-weld heat treatment (PWHT), and the two semi-circular dark areas at the outside surface of the pipe represent “contact burns”. The latter arise from local heat generated where the low-frequency electric current was introduced by rolling contact wheels for the purpose of welding.

A metallographic section across a typical direct-current-welded electric resistance welded (DC-ERW) seam is shown in Figure 2.

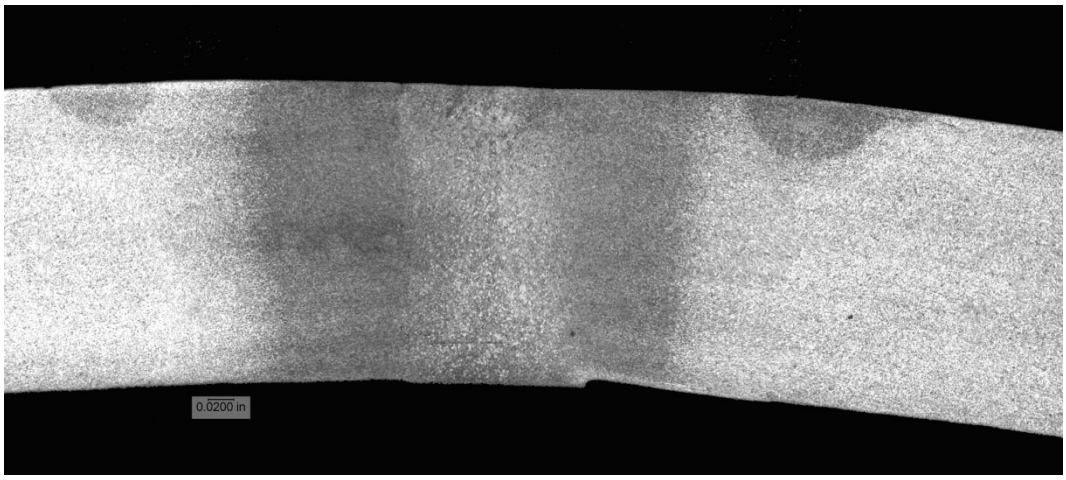

Figure 2. Morphology of a typical DC-ERW seam shown at 10X magnification

The morphology of this DC-ERW seam differs little from that of the LF-ERW seam shown in Figure 1 because the processes were quite similar. The only visible difference is that, in the case of the DC-ERW seam shown in Figure 2, the bond line region is more obvious. It is characterized by larger grain size. The coarse grain structure such as visible in Figure 2 was an unavoidable and undesirable consequence of the deep heat penetration created by low-frequency or direct current. The coarse-grained microstructure typically led to the bond line regions of LF-ERW and DC-ERW seams having high ductile-to-brittle fracture transition temperatures. The resulting bond line regions thus tended to have significantly lower defect resistance at normal ambient temperature than the base metal of the pipe.

A metallographic section across a typical high-frequency-welded electric resistance welded (HF-ERW) seam is shown in Figure 3. HF-ERW seams are typically made with 450 kilocycle electric current.

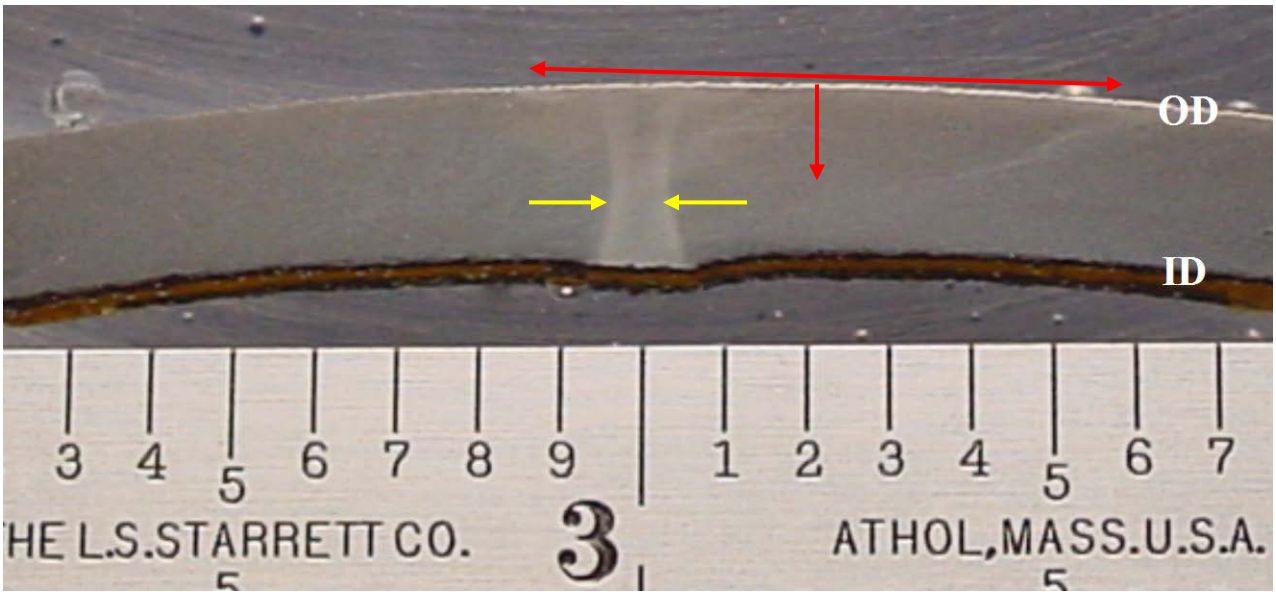

Figure 3. Morphology of a typical HF-ERW seam shown at 4X magnification

The yellow arrows in Figure 3 denote the hour-glass-shaped heat-affected zone typical of an HF-ERW seam. The heat affected zone is much narrower than that of an LF-ERW or DC-ERW seam because of the tendency of the high-frequency current to penetrate less deeply than a low-frequency or direct current. The red arrows show the extent of a slightly shadowed area that is believed to represent the zone of post-weld heat treatment (PWHT).

A higher-magnification view of this seam is shown in Figure 4 (image reversed from that of Figure 3 as the result of different optics).

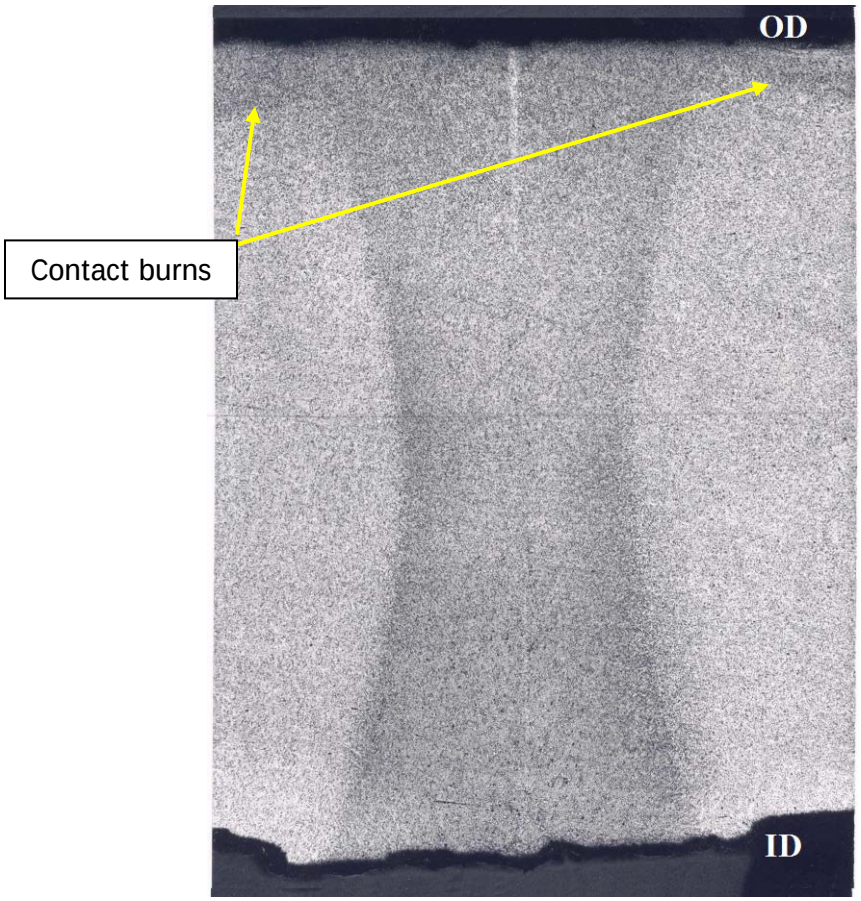

Figure 4. Close-up of a typical HF-ERW seam shown at 12.5X magnification

The bond line of this HF-ERW seam is clearly visible as a narrow white line at the center of the photograph. The white color is attributable to decarburization of the faying surfaces immediately before bonding. Such decarburization does not always appear in the bond line. The contact burns are denoted by arrows. Note that these are much shallower than the contact burns associated with the LF-ERW and DC-ERW seams because of the inability of the high-frequency current to penetrate deeply into the material.

The main advantage of the HF-ERW process over LF-ERW and DC-ERW processes is that it tends to avoid the excess heat penetration and associated grain-coarsening that often affect LF-ERW and DC-ERW seams. As a result HF-ERW bond lines tend to have transition temperatures and toughness more like that of the base metal.

A metallographic section across a typical flash-welded seam is shown in Figure 5. Flash-welded seams were made with direct current heating of the entire edges of a “can” as the edges were forced together. Unlike in the case of LF-ERW seams, DC-ERW seams, and HF-ERW seams only part of the extruded flash of the flash weld was trimmed away. That is typical of a flash weld, it makes flash-welded pipe easy to identify.

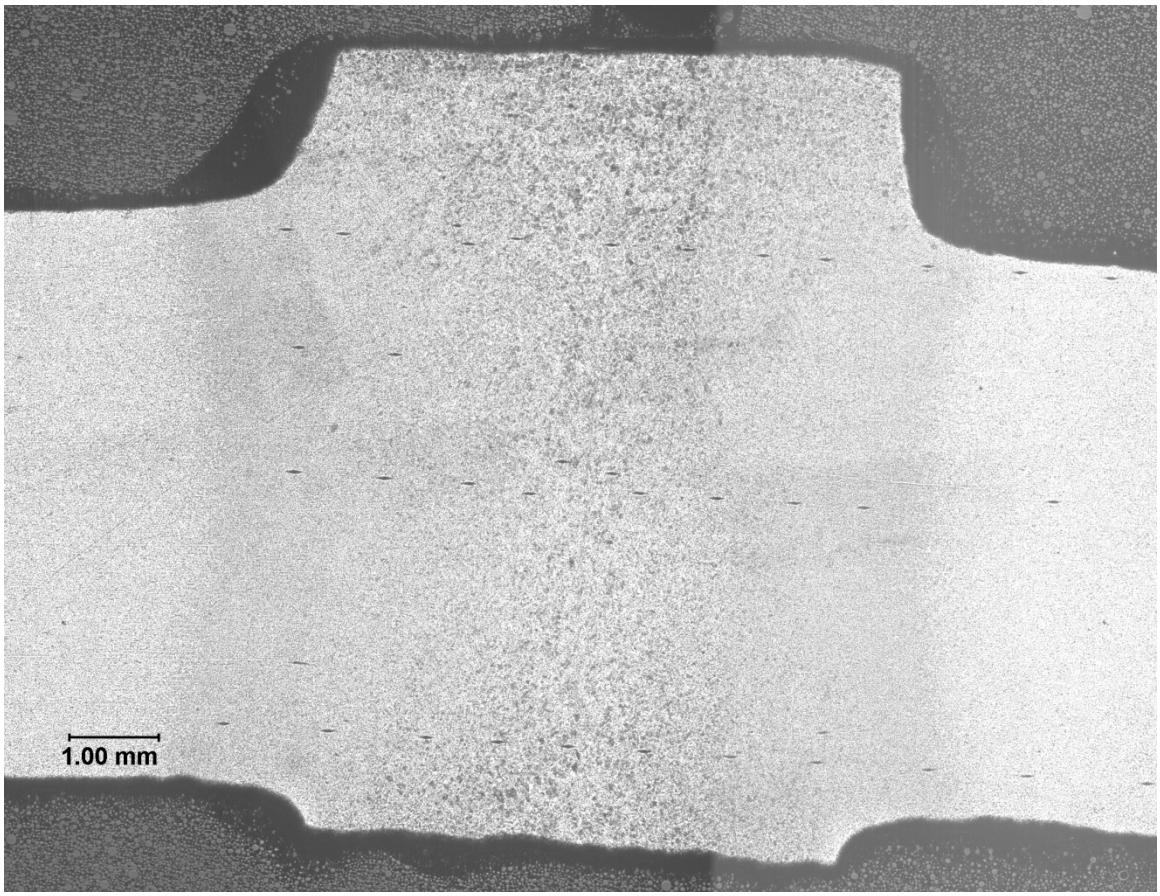

Figure 5. Morphology of a typical flash-welded seam shown at 12X magnification (Note that lines of hardness indentations are visible near both surfaces and at mid-wall. No excessively hard regions were found in this sample.)

The heat affected zone shown for this flash-welded seam is typically wide and contains a band of grain-coarsened material around the bond line region. As stated previously, the grain-coarsened material often translates into high ductile-to-brittle fracture transition temperatures and toughness properties inferior to those of the base metal. Flash-welds typically were not subjected to post-weld heat treatment.

EXAMINING FAILURES OF ERW AND FLASH-WELDED SEAMS VIA METALLOGRAPHY AND FRACTOGRAPHY

Investigation of Hydrostatic Test Failure Caused by a Cold Weld

The following investigation was carried out on one of several hydrostatic test failures that occurred in a hydrostatic retest of an existing pipeline. The pipeline was comprised of 1957-vintage, 12.75-inch-OD, 0.250-inch-wall, X42 pipe. One test break, call it Sample 1, is shown in

Figure 6. The pipe ruptured along its LF-ERW seam at a pressure level of 1,573 (95.5% of SMYS). The length of the rupture was 20 ft, 8 inches (between the arrows in Figure 6). The length of the rupture is 5 to 10 times as long as the length of ductile rupture one would expect from the failure of a defect in the body of the pipe at the same pressure level with water as the pressurizing medium. The fracture opening is very narrow, being less than 1 inch at the widest part. This indicates the relatively low resistance of the seam to fracture propagation.

Figure 6. LF-ERW pipe that ruptured along the seam during a hydrostatic test

As sometimes happens, two anomalies were identified on the fracture surface as possible origins of the fracture. No "chevrons" were present to indicate which one, if either one, was the origin. Both anomalies lay on the bond line and both appeared to be cold weld defects (i.e., lack of fusion). These two anomalies are shown in Figures 7 and 8 as they appeared before the fracture surfaces were removed from the pipe.

Figure 7. Anomaly A on the fracture surface of Sample 1 at 1.1X

Figure 8. Anomaly B on the fracture surface of Sample 1 at 1X

The anomalies shown in Figures 7 and 8 are coated with a dark scale that is probably mill scale formed on a non-bonded portion of the seam while the material was still hot from the welding process. Only a small remaining ligament at the ID surface below each anomaly is coated with rust.

For the purposes of detailed examination of fracture surfaces and to extract appropriate samples for metallographic examination, reasonable size pieces have to be removed from the pipe. Standard practice is to mark samples with paint marker for removal by flame cutting. No flame cutting is allowed within 3 inches of the fracture surfaces along any portion of the fracture surface of interest, and the cut marks at the end of the sample must be at least 3 inches beyond any area of interest. All relevant information as to which side of the fracture the sample comes from and its longitudinal distance from a benchmark such as the upstream girth weld is marked on the sample before cutting. Damp towels are laid over the fracture surfaces to protect them from spatter during flame cutting, and the sample is held in a manner to prevent it from falling and damaging a fracture surface. The samples are allowed to cool before they are handled, and any relevant markings that may have been obscured during cutting are restored.

The fracture surfaces are usually photographed, as is, for the record. In the case of Sample 1, Figures 7 and 8 served that purpose. Each fracture surface is then cleaned in a bath of a water and mild detergent (Alconox®) solution using a soft-fiber-bristle brush. The fracture surfaces are dried with compressed air. They are then examined and photographed as soon as possible. If portions of the surfaces are to be viewed by means of a scanning electron microscope, they are careful extracted by means of a high-speed cut-off wheel and stored in a desiccant container until they can be examined at an outside facility.

The cleaned surfaces in the vicinity of Anomaly A of Sample 1 are shown in Figure 9.

Figure 9. Fracture surface at Anomaly A (OD surfaces back-to-back) at 7/8X

The dark-stained area centered at the 14-inch mark is the anomaly. The remainder of the fracture surface on either side of the anomaly exhibits a repetitive pattern of fracture referred

to as “stitching”. The stitch pattern represents variations in bond strength that were caused by the low-frequency power variations during welding at a too-high welding speed. Stitching likely would not be present on a fracture surface of a seam welded at a lower speed because the heat of welding would have been more uniform. Stitching is not seen on the fracture surfaces of a DC-ERW seam because there is no power variation, and it is not seen on the fracture surfaces of an HF-ERW seam because the frequency of power variation is too high for the welding speed to influence the heat transfer.

The cleaned surfaces in the vicinity of Anomaly B of Sample 1 are shown in Figure 10.

Figure 10. Fracture surfaces at Anomaly B (OD surfaces back-to-back) at 7/8X

The dark-stained area centered at the 19.5-inch mark is the anomaly. Stitching is present on the fracture surfaces on either side of this anomaly as well.

There are no features on either of these fracture surfaces that give any clues as to which of these anomalies (A or B) might be the origin of the rupture. In contrast, the fracture surface show in Figure 11 (taken from another piece of pipe that failed during another cycle of the hydrostatic test of the same pipeline) has distinctive markings called “chevrons” that denote the origin of the fracture. The chevrons sometimes appear on brittle fractures, and they point in the direction opposite that of fracture propagation. Hence, they point toward the origin of the fracture. The yellow arrows in Figure 11 were placed on one of the fracture surfaces in the photograph to show the directions of the chevrons. The red arrows denote the origin of the failure, a small cold weld.

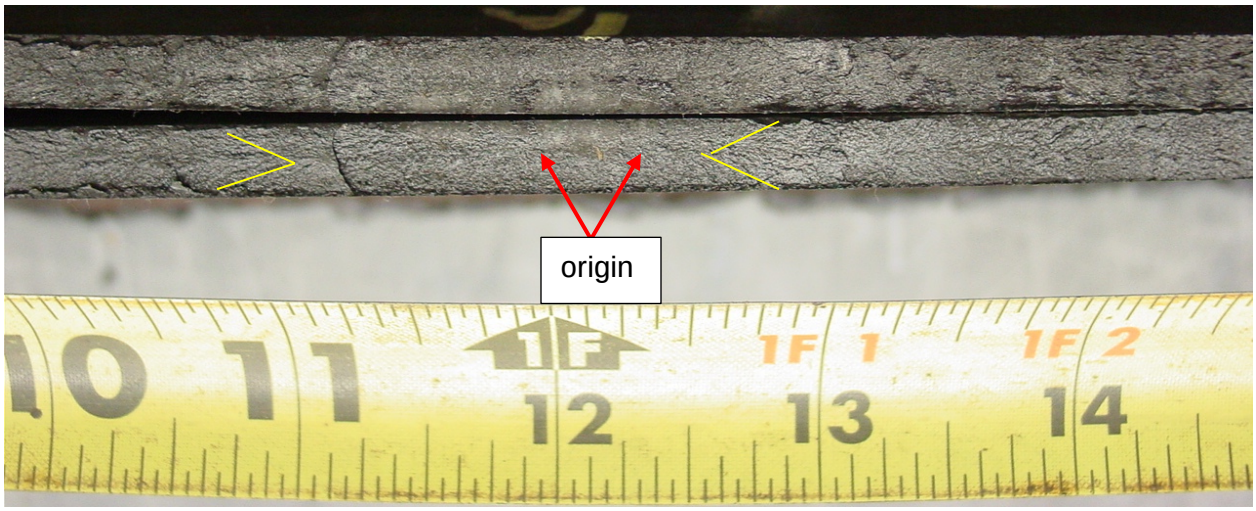

Figure 11. An example of a seam failure where brittle fracture "chevrons" point toward the origin of the failure (OD surfaces back-to-back) at 1.25X

After the fracture surfaces of Sample 1 had been examined, the sides were matched up without touching (to avoid damage from one surface rubbing against the other), and sections across both Anomalies A and B were marked. The objective was to get a common plane through the wall thickness across the fracture. The pieces were saw-cut from both halves of the fracture and matched together but not touching within a mold, and a thermosetting resin was poured into the mold and allowed to harden. The selected common plane was then polished in stages to a 1-micron finish. The resulting metallographic section was then etched in a 5% nital solution (5% nitric acid, balance ethanol). The section across Anomaly A is shown in Figure 12.

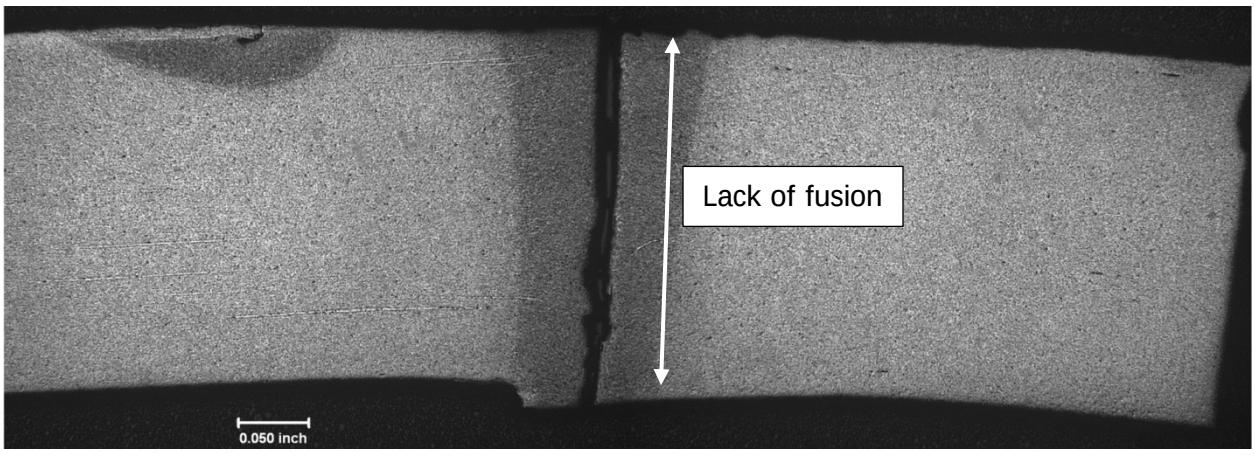

Figure 12. Metallographic section across Anomaly A at 8X

The section across Anomaly B is shown in Figure 13.

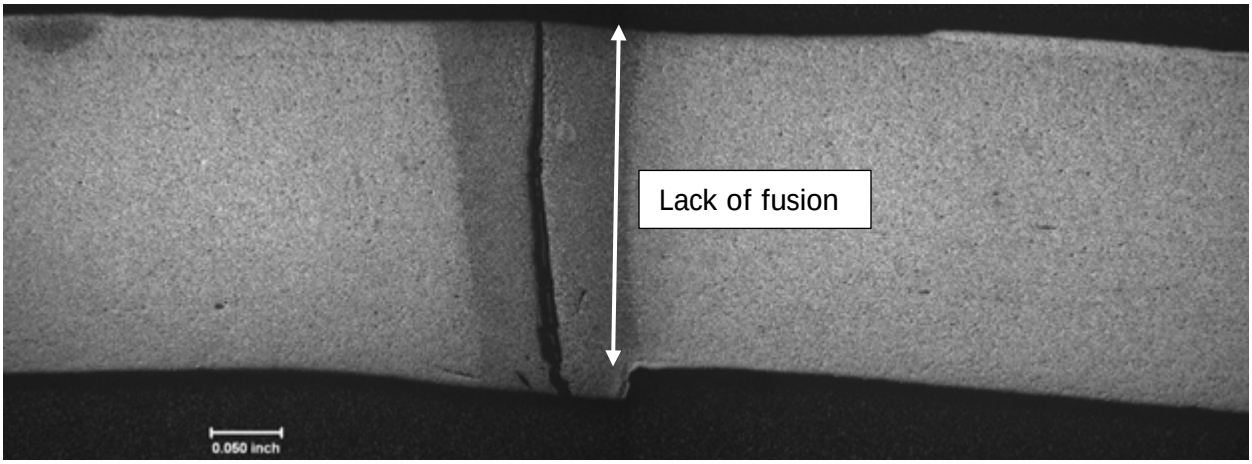

Figure 13. Metallographic section across Anomaly B at 8X

Both anomalies are lack-of-fusion defects or “cold welds”. Anomaly A was about 1.4 inch long. Anomaly B was about 1 inch long. Both were 95% through the wall thickness. They were located about 6 inches apart, so one can probably assume that they did not interact. If that was the case, the longer of the two likely was the origin of the failure.

It is typical for Kiefner to examine a section across an intact portion of an ERW seam in a piece containing a failed ERW seam defect provided that the entire seam was not fractured. Not all of the seam of Sample 1 had been fractured, so a section across an intact portion was taken and is shown in Figure 14.

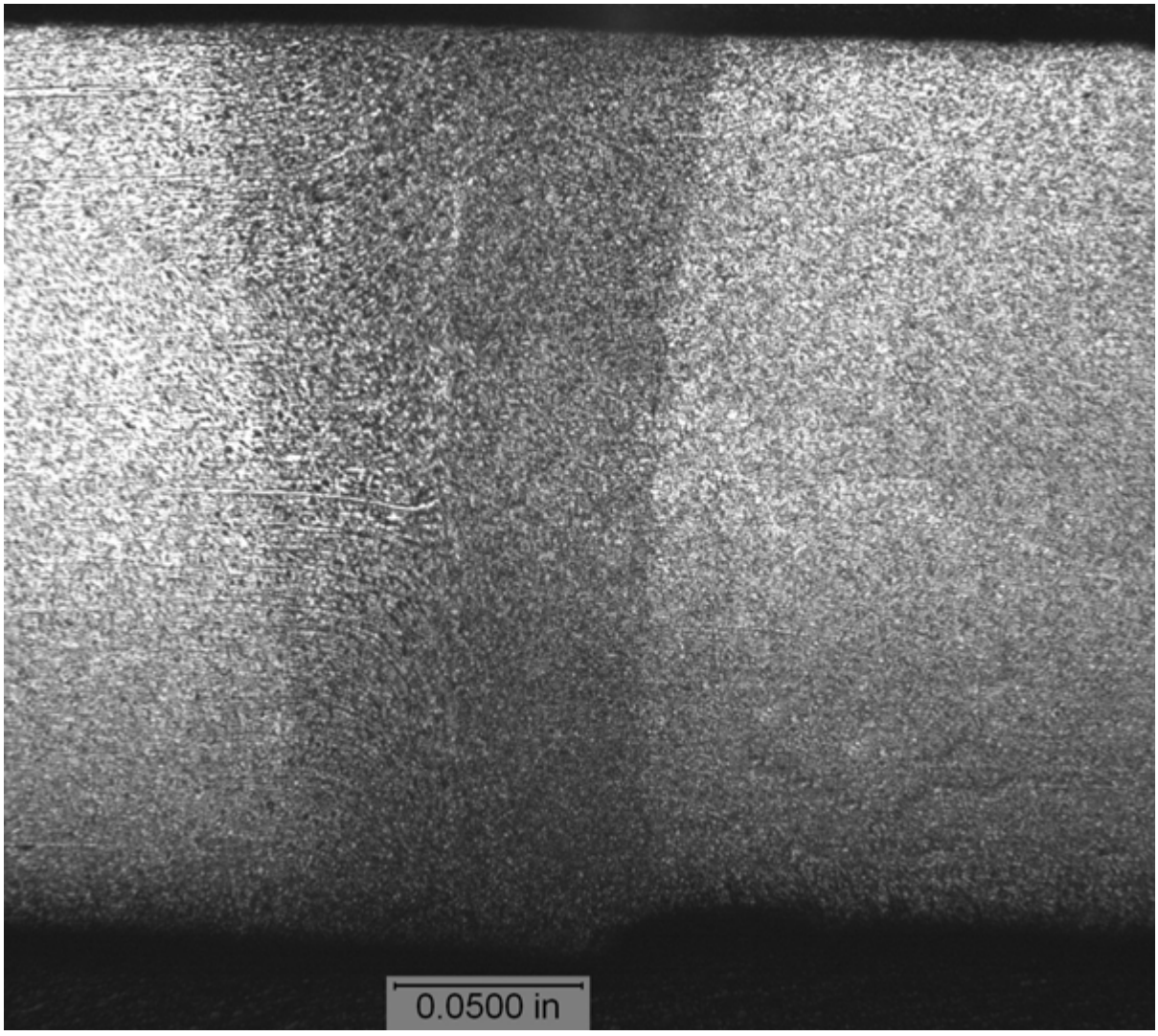

Figure 14. Section across intact portion of the seam of Sample 1 at 20X

This section of the weld exhibits no defects. On the left side of the bond line one can see the flow lines indicative of the upsetting process during welding. The material on the other side looks slightly different suggesting that this pipe may have been made from a slit coil rather than a full-width coil.

Other Investigations of Cold Weld Anomalies

In some cases an anomaly is discovered by an in-service leak necessitating removal of the piece of pipe containing the leak from the pipeline. One such case involved a cold weld in 16-inch-OD, 0.312-inch, X52 LF-ERW 1959-vintage. This defect was found to be leaking in service at 600 psig (29.6% of SMYS) within 1 year after a hydrostatic test to 1248 psig (61.5% of SMYS).

The piece containing the leak is shown, after its removal from service, in Figures 15 and 16.

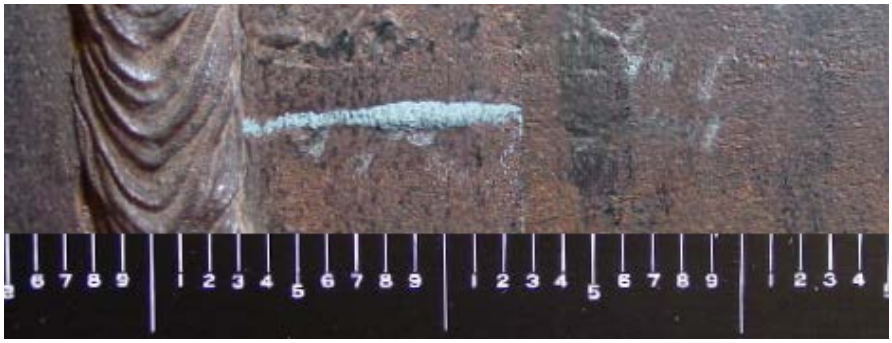

Figure 15. View of the leak at the OD surface (highlighted by magnetic particles)

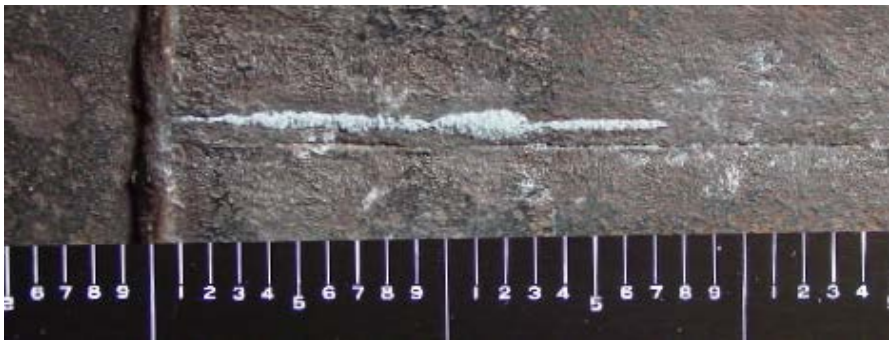

Figure 16. View of the leak at the ID surface (highlighted by magnetic particles)

The leak was located in the ERW seam of the pipe at a girth weld. The sample was chilled in liquid nitrogen and broken apart to expose the surfaces of the leak, and the exposed surfaces are shown in Figure 17.

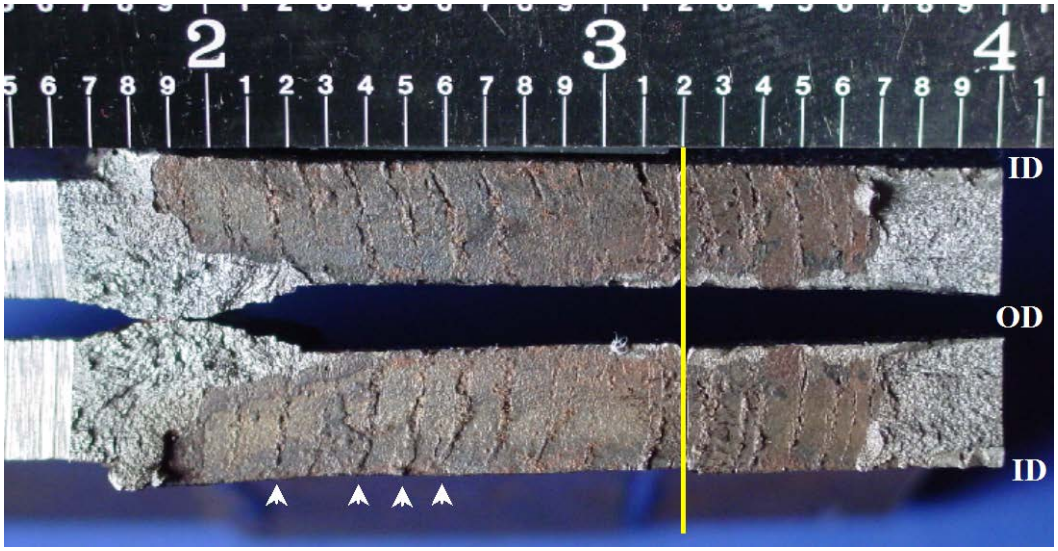

Figure 17. Exposed surfaces of the leak at 2X

This dark-colored area is a cold weld in an LF-ERW bond line. The lighter-colored fracture surfaces on either side of the cold weld were created by impact loading after the sample had been cooled to liquid nitrogen temperature (-320°F). The stitch pattern sometimes seen on fractures in LF-ERW pipe is visible on the mill-scaled surface of the anomaly (white arrows). A cross-section of the anomaly, taken at the location of the yellow line in Figure 17, is shown in Figure 18.

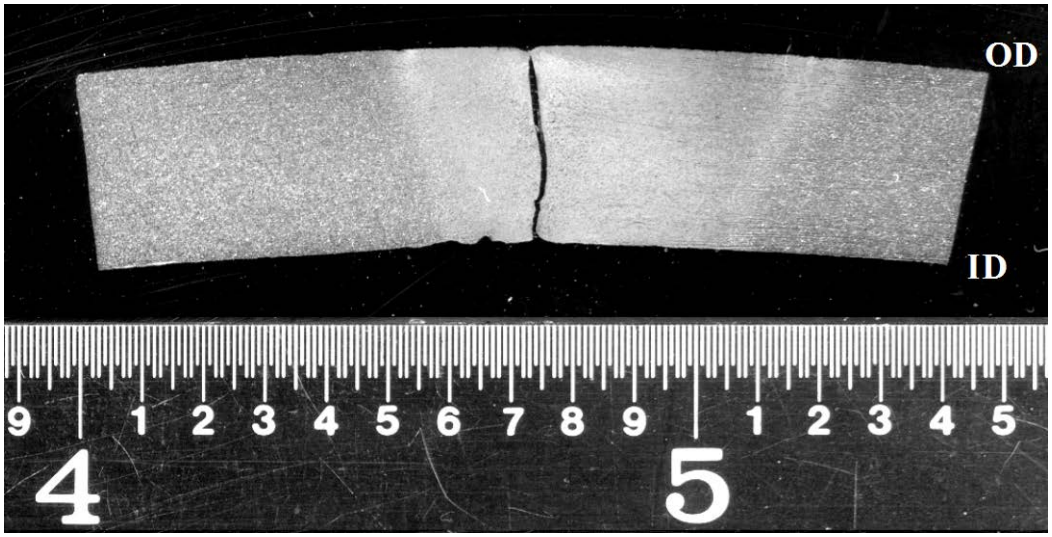

Figure 18. Metallographic section across a cold weld at 3X

A higher magnification view of the anomaly is shown in Figure 19. Flow lines reflecting the upsetting process are clearly visible on both sides of the bond line.

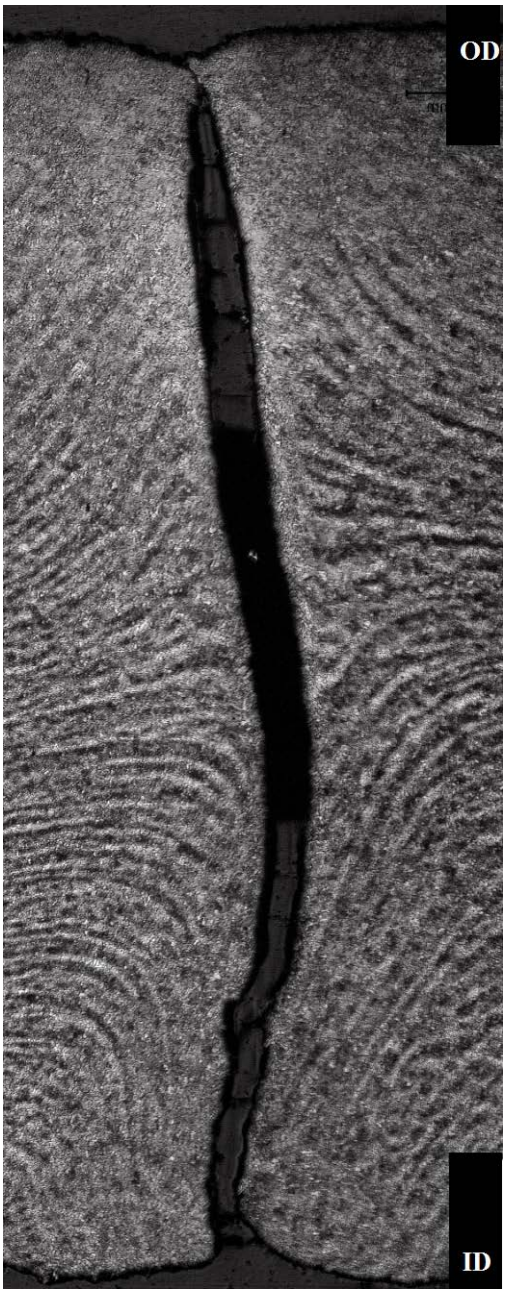

Figure 19. Metallographic section across cold weld at 20X

Cold welds also have been observed in HF-ERW seams. One such short cold weld, also referred to a "penetrator", is shown in Figure 20. This penetrator was found in 10.75-inch-OD, 0.250-inch-wall, X42 HF-ERW pipe when it began leaking in service at 600-psig (30% of SMYS).

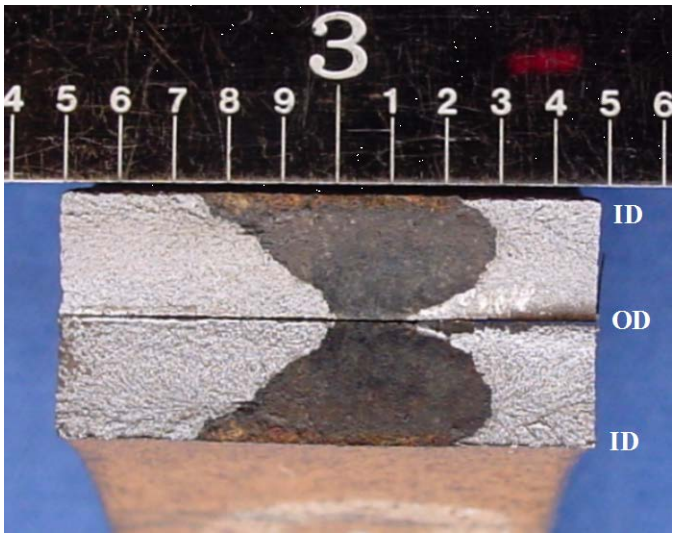

Figure 20. Penetrator as seen after the sample was chilled in liquid nitrogen and broken open at 2.5X

Both of the above leaks occurred after the pipelines had been in service for long periods of time and after having been subjected to higher pressures during hydrostatic testing. Yet, there is no evidence that they leaked during the life of the pipeline until just before they were discovered. It is believed that the mill scale formed at the time of welding prevents leakage as long as it remains intact. Eventually, particularly if the pipe is subjected to a hydrostatic retest at some point, the mill-scale may fracture of otherwise deteriorate sufficiently to allow leakage to develop.

Hook Crack Failures

Hook cracks are anomalies that arise from non-metallic layers or laminations in the base metal that get deformed during the upsetting process at the time of welding. They tend to be located near but not necessarily on the bond line of the seam. Hook cracks have been found in all four types of autogenous seams (i.e., LF-ERW, DC-ERW, HF-ERW, and flash-welded). An example of a hook crack is shown in Figure 21. The hook crack did not extend to either the ID or the OD surface. It penetrated about 15% of the wall thickness. It is likely that the failure of this pipe was not solely the result of this hook crack alone. Toward the OD surface, portions of the fracture involved other hook-shaped layers, no doubt weaker than the base metal. Toward the ID surface it appears that a bond-line weakness also contributed to the failure.

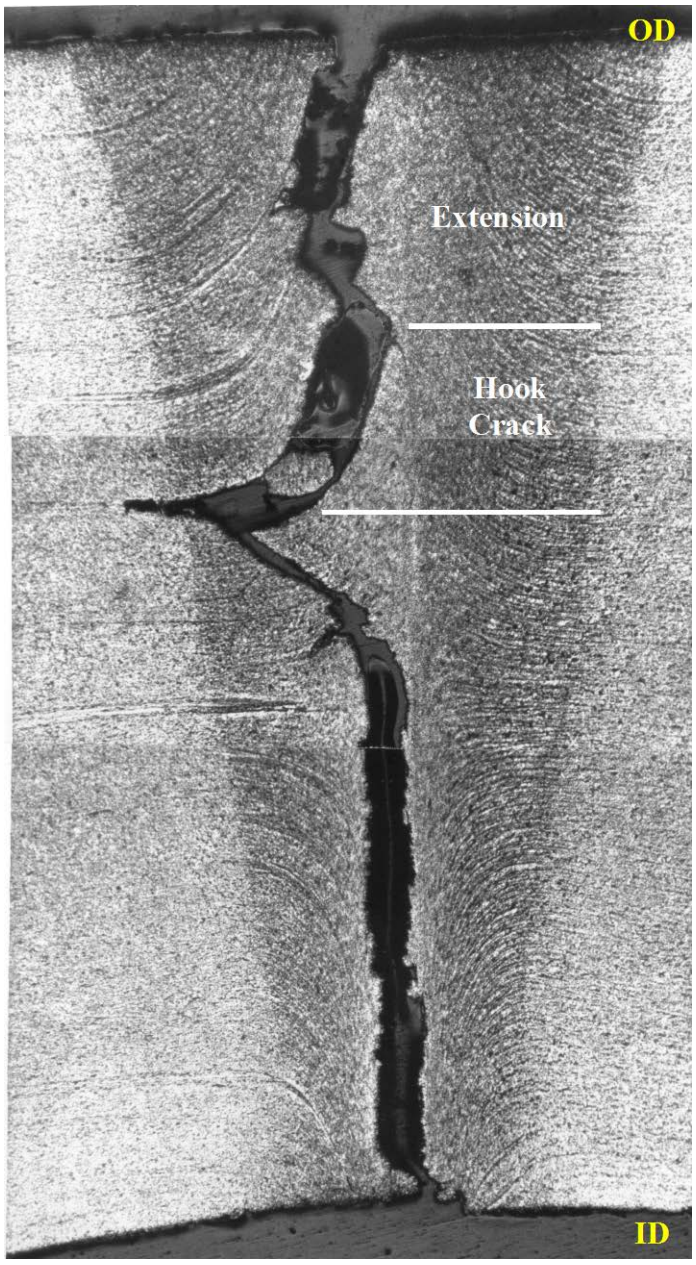

Figure 21. Metallographic section across an HF-ERW seam showing an embedded hook crack at 20X

This anomaly found to be the origin of a hydrostatic test rupture in a 16-inch-OD, 0.308-inch-wall X52, 1967-vintage HF-ERW pipe. This pipe was high-frequency welded, though the heat-affected zone as shown in Figure 21 does not have the hour-glass shape often associated with an HF-ERW seam. The failure pressure was 1675 psig (83.7% of SMYS). The fracture surfaces containing this anomaly are shown in Figure 22.

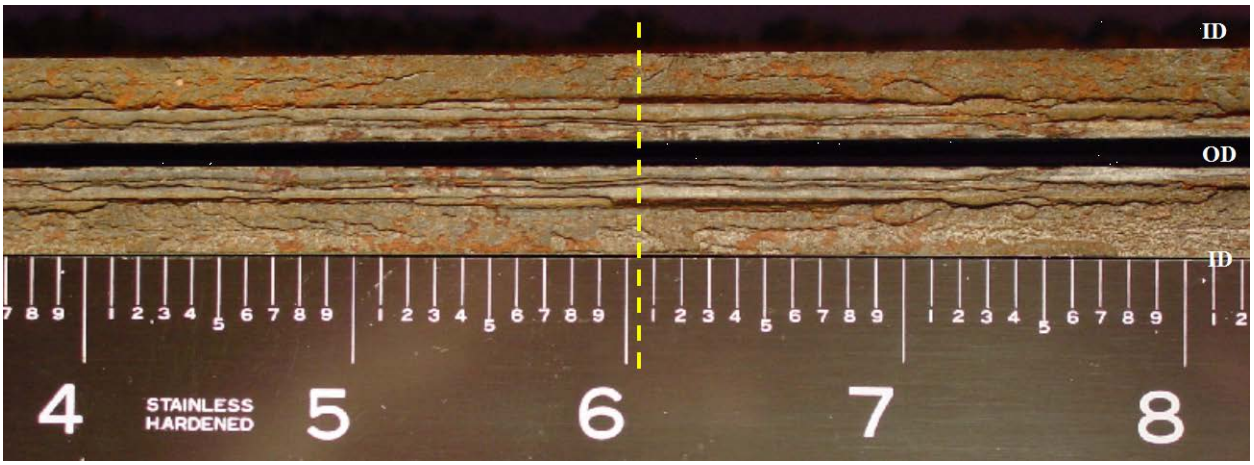

Figure 22. Fracture surfaces containing the anomaly shown in Figure 21 (the metallographic section in Figure 21 was taken at the location of the dashed line) at 1.4X

The fracture surfaces reveal a complex array of layers that suggest fracturing along multiple planes of inclusions and along the bond line. This type of behavior is often seen with "dirty" steels, that is, steels with a lot of non-metallic inclusions. The complexity of the layers makes it next to impossible to define the dimensions of the defect that caused the failure.

The fracture surfaces at another hydrostatic test failure are shown in Figure 23. The origin of the failure was a hook crack. This hook crack was OD-surface-connected and was 7 inches long and 30% through the wall thickness at the point of deepest penetration. It is clearly defined on the fracture surface by its dark gray color.

Figure 23. Fracture surfaces showing a long, mill-scale-coated hook crack at 1.75X

Note that a narrow band of red-brown rust lies adjacent to the hook crack. It is believed that this band represents growth of the hook crack by ductile tearing during a hydrostatic test. This piece of pipe failed in a hydrostatic test at a pressure of 1917 psig (94.0% of SMYS). The pipe

was a 12.75-inch-OD, 0.250-inch-wall, X52, 1961-vintage LF-ERW material manufactured by Lone Star Steel. The metallographic section across this failure is shown in Figure 24. The fact that the heat-affected zone of this seam is practically indistinguishable from the base metal is the result of the full-body normalizing given to each pipe by its manufacturer.

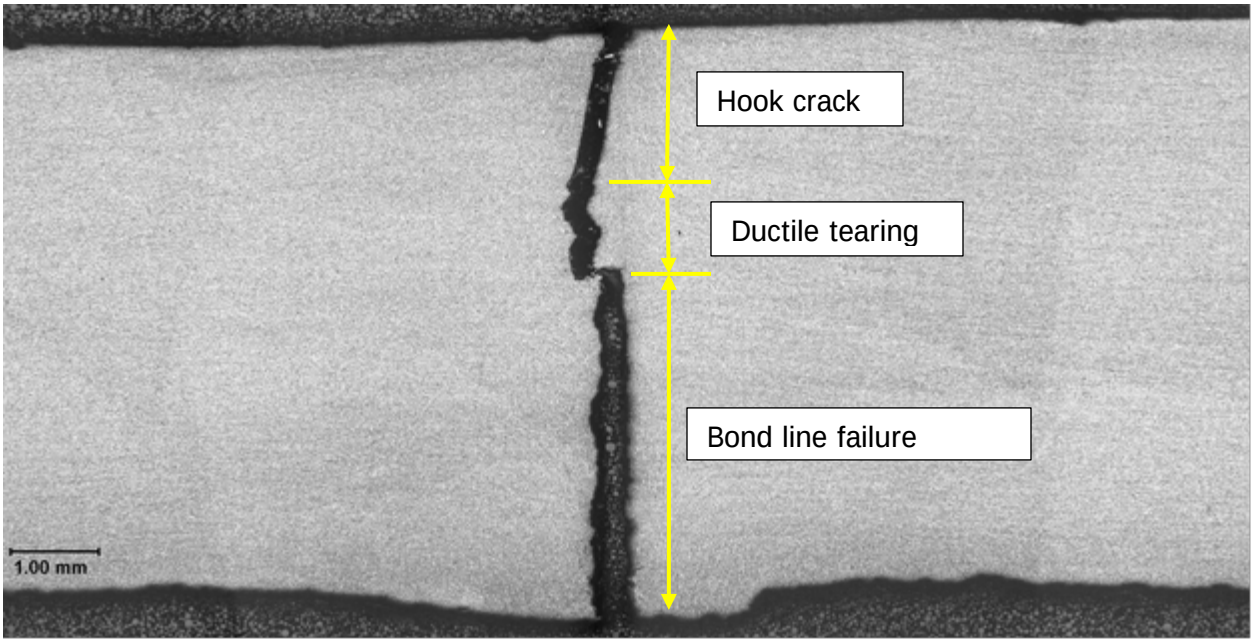

Figure 24. Metallographic section across a failure that originated at an OD-surface-connected hook crack at 10X

The stages of this failure are the initial hook crack, probable ductile tearing during a hydrostatic test, and finally a bond line failure. Using the overall length of the hook crack, its maximum depth of 30% of the wall thickness, and assuming it to have an elliptical shape one can calculate a predicted failure pressure for this anomaly. The flow stress measured for the base metal was 74,000 psi and the base metal full-size-equivalent Charpy upper shelf energy was 44 ft lb. The failure pressure predicted via the Modified Ln-Secant equation is 2,254 psig, 18% higher than the observed failure pressure. Factors that could account for this difference include the possibility that the Charpy upper shelf energy for the zone of the hook crack was significantly less that 44 ft lb, and that part of the failure was in the bond line.

Selective Seam Weld Corrosion Failures

Fractography and metallography are useful for identifying and characterizing failures arising from selective seam weld corrosion. The fracture surfaces of one such failure are shown in Figure 25.

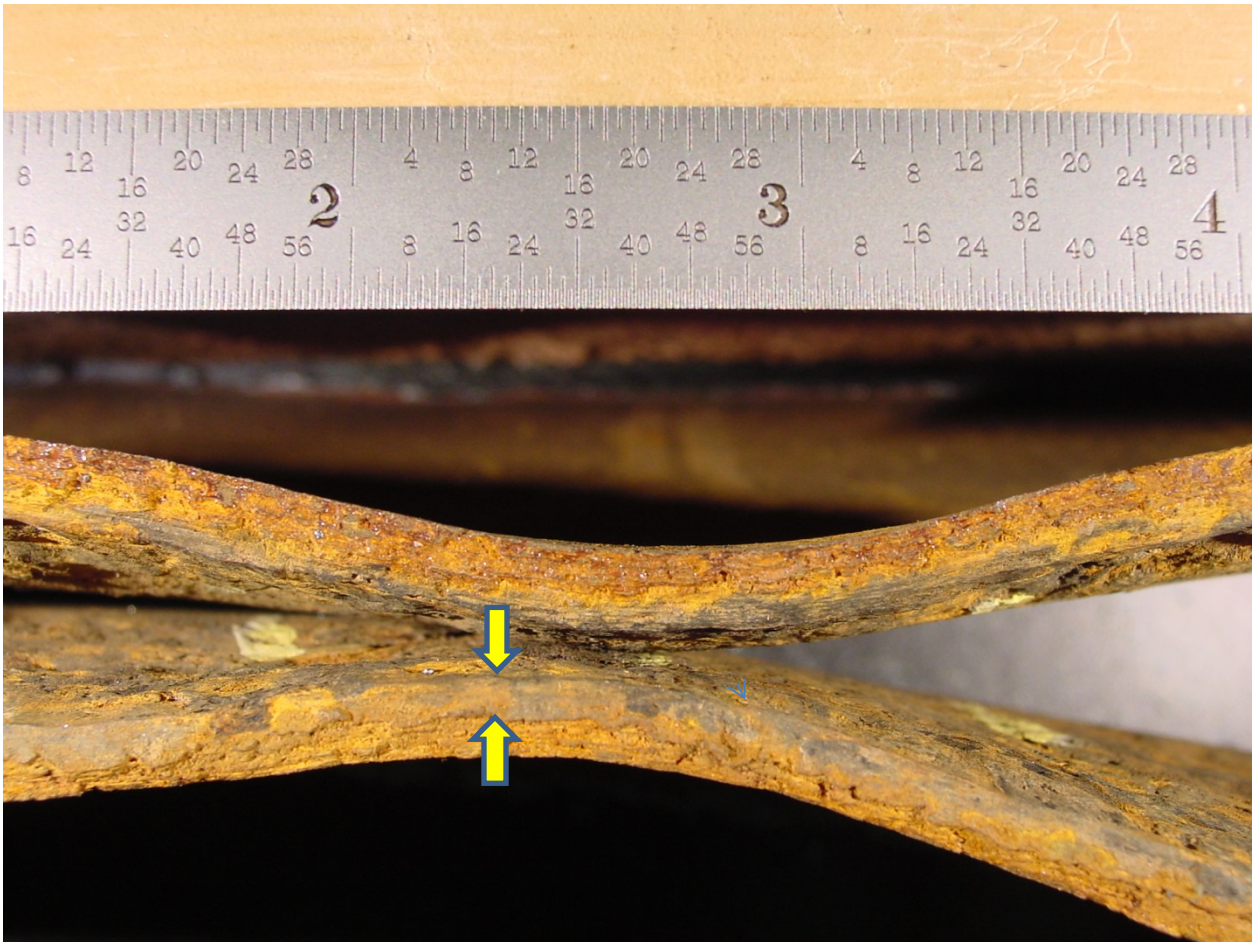

Figure 25. Fracture surfaces of a failure caused by selective seam weld corrosion. Arrows denote missing metal; remainder of the surface is fracture at 2X

This failure occurred in a 12.75-inch-OD, 0.250-inch-wall, X52 LF-ERW, 1958-vintage pipe. The failure occurred in-service at 1,257 psig (61.6% of SMYS). The selective seam weld corrosion had removed as much as 66% of the wall thickness over a length of 6.5 inches. The metallographic section across the seam is shown in Figure 26. The seam corrosion is obviously deeper than that in the surrounding base metal.

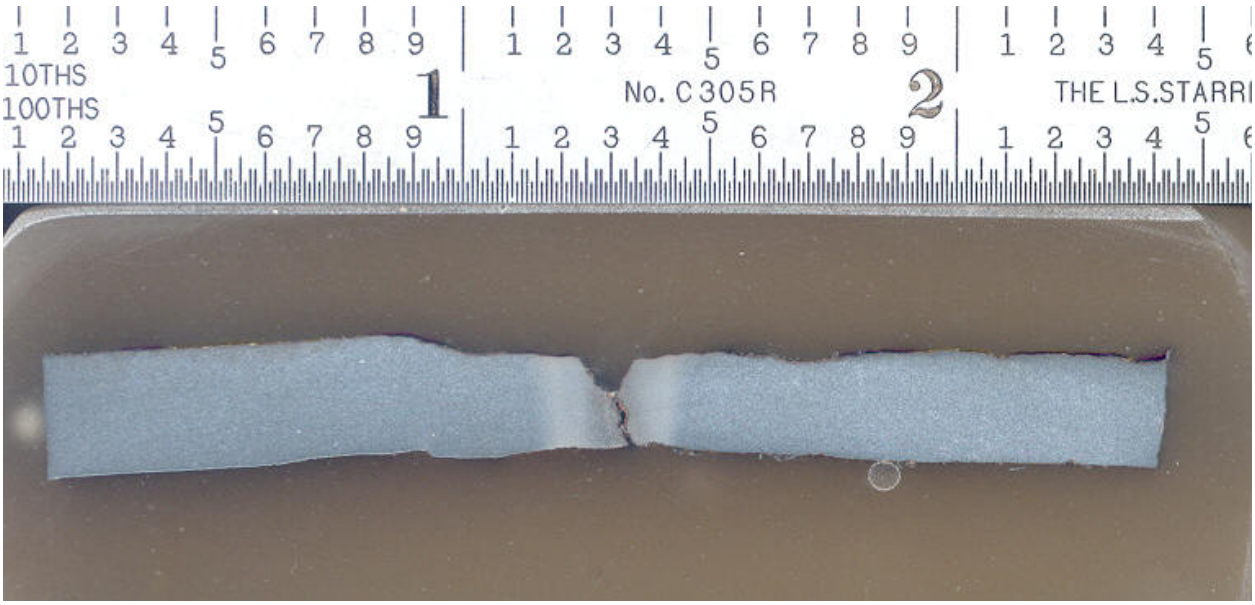

Figure 26. Metallographic section across a failure caused by selective seam weld corrosion at 2.5X

Note that the metal loss in the seam had a fairly blunt shape to it. That and the obvious ductile tearing of the remaining ligament suggest that the failure was ductile rather than brittle. In fact, a calculation via the Modified Ln-Sec equation using the measured flow stress of the base metal (70,000 psi) and the full-size-equivalent Charpy upper shelf energy of the base metal (23 ft lb) results in a predicted failure pressure of 1,183 psig. This value underestimated the actual failure pressure of 1,257 by 6%.

The fracture surfaces of another in-service failure caused by selective seam weld corrosion are shown in Figure 27.

Figure 27. Fracture surfaces of another failure caused by selective seam weld corrosion at 1X

This failure occurred in a 16-inch-OD, 0.375-inch-wall, Grade B, 1946-vintage, LF-ERW pipe. The failure occurred at a pressure level of 120 psig (7.3% of SMYS). Note that the remaining

ligament between the missing metal and the ID-surface is flat. That is a common characteristic of fractures of the bond line of an LF-ERW material.

A metallographic section across the fracture is shown in Figure 28.

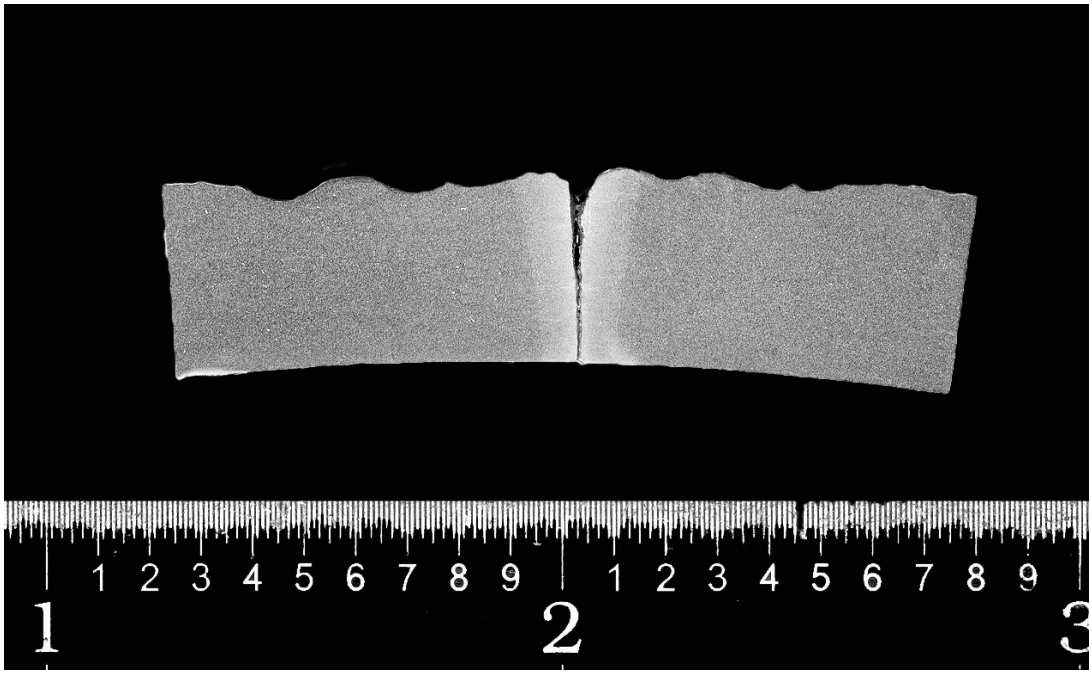

Figure 28. Metallographic section across another failure caused by selective seam weld corrosion at 2.5X

In this case the selective seam weld corrosion is narrow and sharp-tipped. The remaining ligament failed in a brittle manner unlike the case shown in Figure 26. It is speculated that a pre-existing OD-surface-connected bond line defect may have been present in the case of the metal loss shown in Figure 28. Corrosion along the surfaces of such a defect could account for the narrow sharp-tipped appearance of the metal loss.

Fatigue Failures

Fractography and metallography are useful for identifying and characterizing failures arising from pressure-cycle induced fatigue. The fracture surfaces of one such failure are shown in Figures 29 and 30. Figure 29 was taken with a standard optical camera, whereas Figure 30 was taken at low magnification with the aid of an electron microscope. The pipeline involved was comprised of a 1964-vintage, 12.75-inch-OD, 0.203-inch-wall, X52, LF-ERW material manufactured by Bethlehem steel. The pipeline, a hazardous liquid pipeline, failed in service at a pressure level of 990 psig (59.8% of SMYS).

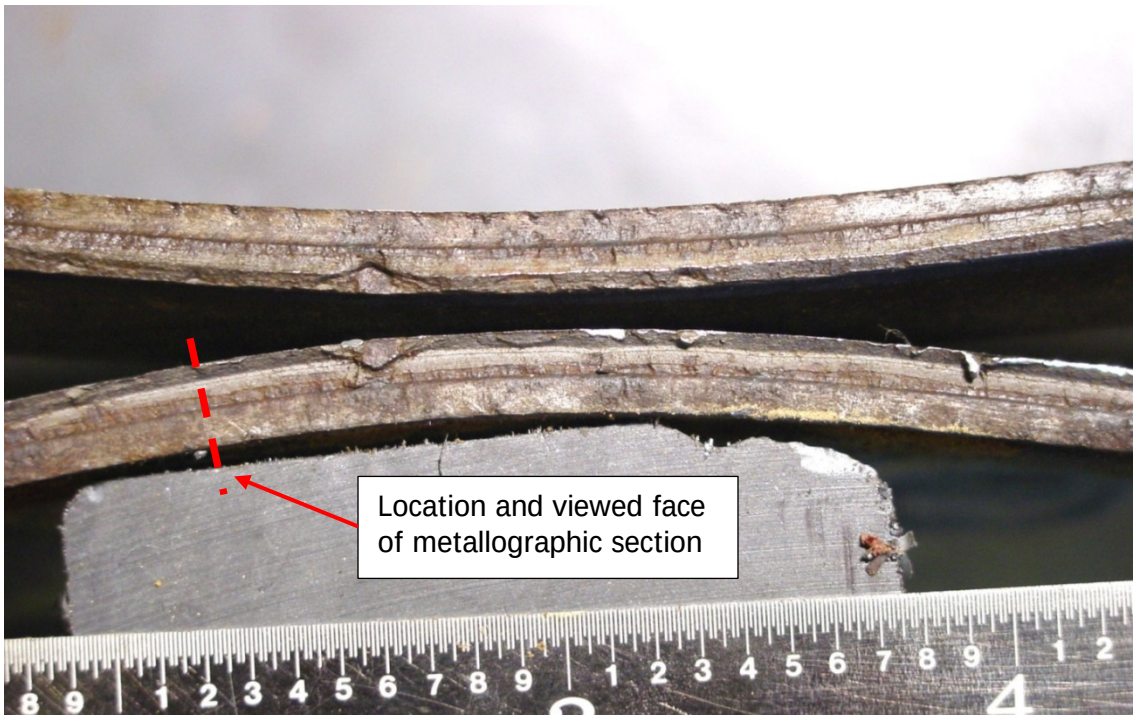

Figure 29. Fracture surfaces of a failure caused by fatigue crack growth from an OD-surface-connected hook crack at 2X

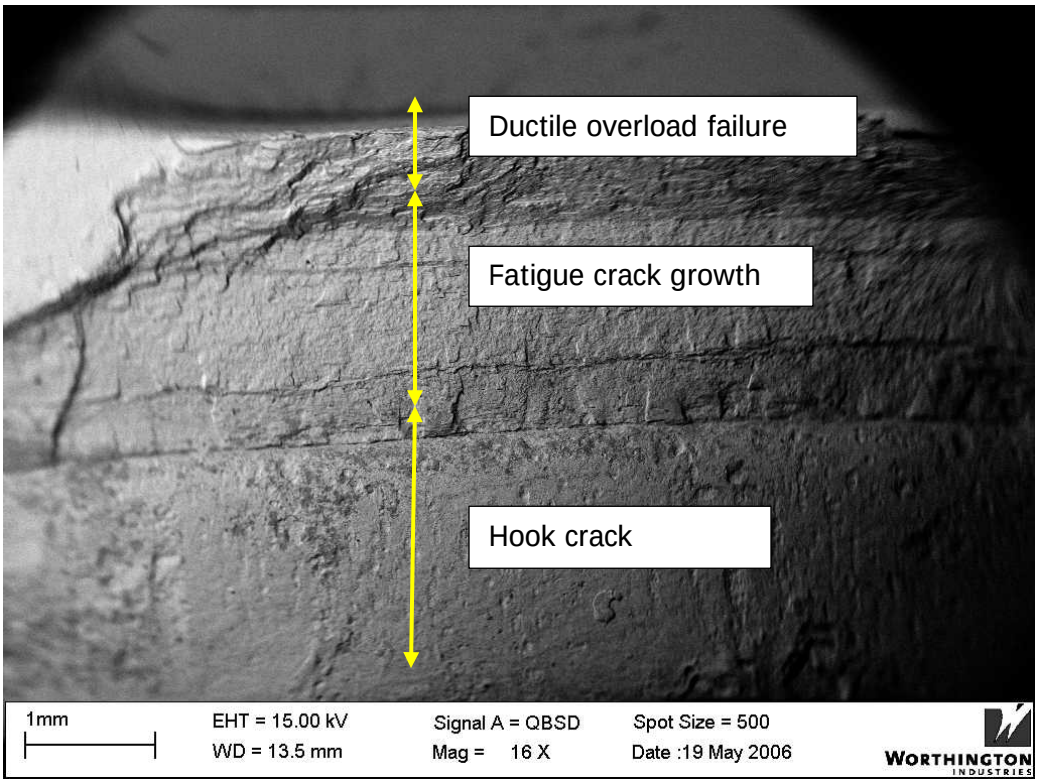

Figure 30. Electron microscope picture of part of the fracture surface of a fatigue failure from a hook crack at 16X

The characteristics of the failure are best observed in Figure 30, although once identified on Figure 30, the features of interest can also be seen in Figure 29. The hook crack was present from the time the pipe was manufactured. At some point during the service life of the pipeline a fatigue crack initiated at the tip of the hook crack. The fatigue crack initiated at numerous locations along the hook crack as evidenced by the step-like appearance along the edge of the smooth hook crack. The steps are often referred to as “ratchet marks”, and they represent individual initial cracks not always on the same plane. After some amount of propagation, these small cracks coalesce into a single crack. In this case the crack continued to propagate fairly uniformly in depth until the stress in the remaining ligament reached the ultimate tensile strength of the a material, and the rupture ensued.

A metallographic section was taken across the failure at the location shown in Figure 29. The section is shown in Figure 31.

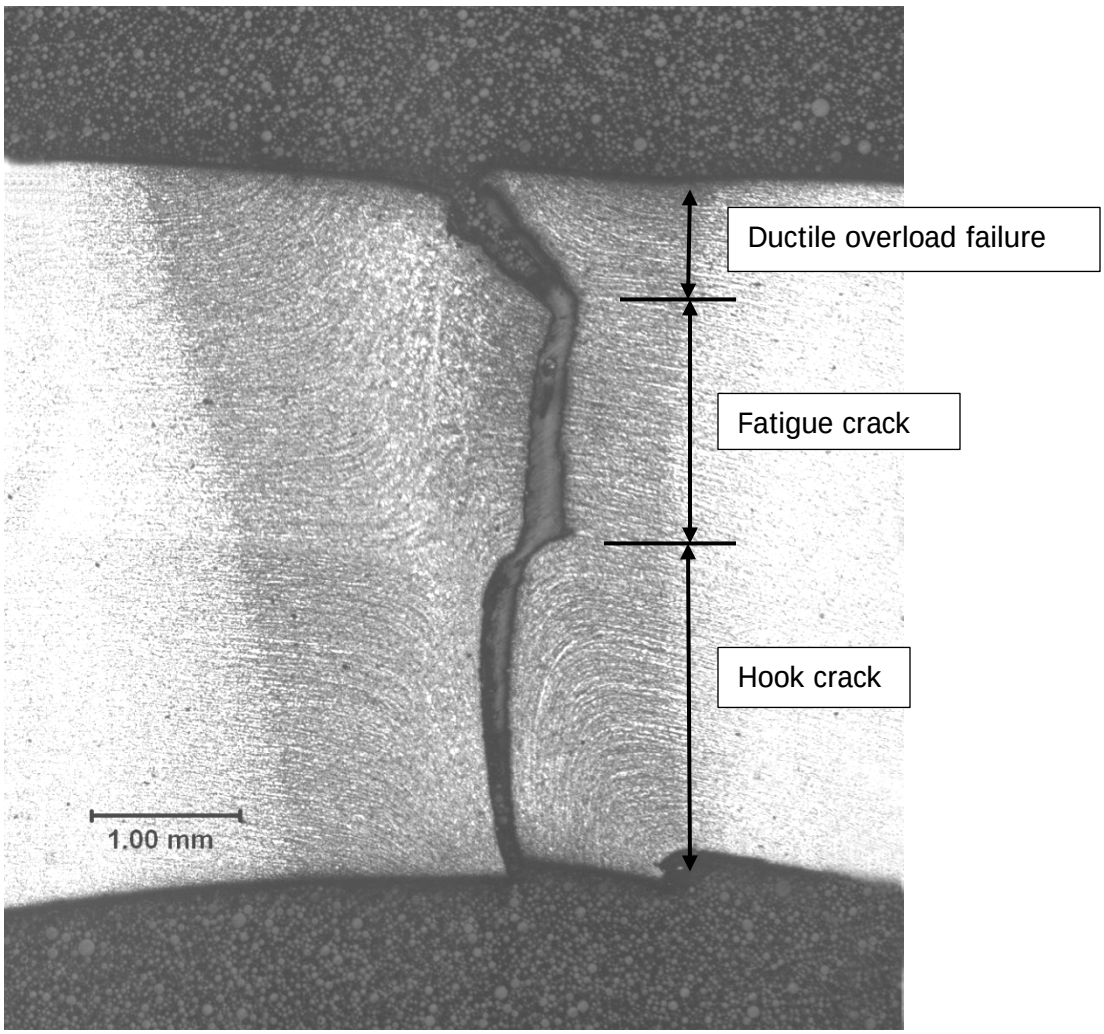

Figure 31. Metallographic section across the fatigue failure at 20X

The metallographic section reveals the relevant features of the failure, the initial hook crack, the fatigue crack growth, and the final overload failure. Pressure-cycle-induced fatigue cracks tend to propagate straight through the pipe wall thickness perpendicular to the maximum principal stress, the hoop stress arising from internal pressure.

It is noted that this fracture was viewed with the aid of an electron microscope. Even at high magnification there was no clear-cut evidence of step by step crack advance (sometimes referred to as “striations”). Kiefner has not had much success at finding striations in conjunction with fatigue failures in the vicinity of ERW seams.

The fracture surfaces of another pressure-cycle-induced fatigue failure are shown in Figures 32 and 33. In this case the failure occurred as a leak, and the fracture surfaces had to be exposed by breaking the sample along the plane of the crack after it had been chilled in liquid nitrogen. The origin of the fatigue crack was an ID-surface-connected hook crack.

Figure 32. Fracture surfaces of a fatigue-induced leak at 2X

I

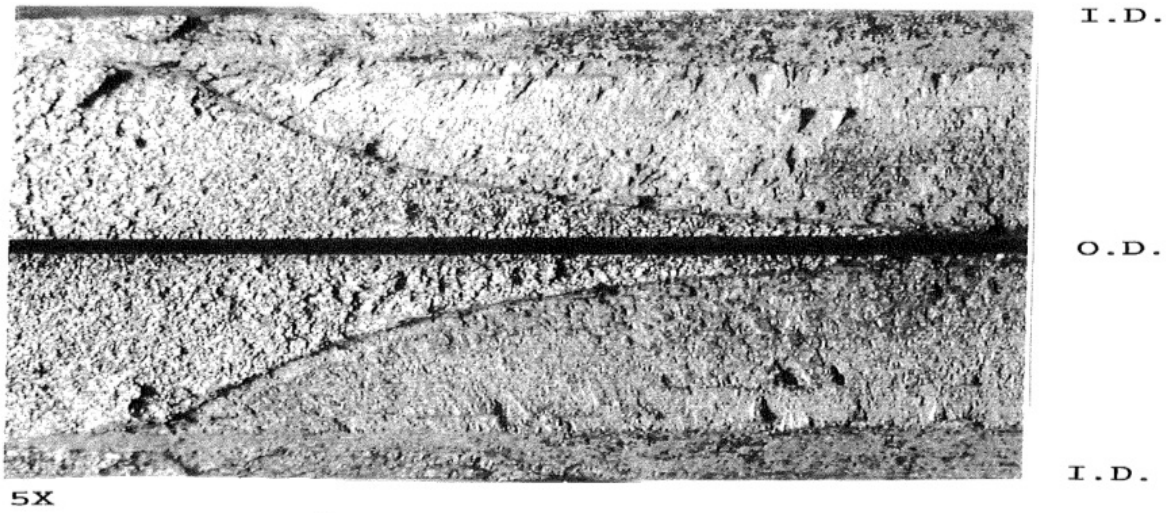

Figure 33 . Fracture surfaces of a fatigue-induced leak at 5X

This anomaly was discovered during a hydrostatic retest of a 26-inch-OD, 0.281-inch-wall, X52, 1956-vintage, flash-welded pipe at a pressure level of 1124 psig (100% of SMYS). Clearly, though, the fatigue crack propagation had taken place while this hazardous liquid pipeline was in service. The fatigue crack initiated in steps (ratchet marks) along the edge of an ID-surface-connected hook crack. The propagation of the fatigue crack is characterized by at least three "re-initiations" as evidenced in Figure 33 by the successive ratchet marks after certain stages of uniform crack growth. It is speculated that the crack growth may have been temporarily retarded on several occasions by large overloads possibly in conjunction with hydrostatic re-tests conducted at various times. In any case, the crack had propagated nearly through the wall before the last hydrostatic test caused the remaining ligament to fail resulting in leakage.

A metallographic section taken at the center of the leak is shown in Figure 34.

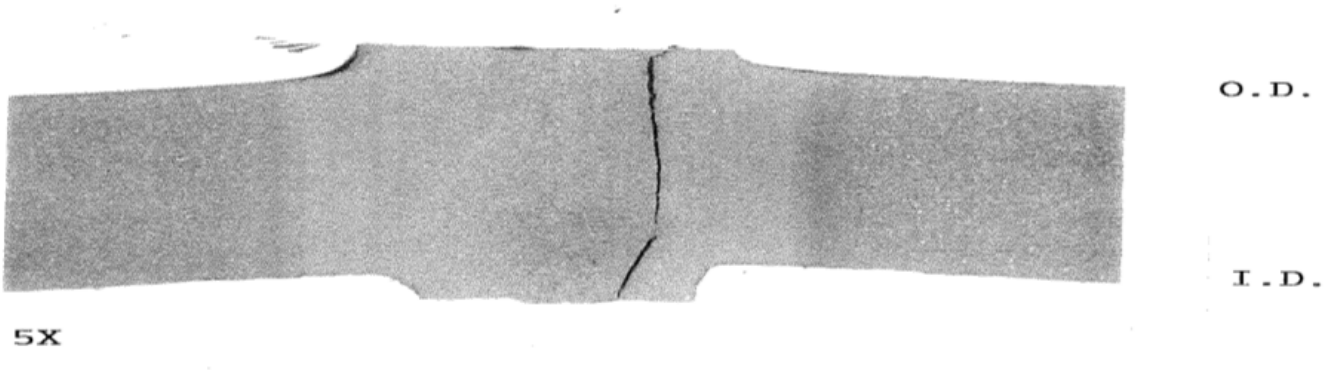

Figure 34. Metallographic section across leak at 5X

The hook crack was ID-surface-connected. The fatigue crack grew almost straight through the wall thickness of the weld flash (thicker than the pipe body). The final ductile overload failure was a slant fracture at the OD surface.

Use of Microhardness Measurements

Microhardness Measurements are used on occasion if excessively hard microstructures are suspected to have played a role in the cause of an ERW or flash-welded seam failure. The locations for appropriate measurements are shown in Figure 35. The sample shown in Figure 35 was taken from a 1962-vintage, 18-inch-OD, 0.219-inch-wall, X52, DC-ERW material. Materials of this type and vintage have been known to be affected by hydrogen stress cracking because of excessively hard heat affected zones. So, hardness measurements were made on this material. As seen in Figure 35, none of the measurements came close to the Vickers 500-gram hardness level of 350 that would tend to raise concern. The importance of Figure 35 is that it shows where the readings should be taken. Three regions; near-OD, near-ID, and mid-wall; should be interrogated. Each traverse should cover 5 to 10 locations (in this case because of the relatively low hardness levels, 5 were sufficient) representing all parts of the HAZ on either side of the bond and the bond line itself. As benchmarks, several base metal reading should be taken as well.

Microhardness Test Results

Job No: [redacted] Project Manager: [redacted]

Sample description: Seam

Scale: Vickers Load: 500 g

Photograph of Sample

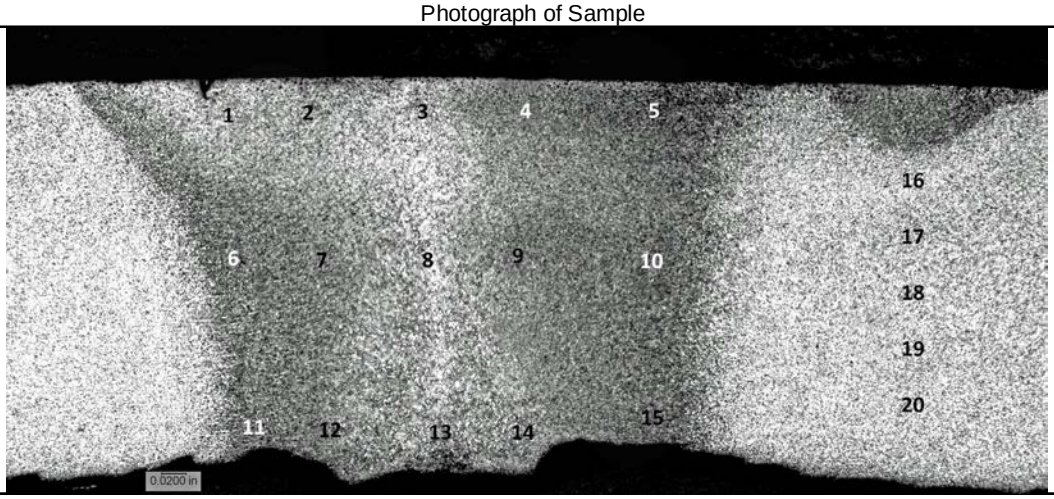

Targeted Locations

1	195.2	VHN	6	194.5	VHN	11	214	VHN	16	210.6	VHN
2	185.8	VHN	7	209.2	VHN	12	221.8	VHN	17	190.8	VHN
3	185.9	VHN	8	220.7	VHN	13	224.2	VHN	18	193.6	VHN
4	181.2	VHN	9	220.5	VHN	14	213.8	VHN	19	190.4	VHN
5	187.6	VHN	10	209.1	VHN	15	202.6	VHN	20	189.3	VHN

Conversion

1	90.5	HRB	6	90.4	HRB	11	94	HRB	16	93.4	HRB
2	88.8	HRB	7	93.2	HRB	12	95.4	HRB	17	89.9	HRB
3	88.8	HRB	8	95.2	HRB	13	95.8	HRB	18	90.3	HRB
4	87.4	HRB	9	95.2	HRB	14	94	HRB	19	89.8	HRB
5	89.3	HRB	10	93.2	HRB	15	92	HRB	20	89.6	HRB